

Università degli Studi di Salerno



Department of Chemistry and Biology

Ph.D. in Chemistry

Polymeric Aerogels

Tutor :

Prof. Gaetano Guerra

Author:

Dr. Simona Longo

Co- Tutor :

Dr. Christophe Daniel

XII cycle 2011-2014

Ai miei splendidi genitori, a mia sorella, al mio Diego.

"[...] La nobiltà dell'uomo, acquisita in cento secoli di prove ed errori, era consistita nel farsi signore della materia, [...] mi ero iscritto a Chimica perché a questa nobiltà mi volevo mantenere fedele, vincere la materia è comprenderla, e comprendere la materia è necessario per comprendere noi stessi [...]"



Primo Levi

Index

Introduction	1
References	11

Part I : Physically Crosslinked Polymeric Aerogel

Chapter 1

Physically Crosslinked Polymeric Aerogel:State of Art

1.1. Introduction	18
1.2. How to prepare physically crosslinked polymeric Aerogel :Sol-Gel Technology	21
1.3. Polymeric Aerogels with Nanoporous Crystalline Phases as Physical Crosslinks	25
1.4. Aerogels with the Nanoporous δ and ϵ Forms of s-PS	25

Chapter 2

Monolithic nanoporous–crystalline aerogels based on Poly (2,6-dimethyl-1,4- phenylene)oxide and Syndiotactic Polystyrene

2.1. Introduction	35
2.2. Preparation and structural characterization of PPO/s-PS aerogels	36
2.3. Properties of aerogels based on nanoporous crystalline PPO	46
2.3.1. Carbon tetrachloride	50
2.3.2. 1,2 - Dichloroethane	51
2.4. Concluding remarks	63

Chapter 3
Monolithic Aerogels Based on
Poly(2,6-diphenyl-1,4-phenylenoxide)and Syndiotactic Polystyrene

3.1. Introduction	65
3.2. PPPO powders and Films	67
3.3. Preparation and structural characterization of PPO/s-PS aerogels	73
3.4. Properties of aerogels based on PPPO	77
3.5. Concluding remarks	84

Chapter 4
Monolithic Aerogels Based on Polyethylene

4.1. Introduction	87
4.2. Polyethylene gels	89
4.3. Preparation and structural characterization of polyethylene aerogels	90
4.4. Concluding remarks	95

References	96
------------	----

**Part II : Nanocomposites Physically Crosslinked Polymeric
Aerogels**

Chapter 1
Nanocomposites Physically Crosslinked Polymeric Aerogels

1.1. Introduction :the concept of Nanocomposites	104
1.2.1 The Nanofillers	107
1.2.2. Reduced Graphene Oxide	110

Chapter 2

Clay exfoliation and polymer/clay aerogels by supercritical carbon dioxide

2.1. Introduction	116
2.2. OMMT exfoliation by scCO ₂	118
2.3. Monolithic nanoporous crystalline s-PS aerogels with large OMMT content	121
2.5 Concluding remarks	134

Chapter 3

Reduced Graphene oxide/Syndiotactic Polystyrene Aerogels

3.1. Introduction	137
3.2. Monolithic nanoporous crystalline aerogels with large GO content	139
3.3. Concluding remarks	

References	156
------------	-----

Part III Experimental Section

Chapter 1

Materials and Samples preparation

1.1. Syndiotactic Polystyrene	164
1.2. Poly(2,6-dimethyl-1,4-phenylene)oxide	164
1.3. Poly(2,6-diphenyl-1,4-phenylene)oxide	164
1.4. Ultra High Molecular weight polyethylene	164
1.5. High surface area graphite and GO preparation	165
1.6. Preparation of physically crosslinked polymeric aerogels	166

1.7. Preparation of s-PS/Clay Gels and Aerogels	167
1.8. Preparation of s-PS/rGO Gels and Aerogels	
Chapter 2	
Techniques	
2.1. Wide angle X-ray diffraction (WAXD)	169
2.2. Fourier Transform Infrared (FTIR)	170
2.3. Raman spectroscopy	171
2.4. Scanning electron microscopy (SEM)	171
2.5. Porosimetry	172
2.6. Thermogravimetric measurements (TGA)	172
2.7. Colorimetric measurements	173
2.8. Dynamic-mechanical analysis	173
References	174
Ringraziamenti	175

List of Abbreviations

BET : Braunauer - Emmett-Teller method

CCl₄: carbon tetrachloride

CO₂ : carbon dioxide

CPN : clay polymer nanocomposites

CVD: chemical vapor deposition

DCB : dichlorobenzene

DCE: 1, 2. dichloethane

GO : graphene oxide

i-P4MP1: isotactic poly(4-methyl-pentene-1)

i-PS : isotactic polystyrene

MCP :mixture critical point

OMMT : organically modified montmorillonite

PE : polyethylene

PPO: Poly(2, 6-dimethyl-1, 4-phenylene)oxide

PPPO : Poly(2, 6-diphenyl-1, 4-phenylene)oxide

PVDF : Polyvinylidene fluoride

P(VDF-HFP) :poly(vinylidene fluoride-cohexafluoropropylene)

scCO₂ : supercritical carbon dioxide

SEM : Scanning electron microscopy

s-PS: syndiotactic polystyrene

TEOS: Tetraethyl orthosilicate

UHMWPE : ultra high molecular weight polyethylene

VOC: volatile organic compound

Introduction

Aerogels are a unique class of materials characterized by a highly porous network of interconnected nanostructures and that exhibit a porosity (non-solid volume) of no less than 50%;^{1a} this type of material results attractive for many applications such as thermal and acoustic insulation, capacitors, or catalysis.²

Aerogels are derived from a gel in which the liquid component of the gel has been replaced with air, by extracting through supercritical drying (sol-gel process).

This allows the liquid to be slowly drawn off without causing the solid matrix in the gel to collapse from capillary action, as would happen with conventional evaporation. For most applications in fact, it is particularly relevant the possibility to obtain wet gel monoliths that can be dried to aerogel monoliths without crushing.

The first aerogels were produced by Kistler from silica gels (Figure 1).¹



Figure 1. Silica aerogel

For half a century this material went relatively unnoticed, due to the notorious difficulties and safety issues relating to its preparation.

Indeed, in the early years, the preparation of aerogels involving the achievement of supercritical conditions for the ethyl alcohol.^{1a}

A fundamental improvement came in the early 1990's when liquid carbon dioxide replaced the ethyl alcohol involved in the gel before the sample was taken through the supercritical process. This allowed scientists to bypass the dangerous pressures and temperatures needed to send the pure ethanol past its supercritical point.

As an example of preparation of the sol of silica particles, silica precursors (silicon alkoxide) are mixed with a hydrolysis agent and a solvent; by condensation reactions a network based on Si-O-Si bridges, is achieved (Figure 2).^{1a}

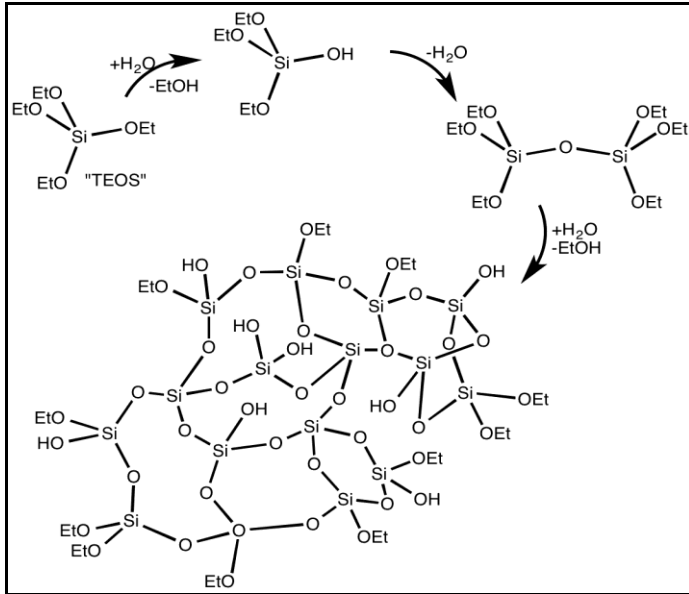


Figure 2. Schematic preparation of Silica Aerogels

Among all known aerogels, silica aerogels are the most popular one.

They possess a wide variety of extraordinary properties; many of them are registered in the Guinness Book of Records for Properties.^{3a} High porosity (~ 99%), high specific surface area (~ 1000 m²/g), low density (~ 0.002 g/cm³), low thermal conductivity (~ 0.01 W/m·K), high optical transition (~ 99%), low refractive index (~ 1.05), low dielectric constant (~ 1.0 -2.0) and low sound velocity (100 m/s) are some of their exceptional properties that make them promising candidates for

many advanced applications. ^{3a-c}Kistler's later work involved aerogels based on alumina, chromia and tin oxide. ¹

Although most aerogels are inorganic, ^{2a-h} many organic and polymeric aerogels, ^{2i, j} have also been developed.

The relevance of polymeric aerogels is mainly related to low cost, robustness, durability and easy processing typical of polymers. Polymeric aerogels are generally characterized, as the other aerogels, by *chemically bonded three-dimensional* networks.

In fact, highly cross-linked aerogels are obtained by systems of resorcinol-formaldehyde, ^{4a-c} melamine-formaldehyde, ^{4d-f} phenolic-furfural, ^{4c, 4g-i} polyurethane-dichloromethane, ^{5a} cresol formaldehyde, ^{5b} phloroglucinol-formaldehyde, ^{5c} epoxy-amine, ^{5d} 1, 3-dimethoxybenzene or 1, 3, 5-trimethoxybenzene formaldehyde, ^{5c, e, f} hydroxylated benzene derivatives-alkyl or aryl aldehydes, ^{5g-i} and aromatic dianhydrides-aromatic diamines or a combined aromatic and aliphatic diamines. ^{5l, m}

A schematic example of the reaction for the formation of chemically crosslinked polymeric gels is shown in Figure 3, which describes the resorcinol-formaldehyde reaction and explains the formation of a crosslinked polymer network. ^{4c} Dry resorcinol formaldehyde aerogels were lastly obtained by the supercritical drying gels with CO₂.

Pekala *et al.* reported the synthesis of resorcinol-formaldehyde

aerogels in details.^{4a, b}

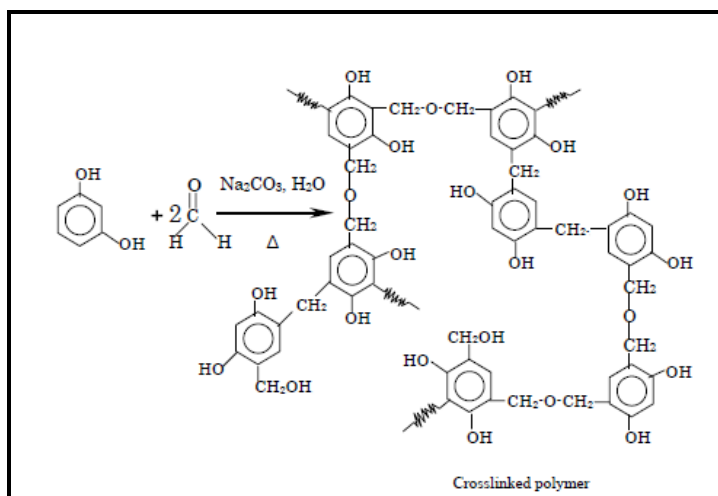


Figure 3. Schematic preparation of Chemically Crosslinked Polymeric Aerogels

In more recent years, polymeric aerogels based on thermoplastic **uncrosslinked** polymers, where the knots of the three-dimensional networks are **physical**, not formed by covalent chemical bonds but by small crystallites, have also been obtained.⁶⁻⁸ These *physically cross-linked aerogels* are generally prepared by supercritical CO₂ extraction of thermoreversible organogels.⁷⁻⁹ In particular hot polymer solution are cooled to lower temperature where gelation occurs.

In this respect is necessary to say that besides aerogels another class of porous materials, is constituted by *semicrystalline*

thermoplastic polymers whose crystalline phase is *nanoporous*, i. e. presents a density lower than the corresponding amorphous phase.^{9,10}

These nanoporous crystalline polymers are able to absorb low molecular mass molecules also when present in traces and have been proposed for molecular separation,¹¹ sensor¹² and catalysis¹³ applications.

The preparation of aerogels with thermoplastic materials exhibiting nanoporous crystalline forms has allowed achieving a special class of *physically cross-linked aerogels*, where the crystallites that constitute the physical knots of the aerogel exhibit a nanoporous-crystalline form.⁷ These nanoporous-crystalline aerogels beside disordered amorphous meso and macro pores (typical of all aerogels) present also all identical nanopores of the crystalline phases.

In particular, monolithic aerogels based on the nanoporous-crystalline δ^{8a-c} and ϵ^{8f} forms of syndiotactic polystyrene (s-PS), which include beside amorphous pores their typical crystalline nanopores (cavities and channels, respectively), have been obtained. The simplest preparation procedure is based on supercritical CO₂ (scCO₂) extraction of an organic solvent being both the liquid of the physical gel and the guest of δ and ϵ

co-crystalline phases.^{8,12}

The fast kinetics and high sorption capacity of VOCs by s-PS nanoporous-crystalline aerogels as well as their good handling characteristics make these new materials particularly suitable as a sorption medium to remove traces of pollutants from water and air.⁸

Very recently, the presence of nanoporous crystalline modifications has been disclosed for another commercial thermoplastic polymer: poly (2, 6-dimethyl-1, 4-phenylene) oxide (PPO).^{10a}

Crystalline modifications, exhibiting largely different X-ray diffraction patterns, have been obtained for this polymer, by gel desiccation procedures as well as by solvent induced crystallization of amorphous films.

Both amorphous and semicrystalline samples of this commercial thermoplastic polymer exhibit a high uptake of large guest molecules (like, e. g., benzene or carbon tetrachloride), both from vapor phases and from diluted aqueous solutions. The semicrystalline PPO samples present guest solubility much higher than fully amorphous PPO samples.

However, the solvent extraction by supercritical CO₂ from PPO gels, with many different solvents, leads to powders rather than to aerogels.^{10a}

Considering the extraordinary properties of aerogels, it is

extremely interesting to make a preparation method of monolithic aerogels, including PPO nanoporous-crystalline phases.

Another interesting commercial polymer, considered in this study for the preparation of physically crosslinked polymeric aerogels, is the poly (2, 6-diphenyl-1, 4-phenylene oxide) (shortly indicated as PPPO).

This polymer is an excellent porous adsorbent for the trapping of many types of volatiles such as halogenated and aromatic compounds, ^{14a-c} normal alkanes, ^{14a, d, e} cycloalkanes, ^{14a} ketones, ^{14a, d-e} alcohols, ^{14a, d-e} and volatile fatty acids ^{14c} mainly from air^{12a, d-e} but also from water. ⁶

Thus, as for most molecular sorption studies ¹⁴ PPPO is used as a semicrystalline powder, is crucial to establish if the occurrence of a nanoporous crystalline phase could be at the origin of the high sorption properties of PPPO and explore the possibility to obtain PPPO aerogels, in attempt to improve the already high sorption of this polymer.

Because of the above and of the emerging interest for these extraordinary materials, the first part of this study will focus on physically crosslinked polymeric aerogels, particularly on aerogels based on PPO and on PPPO, not described in literature previously. Furthermore in the first part is described

the preparation of polyethylene aerogels, also achieved for the first time.

The second part will focus on nanocomposites aerogels. In particular, will be examined syndiotactic polystyrene composites aerogels with:

- Graphene oxide
- Organically modified montmorillonite (OMMT).

Each chapter is closed with a summary that highlight the main achievements of the study. A graphical summary of the thesis structure is shown in Figure 4.

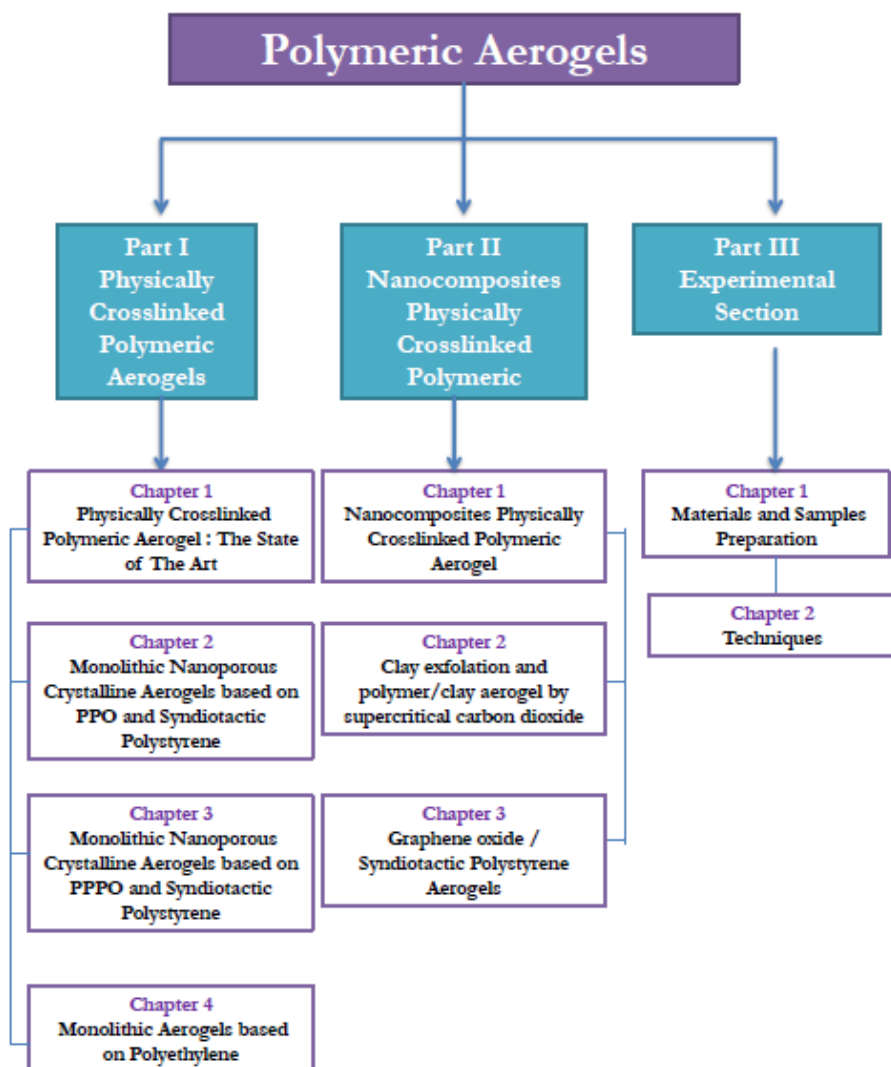


Figure 4. Graphical presentation of the thesis structure.

References

- [1] a) S. S. Kistler, *Nature* **1931**, 127, 741; b) S. S. Kistler, *J. Phys. Chem.* **1932**, 36, 52. b) H. Tamon, et al. *Journal of Colloid and Interface Science*, **1998**, 197(2), 353-359.
- [2] a) Schaefer, D. W. ; Keefer, K. D *Phys. Rev. Lett.* **1986**, 56, 2199. b) Pajonk, G. M. *Appl. Catal.* **1991**, 72, 217.
- c) Mayer, S. T. ; Pekala, R. W. ; Kaschmitter J. L *J. Electrochem. Soc.* **1993**, 140, 446. d) Ward D. A. ; Ko E. I. *J. Catal.* **1994**, **150**, 18. e) Anderson, M. L. ; Stroud, R. M. ; Rolison, D. R. *Nano Letters* **2002**, 2, 235. f) Pierre, A. C. ; Pajonk, G. M. *Chem. Rev.* **2002**, 102, 4243. g) Nielsen, T. K. ; Manickam, K. ; Hirscher, M. ; Besenbacher, F. Jensen T. R. *ACS Nano* **2009**, 3, 3521. h) Wei, T. Y. ; Chen, C. H. ; Chang, K. H. ; Lu, S. Y. ; Hu, C. C. *Chem. Mater.* **2009**, 21, 3228. i) Pekala, R. W. *J. Mater. Sci.* **1989**, 24, 3221. j) Pekala, R. W. ; Alviso, C. T. ; Kong, F. M. ; Hulsey, S. S. *J. Non-Cryst. Solids* **1992**, 145, 90.
- [3] a) Fricke, J., & Emmerling, A. . *Journal of Sol-Gel Science and Technology*, **1999**, 13(1-3), 299-303. b) Fricke, J., & Reichenauer, G. Paper presented at the Materials Research Society Symposia Proceedings, **1986** c) Gurav, J. L., et al. *Journal of Nanomaterials*, **2010**. d) Hrubesh, L. W. *Journal of Non-Crystalline Solids*, **1998**, 225 1), 335-342 (e) Soleimani Dorcheh, A., & Abbasi, M. H. *Journal of Materials Processing Technology*, **2008**, 199(1), 10-26.
- [4](a) Pekala, R. W. : US4873218 **1989** (b) Pekala, R. W. :

US4997804 **1991** (c)Pekala RW. *J Mater Sci* **1989**; 24, 3221-3227.
(d) Pekala, R. W. : US5081163 **1992**, (e)Pekala, R. W. :
US5086085 **1992**, (f)Pekala, R. W. : US5476878 **1995** (g) Pekala,
R. W. : US5556892 **1996** (h) Pekala, R. W. : US5744510 **1998**. (i)
Pekala RW, Alviso CT, Lu X, Gross J, Fricke J. *J. Non-Cryst
Solids*, **1995**; 188, 34-40.

[5] a)Biesmans G, Martens A, Woignier T, Phalippou J. ; *J. Non-
Cryst Solids* **1998**; 225 64-68. b)Li W., Guo S. *Carbon* **2000**, 38:
1520-1523. c) Baumann, T. F., Satcher, Jr., Joe, H., Gash, A. E. :
US20050027027 (**2005**) d)Raman VI, Palmese GR. *Colloids Surf
A Physicochem Eng Asp* **2004**; 241, 119-125. Rhine, W., Wang, J.
Begag, R. : US20040132845 **2004**. e) Baumann, T. F., Satcher,
Jr., Joe, H., Gash, A. E. : US20046806299 **2004**. f) Baumann, T.
F., Satcher, Jr., Joe, H., Gash, A. E. : US20077291653 (**2007**). g)
Chenee, J. -P. P., Liege, R. P., Liege, N. J. :
US20040241237(**2004**). h)Satcher, J. H., Baumann, T. F. :
US20077285575 (**2007**). i) Dietz, S., Nguyen, V. T. :
US20077167354 (**2007**). l) Rhine, W., Wang, J., Begag, R. :
US20050131163 (**2005**). m) Rhine, W., Wang, J., Begag, R. :
US20067074880 (**2006**).

[6]a) Jin, H. ; Nishiyama, Y. ; Wada, M. ; Kuga, S. *Colloids and
Surfaces A: Physicochem. Eng. Aspects* **2004**, 240, 63 b) Gavillon, R. ;
Budtova, T. *Biomacromolecules* **2008**, 9, 269 c) Miao, Z. J. ; Ding,
K. L. ; Wu, T. B. ; Liu Z. M. ; Han B. X. ; An, G. M. ; Miao S.

D. ; Yang G. Y. *Microporous and Mesoporous Materials* **2008** 111, 104 d) Robitzer, M. ; David, L; Rochas, C. ; Di Renzo, F. ; Quignard, F. *Langmuir* **2008**, 24, 12547 e) Quignard, F. ; Valentin, R. ; Di Renzo, F. *New J. Chem.* **2008**, 32, 1300.

[7] a) Beaucage, G. ; Aubert, J. H. ; Lacasse, R. R. ; Schaefer, D. W. ; Rieker, T. P. ; Erlich, P. ; Stein, R. S. ; Kulkarni, S. ; Whaley, P. D. *Journal of Polymer Science: Part B Polymer Physics* **1996**, 34, 3063 b) Dasgupta, D; Nandi, A. K. *Macromolecules* **2005**, 36, 6504, c) Dasgupta, D; Nandi, A. K. *Macromolecules* **2007**, 40, 2008 d) Cardea, S. ; Gugliuzza, A. ; Sessa, M. ; Aceto, M. C. ; Drioli, E. ; Reverchon, E. *ACS Appl. Mater. Interfaces* **2009**, 1, 171. e) Daniel, C. ; Vitillo, J. G. ; Fasano, G. ; Guerra, G. *ACS Appl. Mater. Interfaces* **2011**, 3, 969.

[8] (a) Daniel, C. ; Alfano, D. ; Venditto, V. ; Cardea, S. ; Reverchon, E. ; Larobina, D. ; Mensitieri, G. ; Guerra, G. *Adv. Mater.* **2005**, 17, 1515. (b) Guerra, G. ; Mensitieri, G. ; Venditto, V. ; Reverchon, E. ; Daniel, C. *PCT Int. Appl.* **2005**, WO 2005012402. (c) Malik, S. ; Rochas, C. ; Guenet, J. -M. *Macromolecules* **2005**, 38, 4888. (d) Malik, S. ; Roizard, D. ; Guenet, J. -M. *Macromolecules* 2006, 39, 5957. (e) Daniel, C. ; Sannino, D. ; Guerra, G. *Chem. Mater.* **2008**, 20, 577. (f) Daniel, C. ; Giudice, S. ; Guerra, G. *Chem. Mater.* **2009**, 21, 1028.

[9] a) C. De Rosa, G. Guerra, V. Petraccone, B. Pirozzi, *Macromolecules* **1997**, 30, 4147; b) G. Guerra, G. Milano, V.

Venditto, P. Musto, C. De Rosa, L. Cavallo, *Chem. Mater.* **2000**, 12, 363c) G. Milano, V. Venditto, G. Guerra, L. Cavallo, P. Ciambelli, D. Sannino, *Chem. Mater.* **2001**, 13, 1506; d) E. B. Gowd, N. Shibayama, K. Tashiro, *Macromolecules* **2006**, 39, 8412; e) P. Rizzo, C. Daniel, A. De Girolamo Del Mauro, G. Guerra, *Chem. Mater.* **2007**, 19, 3864; f) V. Petraccone, O. Ruiz de Ballesteros, O. Tarallo, P. Rizzo, G. Guerra, *Chem. Mater.* **2008**, 20, 3663; g) A. R. Alburnia, P. Rizzo, G. Guerra, *Chem. Mater.* **2009**, 21, 3370; h) G. Guerra, C. Daniel, P. Rizzo, O. Tarallo, *J. Polym. Sci. Polym. Phys. Ed.* **2012**, 50, 305.

[10] a) C. Daniel, Longo, S., J. G. Vitillo, G. Fasano, G. Guerra, *Chem. Mater.* **2011**, 23, 3195; b) O. Tarallo, V. Petraccone, C. Daniel, G. Fasano, P. Rizzo, G. Guerra, *J. Mater. Chem.* **2012**, 22, 11672; c) M. Galizia, C. Daniel, G. Fasano, G. Guerra, G. Mensitieri, *Macromolecules* **2012**, 45, 3604; d) C. Daniel, D. Zhovner, G. Guerra, *Macromolecules* **2013**, 46, 449; e) P. Rizzo, G. Ianniello, S. Longo, G. Guerra, *Macromolecules* **2013**, 46, 3995.

[11] a) C. Manfredi, M. A. Del Nobile, G. Mensitieri, G. Guerra, M. Rapacciuolo, *J. Polym. Sci. Polym. Phys. Ed.* **1997**, 35, 133; b) P. Musto, G. Mensitieri, S. Cotugno, G. Guerra, V. Venditto, *Macromolecules* **2002**, 35, 2296; c) K. P. O. Mahesh, M. Sivakumar, Y. Yamamoto, Y. Tsujita, H. Yoshimizu, S. Okamoto, *J. Membrane Sci.* **2005**, 262, 11; d) V. Venditto, A. De Girolamo Del Mauro, G. Mensitieri, G. Milano, P. Musto, P.

Rizzo, G. Guerra, *Chem. Mater.* **2006**, *18*, 2205; e) G. Mensitieri, D. Larobina, G. Guerra, V. Venditto, M. Fermeglia, S. Pricl, *J. Polym. Sci. Part B Polym. Phys.* **2008**, *46*, 8.

[12] a) G. Mensitieri, V. Venditto, G. Guerra, *Sens. Actuators B* **2003**, *92*, 255; b) M. Giordano, M. Russo, A. Cusano, G.

Mensitieri, G. Guerra, *Sens. Actuators B* **2005**, *109*, 177; c) A. Cusano, A. Iadicicco, P. Pilla, L. Contessa, S. Campopiano,

A. Cutolo, M. Giordano, G. Guerra, *J. Lightwave Technol.* **2006**,

24, 1776; d) A. Buono, P. Rizzo, I. Immediata, G. Guerra, *J.*

Am. Chem. Soc. **2007**, *129*, 10992; e) P. Pilla, A. Cusano, A.

Cutolo, M. Giordano, G. Mensitieri, P. Rizzo, L. Sanguigno, V.

Venditto, G. Guerra, *Sensors* **2009**, *9*, 9816; f) M. Erdogan, Z.

Ozbek, R. Capan, Y. Yagci, *J. Appl. Polym. Sci.* **2012**, *123*, 2414.

[13] A. Buonerba, C. Cuomo, S. O. Sanchez, P. Canton, A.

Grassi, *Chemistry-A Eur. J.* **2012**, *18*, 709.

[14] (a) Maier, I. ; Fieber, M. J. *High Resolut. Chromatogr.* 1988,

11, 566–576. (b) Jens Laaks, J. ; Jochmann, M. A. ; Schilling, B. ;

Schmidt, T. C. *Anal. Chem.* 2010, *82*, 7641–7648. (c) Kim, Y. -

H. ; Kim, K. -H. *Anal. Chem.* 2012, *84*, 8284–8293. (d) Alfeeli,

B. ; Taylor, L. T. ; Agah, M. *Microchem. J.* 2010, *95*, 259–267.

(e) Alfeeli, B. ; Jain, V. ; Johnson, R. K. ; Beyer, F. L. ; Heflin, J.

R. ; Agah, M. *Microchem. J.* 2011, *98*, 240–245. (f) Oen, A. M.

P. ; Breedveld, G. D. ; Kalaitzidis, S. ; Christanis, K. ;

Cornelissen, G. *Environ. Toxicol. Chem.* 2006, *25*, 1258–1267.

(g) Barrero-Moreno, J. M. ; Tirendi, S. ; Reniero, F. ; Giordano, G. ; Kotzias, D. *Rapid Commun. Mass Spectrom.* 2008, 22, 471–476. (h) Leva, P. ; Katsoyiannis, A. ; Barrero-Morero, J. ; Kephelopoulos, S. ; Kotzias, D. *J. Environ. Sci. Health, Part B* 2009, 44, 51–57.

Part I : Physically Crosslinked Polymeric Aerogels

Chapter 1

Physically Crosslinked polymeric aerogel:

State of the Art

1.1 Introduction

Gels consist of three-dimensional network structures swollen by a liquid. As mentioned above, for chemical gels, the cross-links that give rise to this network are covalent bonds,¹ whereas, for physical gels the connectedness between polymer chains is achieved by intermolecular physical bonding forming junction zones that can be created and removed by cooling and heating, respectively.²

In particular, for most physical gels,^{3, 4} the junction zones are crystalline regions, organized as fibrils or uncorrelated lamellar platelets, which form monolithic structures because of entanglement.

As introduced, the most efficient method to obtain monolithic aerogels (in the early papers also called nano-structured low density polymer foams)^{3a} from monolithic physical polymer gels is the solvent extraction by supercritical carbon dioxide(scCO₂).

5, 3a, e-j, 4b-h

In particular are well known in literature, monolithic aerogels

based on uncrosslinked polymers obtained by scCO₂ extraction of thermoreversible organogels, based on nitrocellulose,^{5, 3j} isotactic polystyrene (i-PS),^{3c} poly(acrylonitrile),^{3c} polyvinylidene fluoride (PVDF),^{3d, i} poly(vinylidene fluoride-cohexafluoropropylene) P(VDF-HFP),^{3g} polylactic acid,^{3e, f} isotactic poly(4-methyl-pentene-1) (i-P4MP1),^{3h} and hydrogels, based on gelatin,⁵ alginate,^{4e, d, h} chitosan^{4f, g} starch,^{4c} and cellulose,^{4a, b} or by preparing gels of semi dilute polymer (polyethylene^{3a, b} and isotactic polypropylene^{3b}) solutions in a supercritical solvent.

As for aerogels from organogels it has been recognized, since the pioneering studies of Beaucage et al.,^{3c} that their stability is associated with their crystalline phase morphology. In fact, polymer crystallization in solutions leading to spherulitic or other globular morphologies produce unstable gels,^{19h, 2b-e} which, if formed, are crushed as a consequence of drying.^{19h}

On the other hand, stable physical polymeric aerogels are always semicrystalline and their crystalline morphology can be described in terms of uncorrelated lamellar platelets or, more often, of fibrils. This is observed, for instance, for the monolithic aerogels based on i-P4MP1, PVDF, P(VDF-HFP) and s-PS and shown by photographs and SEM images in Figure 2 for a 0.2 gg⁻¹ i-P4MP1 gel in 1, 3, 5-trimethylbenzene.^{3h}

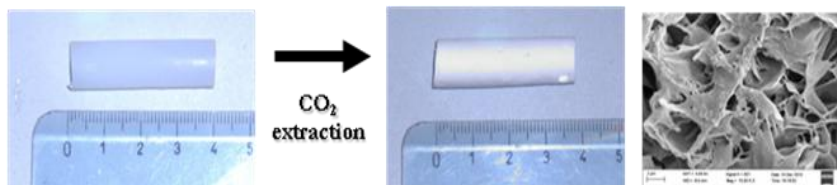


Figure 1.1. Photographs of cylindrical monolithic organogels based on *i*-P4MP1, of the corresponding aerogels obtained by supercritical drying and SEM images of the aerogels.

furthermore, important volume shrinkages have been observed with aerogels obtained from gels which undergo a crystalline phase transition during the extraction process. For example, *i*-P4MP1 is characterized by a complex polymorphic behavior that includes four crystalline phases as well as several cocrystalline phases with low-molecular-mass guest molecules; nevertheless only for a particular crystalline phase gels (Form I, for instance obtained with 1, 3, 5-trimethylbenzene), which maintain this crystalline phase also in their aerogels, both the dimension and shape of the native gel are not altered by the solvent extraction procedure. It is reasonable to expect that, also for other polymers, crystalline phase transitions could be detrimental to the dimensional stability of the physical aerogels.

1.2 How to prepare physically crosslinked polymeric aerogels: Sol - Gel Technology

Generally sol-gel technology describes those processes where a precursor (or a precursors mixture) forming a colloidal solution, which end up with a solid network.⁸ Sol-gel technology has proved to be a versatile and valuable method for production and processing of materials. Metallic, organic, inorganic and hybrid materials can provide valid precursors that can be used for this process. The end products can range from highly advanced materials to materials of general daily use. The importance of the sol-gel process arises from two main causes:

1) production of highly pure materials; 2) creation of novel valuable materials⁹

Figure 1.2 shows a general sol-gel technology sketch of the main most commonly used steps in the sol-gel processes.

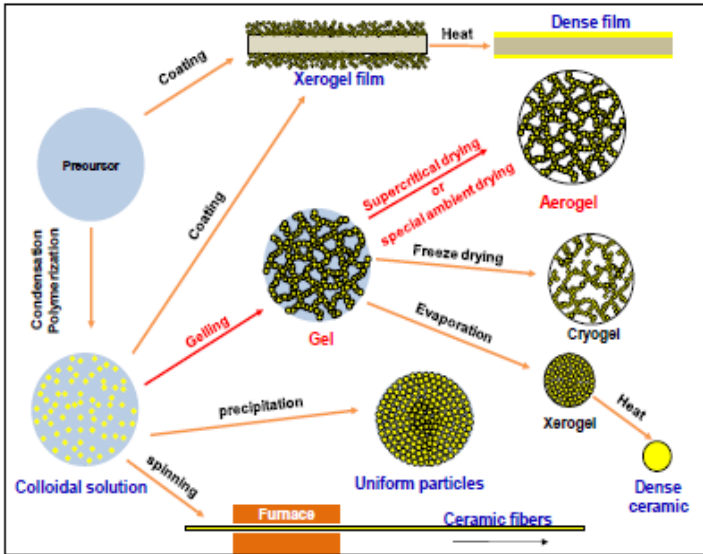


Figure 1.2. General steps involved in the processing of materials using the sol-gel technology and some possible final products structure.

For a broad number of applications, the gel porous network is the key feature for their use. Hence, as aforementioned, it is important to remove the solvent from the network in a way that preserved the internal textural properties of the gel. During solvent evaporation from the gel network the curvature of vapor-liquid interface changes. The curvature of the meniscus decreases with time (Figure 1.3).

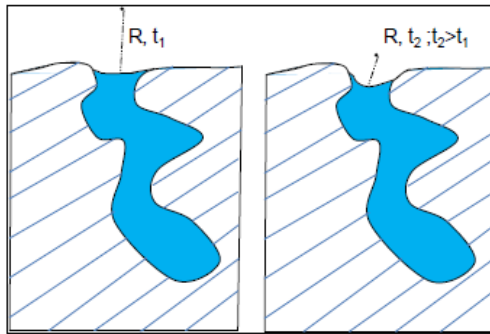


Figure 1.3. Change in liquid-vapor meniscus radius as a function of drying time at the pore surface.

As a result capillary forces take place. The pressure difference between the liquid and vapor phase can be given by Laplace's equation:

$$\text{Eq. 1} \quad \Delta P = -\frac{\sigma \cos \theta}{R}$$

Where σ is the liquid/vapor interfacial surface tension, R is the meniscus radius and θ is the contact angle at which the liquid/vapor interface meets the solid surface. Accordingly the gel structure is subject to compression stresses. Because of the high capillary pressure induced upon solvent evaporation and the fragility of the gel structure, cracks and shrinkages are obtained. Hence, a reduction of the textural properties of the dry gel will be observed.

However, it is possible to reduce the capillary pressure induced during drying by using a solvent which has a low surface tension

value. By means of solvent exchange it is possible to reduce the capillary forces using solvent with lower surface tension.

In particular, as mentioned above, monolithic aerogels based on uncrosslinked polymers have been obtained by scCO_2 . Mechanism of scCO_2 gel drying involves first the formation of a pressurized expanded liquid between scCO_2 and the organic solvent and, secondly its progressive transformation in a supercritical mixture, as long as the concentration of CO_2 in the mixture increases. The supercritical mixture is characterized by a near zero surface tension; this characteristic avoids gel nanostructure collapse. In the subsequent part of the process, the supercritical mixture is progressively removed by continuous flushing of scCO_2 in the pressurized vessel. Therefore, for a successful processing of polymeric gels, the liquid solvent used to produce the gel, should be soluble in scCO_2 at the processing conditions and solvent elimination has to be performed at temperatures and pressures above their mixture critical point (MCP); i. e., at conditions of complete miscibility between solvent and scCO_2 . From a technological point of view, these requisites are relatively simple to be obtained, since the organic solvents ordinarily used (for example, dimethyl sulfoxide, acetone, ethanol, halogenated and aromatic solvents) show a large affinity with scCO_2 and the MCP is located at pressures easily obtainable in a pressurized vessel.

1.3 Polymeric Aerogels with Nanoporous-Crystalline Phases as Physical Cross-Links

It is well known that for a large variety of inorganic, metalorganic as well as organic compounds, the removal of guest molecules from cocrystals can generate nanoporous crystalline phases.¹⁰

As for polymer cocrystalline phases, the removal of the low-molecular-mass guest molecules generates host chain rearrangements, generally leading to crystalline forms that (as usual for polymers) exhibit a density higher than for the corresponding amorphous phase.^{3h, 11} However, in few cases (to our knowledge, up to now only for s-PS¹² and PPO¹³), by using suitable guest removal conditions and preferably extraction by scCO₂,¹⁴ nanoporous crystalline forms, exhibiting a density definitely lower than for the corresponding amorphous phases, can be obtained.

1.4 Aerogels with the Nanoporous δ and ϵ Forms of s-PS

s-PS has been extensively studied and characterized in recent years. This polymer has a complex and widely studied polymorphism, it has 5 crystal structures, α , β , γ , δ , ϵ , and a wide variety of cocrystal structures with different low molecular

weight molecules.¹⁵

The removal of the low-molecular-mass guest molecules from s-PS co-crystals can generate two different nanoporous-crystalline phases.

The first polymeric nanoporous-crystalline form, the δ form of s-PS, ^{12a-d} was patented in 1994. Chains in the helical s(2/1)2 conformation are packed in a monoclinic unit cell with axes $a = 1.74$ nm, $b = 1.185$ nm, $c = 0.77$ nm, and $\gamma = 117^\circ$ whose density is of 0.98 g cm⁻³, i. e., definitely smaller than that one of the amorphous phase (1.05 g cm⁻³).^{12a} The structure presents isolated cavities having a volume close to 0.125 nm³, confined by layers of closely packed alternated enantiomorphous helices, parallel to the ac plane (Figure 1.4 A and A').^{12a, c}

The crystalline cavities are in a number equal to the number of chains and generally can contain one or two guest molecules.^{12a,}

^c It is worth adding that the cavity is rather flat, i. e., presents its maximum dimension (≈ 0.8 nm) nearly perpendicular to the polymer chain axis, while its minimum dimension (≈ 0.3 nm) is essentially along the c axis (Figure 1.4 A and A').^{12c}

The nanoporous ϵ phase of s-PS, ^{12e-g} discovered in 2007,^{12e} presents an orthorhombic unit cell with axes $a = 1.61$ nm, $b = 2.18$ nm, and $c = 0.79$ nm (Figure 1.4 B, B').^{12f} Four chains of s-PS in the s(2/1)2 helical conformation are included in the unit cell, whose density is 0.98 g cm⁻³, i. e., very close to the density of the δ phase.

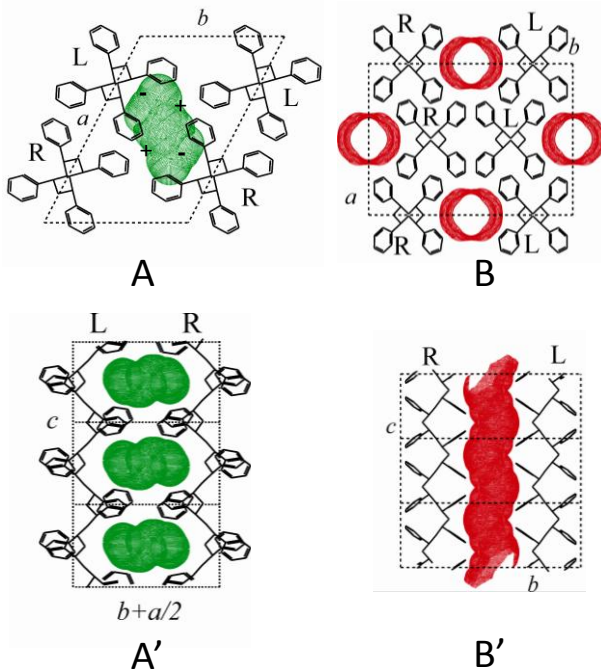


Figure 1.4. A, B) Top and A', B') lateral views of the crystalline structures of the two nanoporous crystalline forms of s-PS. For the A, A') δ and B, B') ϵ forms, the porosity is distributed as cavities and channels, respectively. In (A), the quadrupolar electrostatic field of the cavity is indicated by + and - signs. Reproduced with permission.^{12b} Copyright 2012, John Wiley & Sons Ltd.

The crystal structure is characterized by channel-shaped cavities crossing the unit cells along the c axis and delimited, along b axis, by two enantiomorphous helical chains (Figure 1.4 B, B'). In these channels, guest molecules are generally hosted with their longer molecular axis roughly parallel to the polymer chain axis.

As a consequence of guest sorption in both s-PS nanoporous-crystalline phases, many different cocrystalline forms can be obtained, which have been classified as δ -clathrates,¹⁵ δ -intercalates,¹⁶ or ϵ clathrates.¹⁷

Clathrates present isolated guest molecules in crystalline cavities and channels of δ and ϵ forms, respectively, while intercalates present layers of guest molecules alternated with closely packed layers of alternated enantiomorphous helices that characterize the δ form (Figure 1.4 A).

X-ray diffraction, neutron diffraction, and differential scanning calorimetry characterizations have allowed clarifying that the junction zones of s-PS gels, when prepared by solvents being suitable guests of s-PS cocrystalline forms,¹⁸ are constituted by cocrystalline phases. In particular, the studied gels present δ -clathrate^{18a, d, e, g} or δ -intercalate^{18a, b, c, f, g} phases.

ScCO₂ drying of these gels not only removes solvent molecules leading to stable monolithic aerogels but also removes the solvent molecules being guest of the cocrystalline phase, thus leading to nanoporous-crystalline δ phases (Figure 1.5A), exhibiting a fibrillar morphology (Figure 1.5 A', fibrils of 50–100 nm).^{3b, 5, 19}

High-temperature scCO₂ extraction procedures^{14f} on highly crystalline gels (like those exhibiting the s-PS cocrystalline phase with DCE),^{16c} also allow obtaining high-porosity aerogels exhibiting the γ -form²⁰ (shown in Figure 1.5 B, B') and β -

form ²⁴(not shown here), i. e., aerogels exhibiting dense rather than nanoporous-crystalline s-PS phases as junction zones. ^{19f} These aerogels present a fibrillar morphology with fibril diameters in the range 30–150 nm, similar to those observed for δ -form aerogels, and hence present the disordered porosity of the aerogels whereas do not present the three-dimensionally ordered crystalline nanopores. ^{19f}

Monolithic aerogels exhibiting the nanoporous-crystalline ϵ ^{12e-g} form of s-PS, with its typical crystalline channels, have also been obtained. ^{19f} These aerogels have not obtained by direct gel drying procedures, due to the lack of gels exhibiting ϵ - clathrates. ¹⁷ Robust monolithic ϵ -form aerogels (Figure 1.5 C, C') are instead obtained by treatments of γ -form aerogels (Figure 1.5 B and B ') with chloroform, followed by solvent extraction by scCO₂ at 40 ° C and 200 bar. ^{19f}

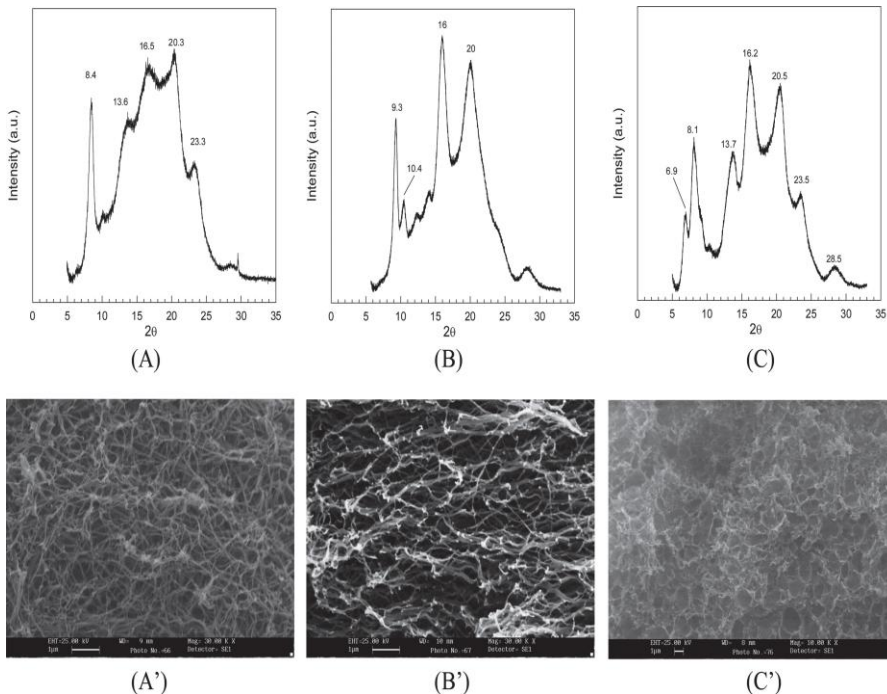


Figure 1.5. X-ray diffraction patterns (Cu-K α radiation) and SEM images of aerogels as obtained from a s-PS gel prepared in 1, 2-dichloroethane (DCE) at $C_{pol} = 0.05 \text{ g g}^{-1}$, after extraction by scCO_2 : A, A' at 40°C , 200 bar (δ -form); B, B' at 130°C , 200 bar (γ -form); C, C' at 130°C 200 bar, followed by room-temperature treatments with chloroform and a second solvent extraction by scCO_2 at 40°C (ϵ -form).

It is worth adding that the density and the total porosity of the physical aerogels can be easily controlled, in wide ranges, by simply changing the gel polymer concentration.

This is shown, for instance in Figure 1.5 A, for aerogels obtained from s-PS/toluene gels where the percentage of

porosity P was estimated from the mass/volume ratio of the aerogel using the relation shown in equation 2:

$$\text{Eq. 2} \quad P = 100 \left(1 - \frac{\rho_{app}}{\rho_{pol}} \right)$$

where ρ_{pol} is the density of the polymer matrix (e. g., equal to 1.02 g cm^{-3} , for δ -form s-PS samples with a crystallinity of nearly 40%) and ρ_{app} is the aerogel apparent density calculated from the mass/volume ratio of the monolithic aerogels.

The SEM images of Figure 1.6 B–D show that, while the aerogel porosity changes in a wide range, the morphology remains essentially unaltered, with fibrils maintaining diameters in the range 50–100 nm.

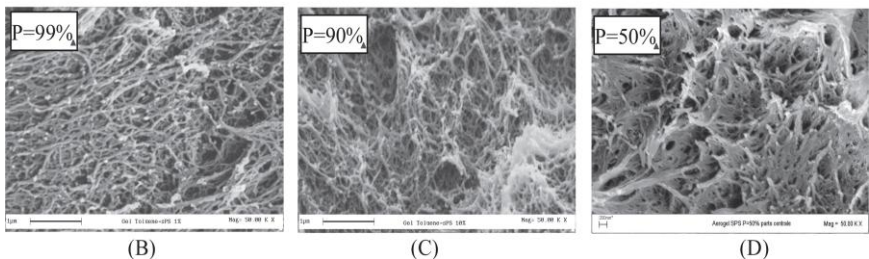
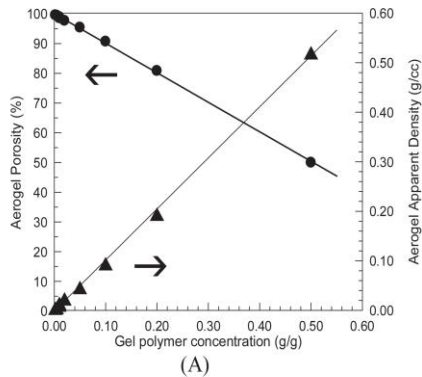


Figure 1. 6. A) Dependence of porosity (circles) and apparent density (triangles) of δ -form s-PS aerogels on the polymer concentration in toluene gels, as observed for scCO₂ extraction at 40 ° C, 200 bar; B–D) SEM images of the aerogels presenting a porosity of 99% B), 90% C), and 50% D).

As generally done for porous materials, the surface area of the obtained aerogels has been studied by BET experiments like those reported in Figure 1.7 and Table 1. From these and other analogous experiments, it is possible to conclude that N₂ sorption ability and surface area of s-PS samples are:

- i) higher for samples including the nanoporous crystalline phases (δ or ϵ) than for the corresponding samples exhibiting dense crystalline phases (α , β or γ);
- ii) highest for samples including the nanoporous-crystalline δ phase;

- iii) always higher for aerogels than for powders;
- iv) increasing with the aerogel porosity.

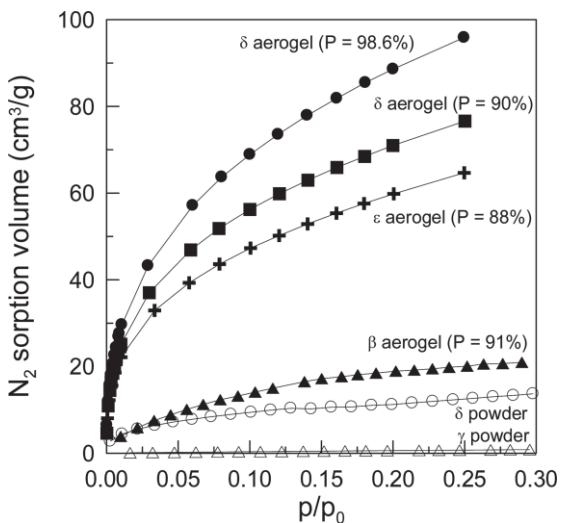


Figure 1.7. Volumetric N_2 adsorption isotherms recorded at 77 K for s-PS powders (empty symbols) and aerogels (filled symbols), presenting different crystalline phases. For the aerogels the porosity is indicated as P , close to each curve. Reproduced with permission. ³⁶Copyright 2010, American Chemical Society.

s-PS sample	N ₂ sorption at p/p° = 0.1 (cm ³ g ⁻¹)	BET (m ² g ⁻¹)
γ-powder	0.3	4
δ-powder	9	43
β-aerogel (P=91%)	14	70
ε-aerogel (P=88%)	47	230
δ-aerogel (P=90%)	56	290
δ-aerogel (P=98%)	69	348

Table 1.1. N₂ sorption at p/p° = 0.1, expressed as cm³ g⁻¹, and BET surface area, expressed as m² g⁻¹ for the s-PS powders and aerogels of Figure 6.

It is worth adding that aerogels based on other polymers, exhibiting dense crystalline phases, present surface areas similar to those observed for the β -form s-PS aerogels and much lower than those obtained for nanoporous-crystalline (δ and ε) s-PS aerogels. For instance, S_{BET} is lower than 90 and 70 m² g⁻¹ for all the prepared i-P4MP1^{3h} and PVDF³ⁱ aerogels, respectively.

Chapter 2

Monolithic nanoporous–crystalline aerogels based on Poly(2, 6-dimethyl-1, 4 phenylene)oxide and Syndiotactic Polystyrene

2. 1 Introduction

As discussed in the introduction, very recently the presence of nanoporous crystalline modifications has been disclosed for another commercial thermoplastic polymer: poly(2, 6-dimethyl-1, 4-phenylene)oxide (PPO).^{13a}

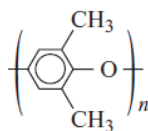


Figure 2. 1. Chemical structure of PPO repeating unit

However, extraction from PPO gels of the solvent, independently of its chemical nature and of the extraction procedure, leads to powders rather than to aerogels.^{13a}

In this chapter, the preparation of monolithic aerogels, including PPO nanoporous–crystalline phases, is reported.

The described preparation method is based on the formation in the gels (and in the derived aerogels) of fibrillar crystalline morphology as a consequence of blending PPO with s-PS. The

method, by using gels with suitable PPO/s-PS compositions, also allows the formation of monolithic aerogels that include, beside amorphous nanopores, nanoporous–crystalline phases of both PPO and s-PS.

2. 2 Preparation and structural characterization of PPO/s-PS aerogels

X-ray diffraction patterns of physical PPO gels with a polymer content in the range 30–40 wt%, with four different solvents, are shown in Figure 2. 2 A–D. All these patterns show, beside broad amorphous halos associated with the solvent and the polymer amorphous phase, well-defined crystalline peaks associated with the three-dimensional physical networks holding up the gel. In particular, the gels including decalin and α -pinene (Figure 2. 2 A and 2. 2 B, respectively) exhibit diffraction peaks of the corresponding co-crystalline phases with PPO.

In particular, the 101, 110, 102, 200, 201, 211, 220 and 221 reflections of the PPO/ α -pinene cocrystalline form, located at $2\Theta_{\text{Cu-K}\alpha} \sim 8. 9^\circ, 10. 5^\circ, 13. 1^\circ, 15. 0^\circ, 15. 8^\circ, 17. 5^\circ, 21.3^\circ$ and 21.8° ,^{22,23} are clearly apparent in Figure 2.2B.

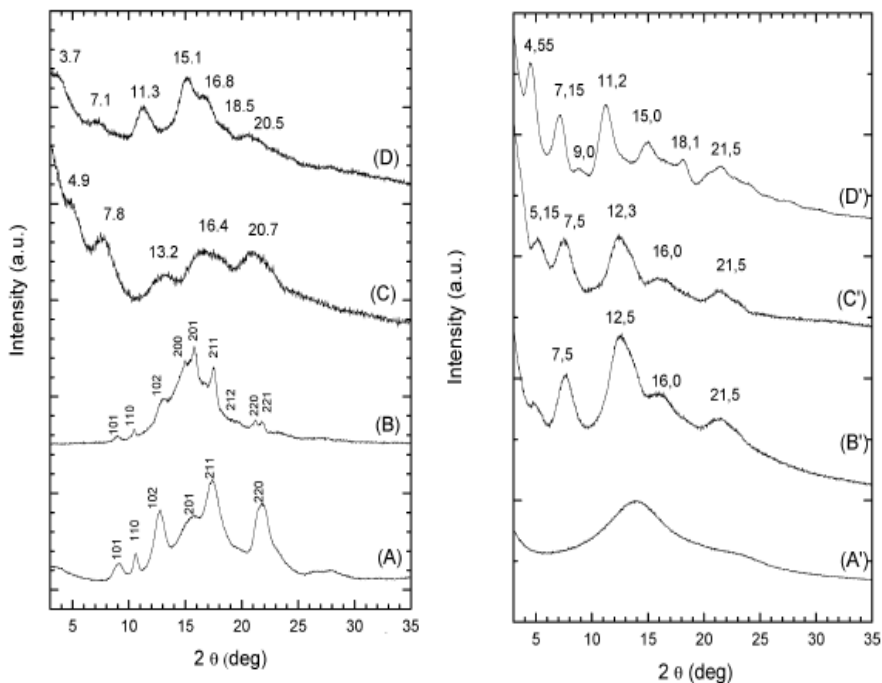


Figure 2. 2. X-ray diffraction patterns (Cu-K α radiation) of PPO gels (PPO content 30–40 wt%), prepared with different solvents (A–D), and of the corresponding powders, as obtained by complete solvent extraction by scCO₂ (A'–D'): (A, A') in decalin; (B, B') in α -pinene; (C, C') in benzene; (D, D') in carbon tetrachloride.

As for the gel with decalin, peaks at $2\Theta_{\text{Cu-K}\alpha} \sim 9.1^\circ, 10.6^\circ, 12.7^\circ, 17.4^\circ$ and 21.8° are observed (Figure 2. 2 A), which, from analogy with the X-ray diffraction pattern of the co-crystalline phase with α -pinene, can be indexed as 101, 110, 102, 211 and 220–221, respectively. The gels including CCl₄ (Figure 2. 2 C) and benzene (Figure 2. 2 D) show diffraction patterns that are

different from those of the co-crystals with α -pinene and decalin gels but also definitely different from each other as well as from those of the known PPO crystalline modifications.^{22,24}

The solvent removal from all these physical gels by supercritical carbon dioxide does not lead to aerogels,^{13a} as observed instead for many other thermoplastic polymers,¹⁹ but only leads to powders. These powders can be amorphous (Figure 2. 2A') or can exhibit a PPO crystalline modification (Figure 2. 2 B'-D'). In particular, as a consequence of complete benzene and CCl₄ removal from their gels (Figure 2. 2 C' and 2. 2 D'), the limit nanoporous crystalline modifications with highest and lowest diffraction angles (similar to those described in the first and last columns of Table 1 of ref. 13a) are obtained, respectively.

It is worth noting that the X-ray diffractions of the gels of Figure 2.2 C, D are similar to those of the corresponding nanoporous– crystalline phases of Figure 2.2 C', D'. This similarity suggests the presence in these gels of co-crystalline phases, being structurally related to the corresponding nanoporous–crystalline phases.

In particular, the shift to a higher 2Θ value (from 3.7° up to 4.55° and from 4.9° up to 5.15°) observed for the lowest diffraction peak, as a consequence of CCl₄ and benzene removal from their PPO gels, suggests unit cell reductions as a consequence of removal of guest molecules from the co-

crystalline phases.

Hence, the present results confirm that, independently of the nature of the solvent in the gels and of the nature of the crystalline phase holding up the gel, solvent removal procedures lead to powders or extremely brittle samples rather than to robust aerogels.

This is shown for instance for the PPO gel in 1,2-dichloroethane with a polymer content of 20 wt%, in Fig. 2. 3.

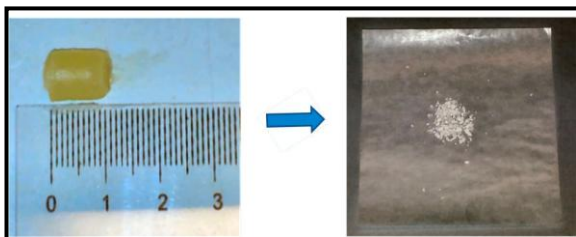


Figure 2. 3. Photographs of pieces of PPO gel prepared in 1, 2-dichloroethane with a polymer concentration of 20 wt%, before and after complete solvent extraction via supercritical carbon dioxide (units on the ruler are cm).

Monolithic physically crosslinked aerogels can be instead easily prepared from mixed PPO/s-PS gels, by the usual scCO_2 extraction procedure, provided that the s-PS fraction is higher than 0.05.

s-PS has been selected because it easily forms aerogels¹⁹ and because PPO and s-PS dissolve in the same solvents. In addition PPO and s-PS are fully miscible in their amorphous phases.²⁵

An example of a PPO/s-PS, 90/10 gel in 1, 2-dichloroethane

with a polymer content of 20 wt%, is shown in Figure 2. 4.

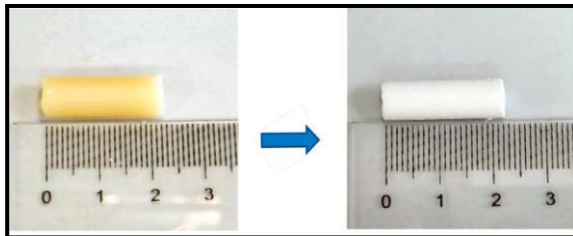


Figure 2. 4. Photographs of pieces of 90/10 w/w PPO/s-PS gels prepared in 1, 2-dichloroethane with a polymer concentration of 20 wt%, before and after complete solvent extraction via supercritical carbon dioxide (units on the ruler are cm).

The obtained aerogels exhibit a toughness comparable to those of s-PS aerogels and the monoliths do not break even after heavy handling.

The X-ray diffraction patterns of aerogels obtained from gel in 1, 2-dichloroethane¹⁸ (DCE) with a polymer content of 20 wt% are shown, for instance, in Figure 2. 5.

The s-PS aerogel (Figure 2. 5A) shows strong reflections located at $2\theta_{(Cu-K\alpha)} \sim 8.3^\circ$ (010), 20.7° and 23.5° , indicating the presence of the nanoporous δ -form.¹⁴

The PPO/s-PS aerogels, for low PPO contents ($x_{PPO} = 0.25$, Figure 2. 5B), show only the crystallinity of the δ form of s-PS. For intermediate polymer composition (e. g. $x_{PPO} = 0.50$, Figure 2.5C) both s-PS and PPO crystallinities are clearly present. As for the PPO crystallinity, well apparent for $x_{PPO} > 0.5$, diffraction peak positions change with x_{PPO} . In fact, for the pure

PPO powder, as obtained by DCE removal from the corresponding gel, diffraction peaks at 4.95° , 7.65° , 12.3° , 16.1° , 21.5° are observed (Figure 2. 5F), which are not far from those observed for powders obtained by desiccation of benzene gels (Figure 2. 2 C', indicated as high limit diffraction angles in the first column of Table 1 in ref. 13a).

As the PPO fraction decreases, a progressive shift of the PPO crystalline peaks is observed and for $x_{\text{PPO}} = 0.50$ (Figure 2. 5C) the diffraction peaks are observed at 4.4° , 7.15° , 11.2° , 15.0° and 18.1° , i. e. at 2Θ values lower than those of powders obtained by desiccation of carbon tetrachloride gels (Figure 2. 2 D', indicated as low limit diffraction angles in the last column of Table 1 in ref. 13a). The formation of PPO physical aerogels, already in the presence of small amount of s-PS, clearly indicates a strong influence of s-PS on PPO crystallization.

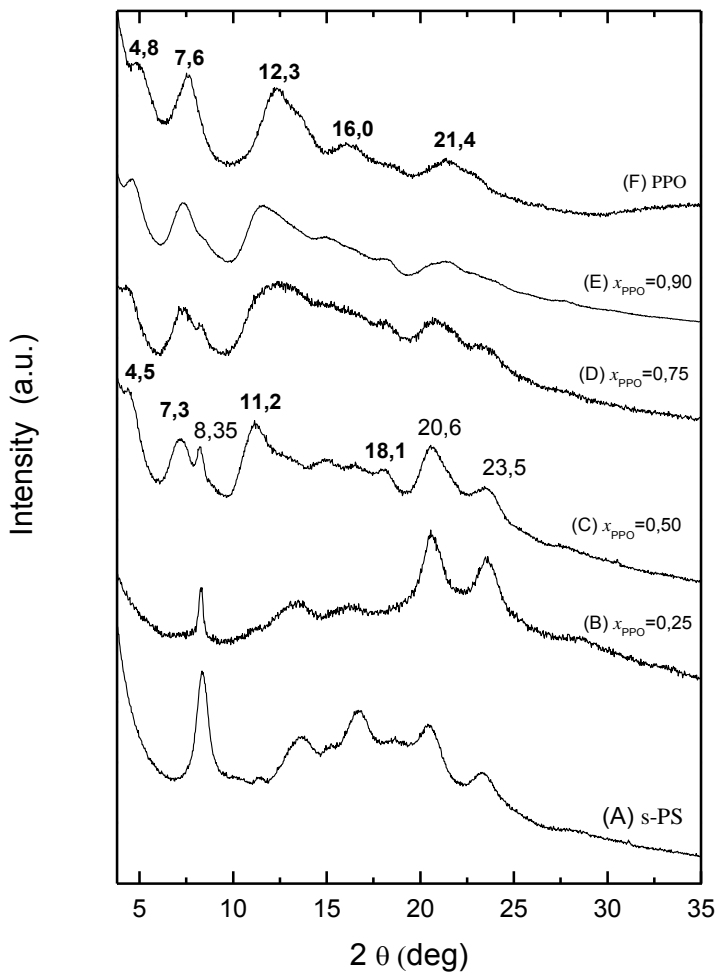


Figure 2. 5. X-ray diffraction patterns (CuK α radiation) of PPO/s-PS gels in DCE, prepared with polymer content of 20wt%, after complete solvent extraction by scCO₂, for different PPO fraction: (A) s-PS aerogel; aerogels with (B) $x_{\text{PPO}} = 0.25$, (C) $x_{\text{PPO}} = 0.50$, (D) $x_{\text{PPO}} = 0.75$, (E) $x_{\text{PPO}} = 0.9$; (F) PPO powder. For some patterns (C and F), diffraction peaks of PPO and s-PS (δ form) are labeled by bold and italics numbers, respectively.

This influence is confirmed by the remarkable shift between PPO crystalline modifications (approximately from the limit

modification with lowest diffraction angles toward the limit modification with highest diffraction angles), which is induced by the increase of the s-PS content in the blend (Figure 2. 5).

The observed s-PS influence on PPO crystallization is not surprising, due to the well-known miscibility of the two polymers in their amorphous phases, as already mentioned previously.²⁵

In fact, it has been clearly established that PPO is able to alter the s-PS polymorphic behavior, favoring the densest and thermodynamically stable β crystalline form,²⁶ both for melt crystallization^{25a} and for solvent-induced crystallization from the amorphous state.^{25b}

The patterns of Figure 2. 5 show that, in turn, s-PS is able to alter the PPO polymorphic behavior favoring, for solution crystallization, the crystalline modifications exhibiting highest diffraction angles.

Scanning Electron Microscopy (SEM) images of some of the samples of Figure 2. 5 are shown in Figure 2. 6. The differences between the morphologies of the s-PS and PPO semicrystalline samples prepared in the same conditions are remarkable.

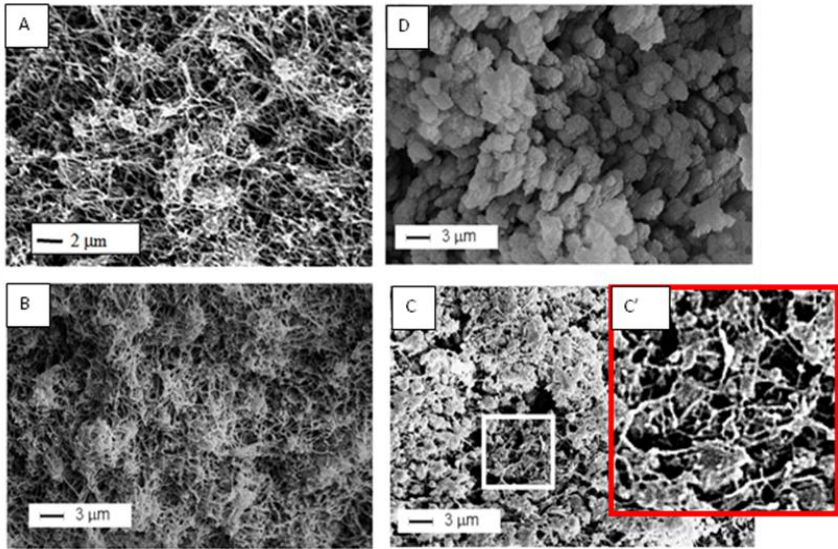


Figure 2. 6. SEM images of samples, as prepared from DCE gels with polymer content of 20wt%, after complete solvent extraction by scCO₂: (A) s-PS δ form aerogel; (B) aerogel with $x_{PPO} = 0.5$; (C, C') aerogel with $x_{PPO} = 0.90$; (D) PPO powder.

In fact, the δ form s-PS aerogel (Figure 2. 6A) presents a fibrillar morphology with fibril diameters of 60–150 nm, while the PPO nanoporous–crystalline powder exhibits granules of micrometric size, possibly constituted by aggregates of spherulites (Figure 2. 6D). The SEM images of the aerogels obtained from PPO/s-PS blends (Figure 2. 6B, C) clearly show the maintenance of the fibrils typical of s-PS aerogels, together with a size reduction of the PPO granules (whose diameter becomes roughly lower than 1 μ m). Hence, the miscibility between the amorphous phases of PPO and s-PS leads to finer PPO morphologies. It is reasonable

to hypothesize that the maintenance of the fibrillar morphology of the s-PS crystalline phases in mixed gels and aerogels (Figure 2. 6B, C) makes for feasible PPO-rich monolithic aerogels.

Monolithic aerogels can be obtained from PPO/s-PS gels for a large range of polymer concentrations. Infact aerogels from gels with 5, 10, 20 and 30 wt% of polymer, with $x_{\text{PPO}} = 0.50$, have been achieved.

2.3 Properties of aerogels based on nanoporous-crystalline PPO

Total surface areas and micropore areas, as obtained from N₂ isotherms (BET experiments) for the mixed PPO/s-PS aerogels are compared in Table 2.1 and Figure 2.7. The surface area increases with the PPO content (Figure 7A), but only for aerogels with crystalline PPO. In fact, for instance, the sample with $x_{\text{PPO}} = 0.25$ exhibiting only the s-PS crystallinity (Figure 2.5B) shows a surface area close to that one of the pure s-PS aerogel. A linear increase of the surface area of the aerogels is instead observed with their content of crystalline PPO ($x_{\text{PPO, crys}}$), as clearly shown by Figure 2.7B.

The predominant contribution of PPO crystallinity to the aerogel surface area is also confirmed by comparing aerogels exhibiting equal PPO content. In fact, the high-porosity PPO/s-PS - 50/50 wt% aerogel prepared from diluted gels ($C_{\text{pol}} = 5$ wt%, 7th line in Table 2.1), which present a low degree of crystallinity, exhibit surface area nearly three times lower than for the denser highly crystalline aerogels, as obtained from more concentrated gels ($C_{\text{pol}} = 10-30$ wt%, last three lines in Table 2.1).

x_{PPO}	C_{pol} (wt%)	$x_{\text{PPO, crys}}$	S_{BET}^a ($\text{m}^2 \text{g}^{-1}$)	S_{micro}^b ($\text{m}^2 \text{g}^{-1}$)	x_{PPO} (%)
s-PS	20	0	206	27	0
0.25	20	0	217	49	0
0.5	20	0.24	337	118	48
0.75	20	0.27	341	141	36
0.9	20	0.53	483	172	58
PPO (powder)	25	0.59	535	195	59
0.5	5	0.08	112	19	15
0.5	10	0.20	273	92	39
0.5	20	0.24	337	118	48
0.5	30	0.18	343	108	35

^aTotal area evaluated following the BET model in the standard $0.05 < P/P_0 < 0.25$ pressure range.

^bMicropore area obtained from the t-plot.

Table 2. 1. Total surface area (S_{BET}) and micropore area (S_{micro}), expressed as $\text{m}^2 \text{g}^{-1}$, of the polymeric aerogels, as obtained for PPO/s-PS blends presenting different PPO weight fractions (x_{PPO}), as prepared from DCE gels presenting different polymer content (C_{pol}). The aerogel fraction constituted by crystalline PPO ($x_{\text{PPO, crys}}$), as evaluated from the patterns of Figures 2 and 4, and the degree of crystallinity relative to the PPO fraction (x_{PPO}), as evaluated by the X-ray diffraction patterns of Figures 2 and 4, are also indicated.

Particularly interesting is the comparison of the dependence of S_{BET} on the apparent density for s-PS and PPO/s-PS aerogels, which is shown in Figure 2. 7C. In fact, while for s-PS aerogels the surface area, S_{BET} , increases as expected when the density decreases, the opposite unexpected behavior is observed for the PPO/s-PS aerogels. This behavior can be rationalized by the achievement of maximum content of nanoporous-crystalline phase of PPO only for denser PPO/s-PS aerogels ($C_{\text{pol}} \geq 10$ wt%, Table 2. 1).

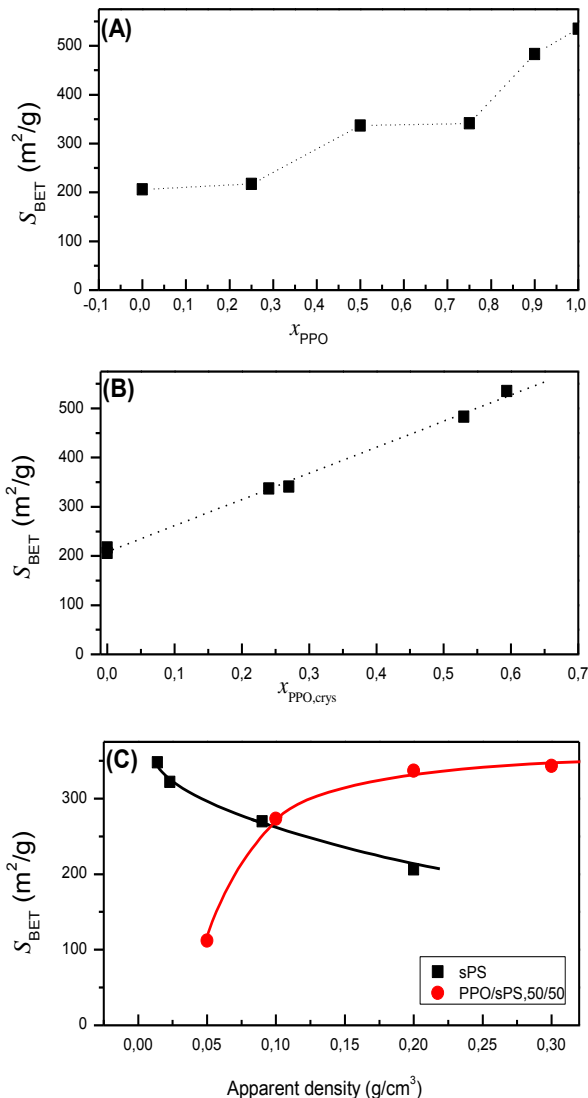


Figure 2. 7. Surface area (S_{BET} , $\text{m}^2 \text{g}^{-1}$) of PPO/s-PS aerogels (prepared from DCE gels and after complete solvent extraction by scCO_2), as evaluated by the BET model in the standard 0. 05, P/P₀, 0. 25 pressure range: (A, B) from gels with a polymer content of 20 wt% (aerogel apparent density of $0. 2 \text{ g cm}^{-3}$) versus the PPO fraction (x_{PPO} ; A) or versus the crystalline PPO fraction ($x_{\text{PPO, crys}}$; B); (C) versus the aerogel apparent density, for $x_{\text{PPO}} = 0. 50$.

For these monolithic PPO-based aerogels, exhibiting high surface areas (up to 350-500 m² g⁻¹), also for densities higher than 0.2 g/cm³, the uptake of pollutant molecules as guest of the nanoporous-crystalline phases is expected to be large, mainly if expressed as content per volume rather than per weight.

The chosen pollutants for sorption test are the carbon tetrachloride (CCl₄) and 1,2 dichloroethane (DCE). The reasons which led to this choice are described in the following paragraphs.

2. 3. 1 Carbon tetrachloride

Carbon tetrachloride is readily volatile at ambient temperature and degrades very slowly, (85 years ²⁷)so it has gradually accumulated in the environment.

The primary routes of potential human exposure to carbon tetrachloride are inhalation, ingestion, and dermal contact. The general population is most likely to be exposed to carbon tetrachloride through air and drinking water. In 1988, EPA's Toxics Release Inventory listed 95 industrial facilities that produced, processed, or otherwise used carbon tetrachloride and reported environmental releases of carbon tetrachloride totaling 3. 9 million pounds (TRI 2009).

Exposure to carbon tetrachloride may also occur by dermal contact with tap water (e. g., during bathing). Surveys have found that about 99% of all groundwater supplies and 95% of all sur-

face-water supplies contain carbon tetrachloride. Exposure to carbon tetrachloride by ingestion may occur through consumption of contaminated drinking water or food.^{27a}

In this regard, damage to a prolonged exposure to high concentrations of carbon tetrachloride can affect the central nervous system, degenerate the liver^{27b} and kidneys^{27c}, could result in cancer^{27f}, coma and even death.^{27d}

In 2008, a study of common cleaning products found the presence of carbon tetrachloride in "very high concentrations" (up to 101 mg/m³) as a result of manufacturers' mixing of surfactants or soap with sodium hypochlorite (bleach).^{27g} Carbon tetrachloride is also both ozone-depleting^{27h} and a greenhouse gas.²⁷ⁱ

2.3.2 1, 2-Dichloroethane

Dichloroethane (DCE) is toxic (especially by inhalation due to its high vapour pressure), highly flammable, and carcinogenic.^{28a}

Its high solubility and 50-year half-life in anoxic aquifers make it a perennial pollutant and health risk that is very expensive to treat conventionally, requiring a method of bioremediation.

The general population is exposed to 1,2-dichloroethane primarily from inhalation of ambient air, particularly near point sources. Other potential routes of exposure for the general population include ingestion of DCE in contaminated drinking

water or food items and dermal absorption. In addition, inhalation exposure may occur from DCE that has volatilized from water during activities such as cooking, bathing, showering, and dishwashing, if DCE is in the water supply. Occupational exposure to this pollutant occurs through inhalation and dermal contact with the compound at workplaces where it is produced or used. Children are expected to be exposed to DCE by the same routes as adults.^{28b}

For these reasons, a material suitable to absorb these pollutants, even at low concentrations, is very interesting.

For the selected pollutants sorption measurements from vapors at low activity and from diluted aqueous solutions have been carried out with these PPO rich aerogels.

In Figure 2. 8 are reported the CCl_4 sorption experiments at 35°C at pressures lower than $0.08 P/P_0$ for s-PS/PPO aerogels with different content of PPO, a pure δ s-PS aerogel and amorphous and semicrystalline PPO powders. We can observe that the sorption capacity of pure semi-crystalline PPO is higher than amorphous PPO and than s-PS δ aerogel. In particular at $0.01 P/P_0$ the CCl_4 uptake in the semi-crystalline PPO samples is c.a 2 times higher than δ s-PS and 3 times higher than amorphous PPO.

The sorption results obtained with PPO-s-PS aerogels can be explained on the basis of X-ray diffraction patterns reported in

Figure2. 5.

s-PS/PPO aerogel with $\chi_{\text{PPO}}=0.25$ shows a lower sorption capacity than the s-PS δ aerogel. This can be clearly explained by the absence of PPO crystallization in these condition as shown in Figure2. 5B which leads to a sorption capacity lower than the s-PS δ phase. For PPO contents of $\chi_{\text{PPO}}=0.50$, $\chi_{\text{PPO}}=0.75$ the sorption uptakes are similar and are intermediate between the uptakes of pure PPO and d s-PS.

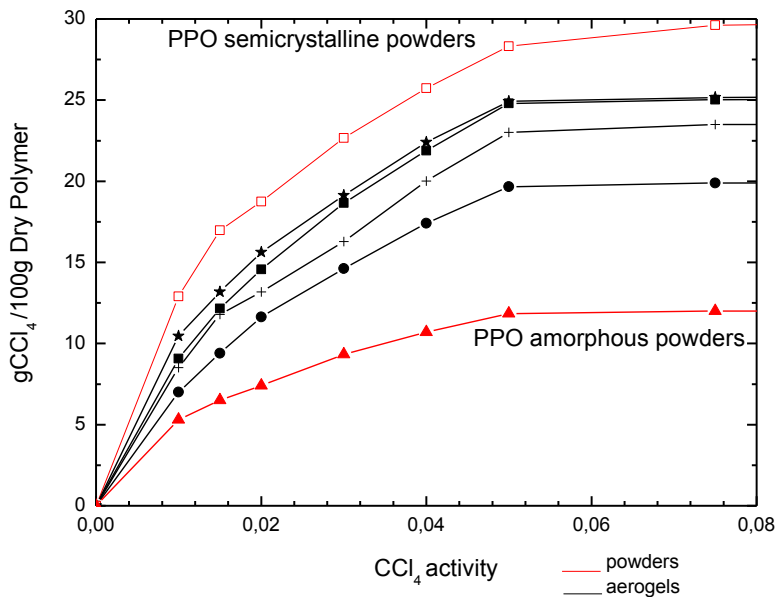


Figure 2. 8. CCl₄ sorption experiments at 35°C at pressures lower than 0.08 P/P₀ on : amorphous PPO (red solid triangles); s-PS/PPO aerogel $\chi_{\text{PPO}}=0.25$ (black solid circles); δ s-PS aerogel (black plus symbols); s-PS/PPO aerogel $\chi_{\text{PPO}}=0.50$ (black solid squares); s-PS/PPO aerogel $\chi_{\text{PPO}}=0.75$ (black stars symbol); semicrystalline PPO (red empty squares)

In order to further characterize the sorption capacity and kinetics of s-PS/PPO aerogels and to assess possible uses of this new material, sorption measurements of diluted organic compounds from diluted aqueous solutions have been conducted at room temperature. In particular the equilibrium uptake of CCl_4 and DCE from diluted aqueous solutions has been investigated for s-PS/PPO aerogels with $\chi_{\text{PPO}}=0.50$ ($C_{\text{pol}}=20\%$) and for δ s-PS aerogel ($C_{\text{pol}}=1\%$).

In Figure 2.9 are reported the FTIR spectra a s-PS/PPO aerogel (A) and of a δ s-PS aerogel (B) before (black curves) and after (red curves) immersion in a CCl_4 aqueous solution at 10 ppm.

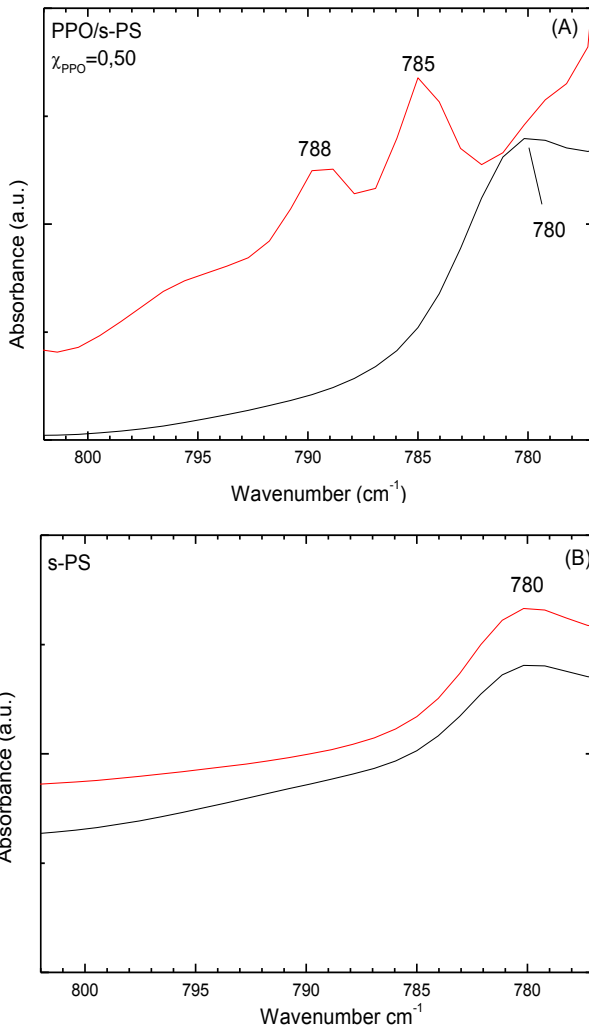


Figure2. 9 FTIR spectra of s-PS/PPO aerogel ($\chi_{\text{PPO}}=0.5$) $C_{\text{pol}}=20\%$ (A) and δ s-PS aerogel ($C_{\text{pol}}=1\%$) (B) before (black curves) and after (red curves) equilibrium CCl_4 sorption from its aqueous 10ppm solutions. .

The appearance of the peaks at 788 and 785 cm⁻¹ clearly indicates the occurrence of a substantial sorption of CCl_4 , which

has been quantified by thermogravimetric analysis (Figure 2. 10). Measurements confirm that the guest is selectively adsorbed by the PPO phase of the PPO/s-PS aerogel (13%), infact in δ s-PS aerogel the amount of adsorbed guest is less than 0, 5%. Then, a CCl_4 selective uptake from PPO in the PPO/s-PS aerogels is effectively present. In the same conditions, the CCl_4 uptake from the PPO/s-PS - 90/10wt% aerogel with crystalline PPO (of Figure 2.5E), exhibiting surface area higher than for 50/50 aerogels (Table 2), is close to 19wt%.

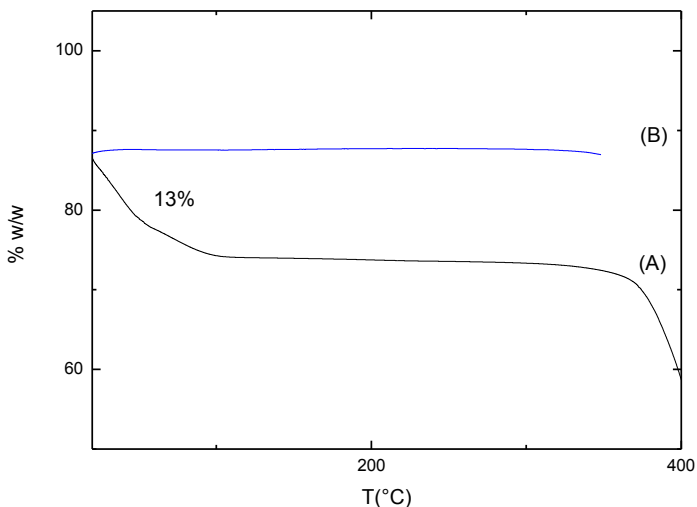


Figure 2. 10 Thermogravimetric measurements of CCl_4 amount in s-PS/PPO ($\chi_{\text{PPO}}=0.5$) $C_{\text{pol}}=20\%$ (A) and δ s-PS aerogel ($C_{\text{pol}}=1\%$)(B) after equilibrium CCl_4 (10ppm) sorption from its aqueous 10ppm solutions.

It is worth adding that, with respect to films, the macropores of the aerogels not only result in an increase in the guest sorption

kinetics but can also increase the uptake values for molecules presenting a poor solubility in the polymer amorphous phase.

The CCl_4 uptake in PPO films has been also investigated and FTIR spectra collected before and after immersion of a PPO film in a 10ppm aqueous solutions is reported in Figure 2.11.

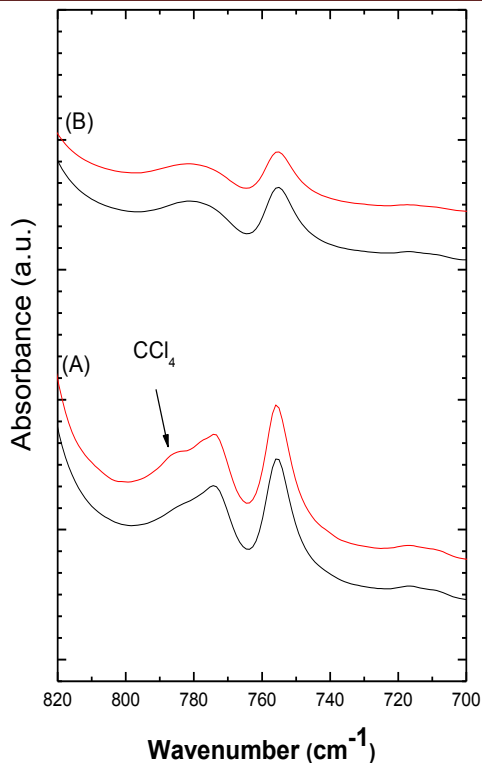


Figure 2.11 FTIR spectra of semicrystalline PPO film (A) amorphous PPO film (B) before (black curves) and after (red curves) equilibrium CCl_4 sorption from its aqueous 10ppm solutions.

In similar conditions the CCl_4 uptake from the film samples for dilute aqueous solutions is less than 1%, also for this reason the achievement of monolithic aerogels that include the crystalline pores of both PPO and s-PS is a very important result.

As mentioned above the sorption measurements have been also carried out with DCE dilute aqueous solutions for s-PS/PPO aerogels with $\chi_{\text{PPO}}=0.50$ ($C_{\text{pol}}=20\%$). Figure 2.12 shows the FTIR spectra for s-PS/PPO aerogel $\chi_{\text{PPO}}=0.50$ ($C_{\text{pol}}=20\%$)

before (B) and after (C) equilibrium DCE (blue curve) sorption from a 10 ppm aqueous solutions. Spectral subtraction is also shown (C-B).

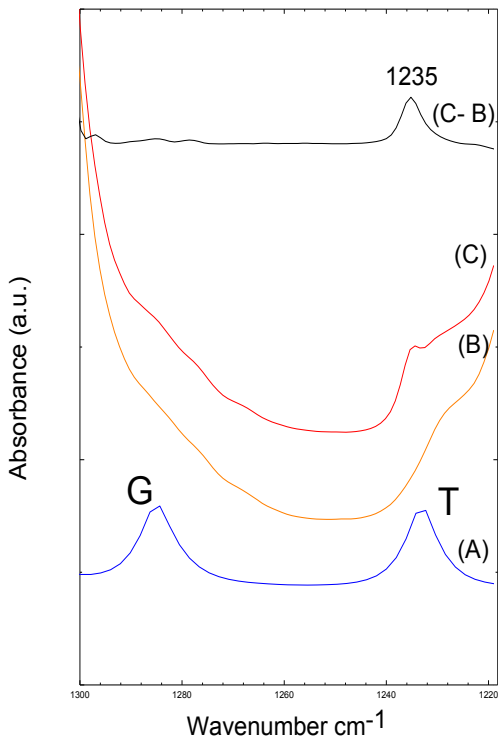


Figure 2. 12 FTIR spectra of DCE with gauche and trans peaks (A) s-PS/PPO aerogel ($\chi_{\text{PPO}}=0.5$) $C_{\text{pol}}=20\%$ before (B) and after (C) equilibrium DCE sorption from its aqueous 10ppm solutions. The black curve shows the subtraction between (C-B)

In figure 2.12, gauche (G) and trans peaks (T) of DCE are shown ^{19c}. After immersion only peak of trans conformer is observed (1235 cm⁻¹) as evidenced by spectral subtraction

(Figure 2.12 C-B); it means that DCE is selectively adsorbed by δ s-PS phase of the s-PS-PPO aerogel. ^{19c}

The amount of DCE has been quantified by thermogravimetric measurements, and is equal to 2.5% while for δ s-PS aerogel ($C_{\text{pol}}=1\%$) the DCE uptake from dilute aqueous solutions (10 ppm) is 5%. ^{19b}

So, in the same condition, the DCE is selectively adsorbed from δ s-PS in s-PS/PPO aerogel, while CCl_4 is adsorbed quickly and in large quantities only from PPO in s-PS/PPO aerogel with $\chi_{\text{PPO}}=0.50$ and $\chi_{\text{PPO}}=0.90$ ($C_{\text{pol}}=20\%$).

This inverse selectivity trend is outlined in Fig 2.13.

It's important to specify that for the gravimetric sorption isotherm at 35°C and at a pressure of $0.1 P/P_0$, we observe an higher CCl_4 uptake (green curve) than from the aqueous 10 ppm solution, also for the pure δ s-PS. Much likely this is caused by the formation of a hydrated species of carbon tetrachloride in the aqueous solution, ²⁹ which increases the guest size thus decreases the CCl_4 uptake.

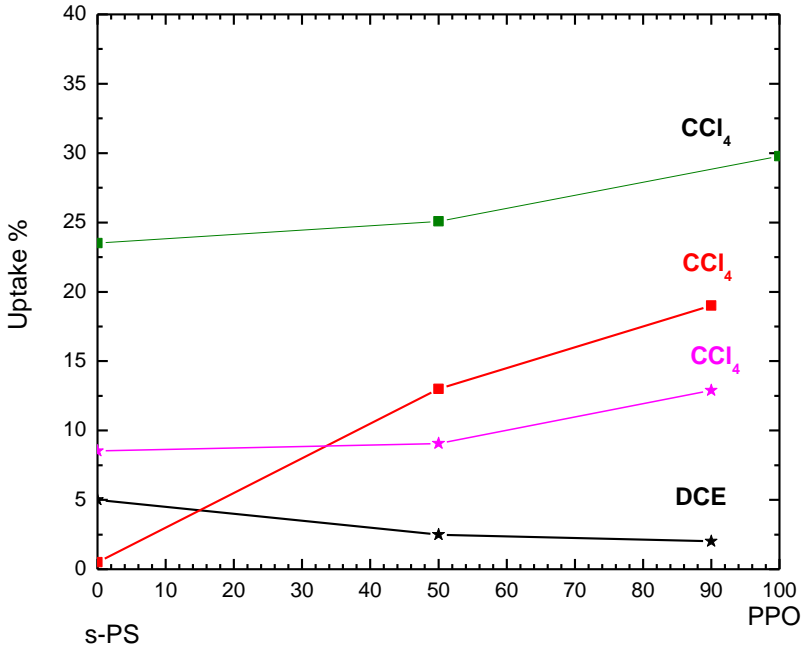


Figure 2. 13. Percentage uptake vs PPO increasing concentration, from : DCE diluted aqueous solutions (10 ppm)(black curve), CCl₄ diluted aqueous solutions (10 ppm)(red curve). The magenta curve is the sorption isotherms at 35 ° C and at a pressure of 0. 01 P/P₀ CCl₄ and the green curve is the sorption isotherms at 35 ° C and at a pressure of 0. 1 P/P₀ CCl₄.

For these monolithic nanoporous crystalline aerogels based on PPO, sorption properties were preliminarily valuated for aniline, a pollutant of great relevance, produced in very large amounts.³⁰ The largest users of aniline are companies that make isocyanates, especially methyl diphenyl diisocyanate. Other companies use aniline to make pesticides, dyes, and rubber. Companies also use smaller amounts of aniline to make drugs, photographic chemicals, varnishes, and explosives.

This substance may be hazardous to the environment; with special attention given to fish, crustaceans, and birds. Tests by the aniline industry show that aniline is highly toxic to aquatic life. Aniline causes germination decrease, stunting, and size decreases (among other effects) on numerous agricultural crops. It is also moderately adsorbed to organic material in the soil. On this basis, an absorbent material for this pollutant, even in traces, would be actually very useful. The aniline uptake from 10ppm aqueous solution, evaluated by thermogravimetric measurements is close to 8%.

2. 4 Concluding remarks

X-ray diffraction patterns of PPO gels with different solvents have shown the presence of co-crystalline phases acting as knots of their physical cross-linking. In particular, the well-known PPO co-crystalline phases with decaline and α -pinene have been observed for the corresponding PPO gels. Moreover, the patterns of gels with carbon tetrachloride and benzene strongly suggest the presence of respective co-crystalline phases, being rather similar to the two limit nanoporous-crystalline modifications of PPO.

All attempt to obtain monolithic aerogels from PPO gels were unsuccessful. PPO based monolithic aerogels were instead easily obtained starting from mixed PPO/s-PS gels. SEM experiments suggest that the stability of PPO/s-PS aerogels is due to the s-PS fibrillar morphology, which is still clearly apparent for PPO/s-PS - 90/10 wt% aerogels.

X-ray diffraction experiments show that these mixed aerogels can exhibit nanoporous-crystalline phases of both polymers. However, aerogels with high degrees of PPO crystallinity (in the range 35-50%) can be easily obtained only for high PPO fractions ($x_{\text{PPO}} \geq 0.5$) and high density ($\rho_{\text{app}} \geq 0.1 \text{ g/cm}^3$).

These nanoporous-crystalline PPO rich and dense aerogels present high surface areas (up to $480 \text{ m}^2\text{g}^{-1}$) and high guest

solubilities and diffusivities, due to the presence of the crystalline cavities of both polymers, and hence are particularly suitable for removal of traces of organic pollutants from water and air. For instance, the carbon tetrachloride uptake from 10 ppm aqueous solutions for these aerogels can be as high as 19 wt%, while the corresponding uptake for s-PS aerogels and PPO films is lower than 1 wt %, after 3 days of exposure.

The increase of the surface area and of the sorption ability of PPO/s-PS aerogels with the PPO crystallinity clearly confirms the nanoporous nature of the PPO crystalline modifications.

Chapter 3

Monolithic Aerogels Based on Poly(2, 6-diphenyl-1, 4-phenyleneoxide) and Syndiotactic Polystyrene

3.1 Introduction

Poly(2,6-diphenyl-1,4-phenylene oxide) (shortly indicated as PPPO), which was patented in 1969,³¹ has been mainly developed with the trade name Tenax as a porous column packing polymer for gas chromatography.³²

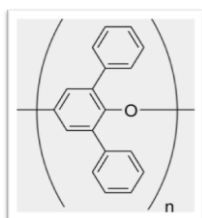


Figure 3.1. Chemical structure of PPPO repeating unit

It is widely reported in literature (about 800 papers) that PPPO is an excellent porous adsorbent for the trapping of many types of volatiles such as halogenated and aromatic compounds,^{33a-c} normal alkanes,^{33a, d, e} cycloalkanes,^{33a} ketones,^{33a, c-e} alcohols,^{33a, c-e} and volatile fatty acids^{33c} mainly from air^{33a, 33c-e} but also from water.^{33d} Furthermore PPPO, generally provided in granular form, has several attractive features for a use as a porous material in air analysis: it is thermally stable (up to 350 °C),³⁴

presents a low water retention,^{33a} and is relatively resistant to oxygen. Thus PPPO is largely used as an adsorbent material in standard methods for routine air monitoring^{35a} or for the study of specific industrial emissions.^{35b-d}

Since as for most molecular sorption studies^{32, 33, 35b-d} PPPO is used as a semicrystalline powder, the experimental results described in this chapter focus on two main goals :

- Establish if the occurrence of a nanoporous crystalline phase could be at the origin of the high sorption properties of this polymer.
- Explore the possibility to obtain PPPO aerogels, in the attempt to improve the already high sorption capability.

3.2 PPPO Powders and Films

In order to better understand PPPO sorption properties, volatile organic compounds (VOCs) uptake were evaluated for different samples. PPPO samples chosen for the analysis are:

- Commercial PPPO powder
- PPPO amorphous films obtained by casting in CHCl_3 at 20°C .
- PPPO amorphous films obtained by casting in CHCl_3 at 135°C .
- PPPO amorphous powder obtained by concentrated solution ($C_{\text{pol}}=20\%$), successively extracted by supercritical CO_2 .

The X-ray diffraction patterns of powders obtained from a concentrated CHCl_3 solution ($C_{\text{pol}}=20\text{wt}\%$) by scCO_2 extraction and of films obtained by casting from CHCl_3 solutions at 135°C and at 20°C , are shown in Figure 3. 2 B–D, respectively. The three patterns present the typical PPPO amorphous halo with two maxima,³⁶ which are however centered at definitely different 2θ values: at 8.6° and 17.3° for the scCO_2 extracted powder while in the ranges $8.8\text{--}9.1^\circ$ and $17.7\text{--}18.0^\circ$ for the films. The most dense amorphous sample (corresponding to the pattern shifted at highest 2θ values of Figure 3. 2D) is obtained for the

low temperature solution casting procedure while the less dense amorphous sample (corresponding to the pattern shifted at lowest 2θ values of Figure 3. 2B) is obtained for the powder obtained by sudden solvent removal by $scCO_2$. The samples of Figure 3. 2 have been compared as sorbent materials for carbon tetrachloride (CCl_4) vapor at low activity.

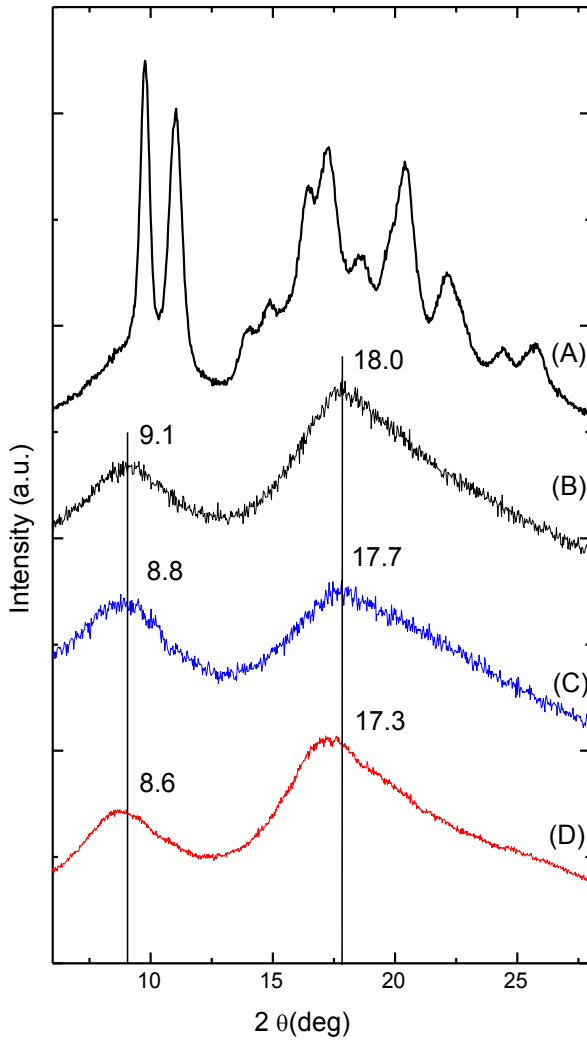


Figure 3.2 X-ray diffraction patterns (CuK α radiation) of: (A) commercial Tenax TA, (B) Tenax TA amorphous films obtained by casting in CHCl₃ at 20°C and at 135°C, (C) Tenax TA amorphous powder obtained by concentrated solution ($C_{\text{pol}}=20\%$) and successively extracted by supercritical CO₂.

Gravimetric CCl_4 sorption isotherms, at 35 °C and at activities (p/p^0) up to 0. 2, are reported in Figure 3. 3.

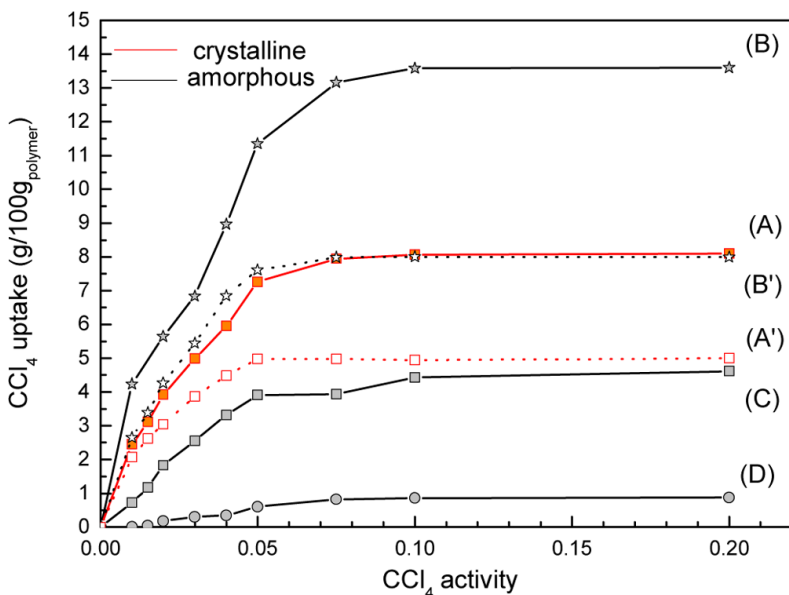


Figure 3. 3. CCl_4 sorption isotherms at 35 °C for PPPO samples: (A) as received commercial semicrystalline Tenax TA powder; (B) fully amorphous powder, obtained by scCO_2 extraction of a concentrated solution; (C, D) fully amorphous films obtained by casting in CHCl_3 at (C) 135 and (D) 20 °C. The dotted curves with empty symbols (A' and B') indicate the sorption isotherms of the semicrystalline and amorphous powders A and B after annealing at 220 °C.

For the entire CCl_4 activity range, the equilibrium uptake from the amorphous powder (Figure 3.3B) is much higher than from the two amorphous films (Figure 3.3 C, D) and also higher than for the commercial semicrystalline powder (Figure 3. 3A). For

instance, the equilibrium sorption at $p/p^\circ = 0.10$ for the amorphous powder is nearly 14 wt % while for the semicrystalline powder is nearly 8 wt % and for the amorphous films cast at 135 and 20 °C is lower than 5 and 1 wt %, respectively.

The different values of the CCl_4 sorption uptake obtained with the cast films and the amorphous powder can be attributed to the different density of the amorphous phases obtained in the three samples. In fact the most dense sample (i. e., cast film prepared at 20 °C) is characterized by the lowest CCl_4 uptake (Figure 3. 3 D) while the less dense sample (i. e., powder obtained by scCO_2 extraction of a concentrated solution) presents the highest CCl_4 uptake (Figure 3. 3 B)

The guest uptake from the semicrystalline sample (Figure 3. 3A), is roughly equal to 60% of the guest uptake of the amorphous powder (Figure 3. 3B), i. e., close to the amorphous content of the semicrystalline powder.

This indicates that, as generally occurs for polymers, guest uptake is essentially due to only the amorphous phase and that, differently from the case of s-PS and PPO, the crystalline phase of PPPPO is not nanoporous.

It is worth adding that annealing procedures on both amorphous and semicrystalline samples, which do not alter significantly their degree of crystallinity, can largely reduce the

pollutant uptake. For instance, gravimetric CCl_4 sorption isotherms, of the amorphous and semicrystalline powders of curves A and B, after treatment at $220\text{ }^\circ\text{C}$ (i. e., glass transition temperature of PPPO³⁶) for 240 min (reported as A' and B' curves, with empty symbols and dotted curves in Figure 2), show a reduction of the guest uptake of roughly 40%. This reduction of pollutant uptake is due to the expected densification of the amorphous phases, occurring by thermal treatments close to T_g .^{37a, b}

Hence, our results indicate that the free volume of PPPO amorphous phases is largely dependent on the preparation procedure as well as on the thermal history and thus important differences of the guest uptakes may be observed in amorphous PPPO samples.

3.3 Preparation and structural characterization of PPPO/s-PS aerogels

PPPO is easily dissolved in many organic solvents (e. g., CHCl_3 , CH_2Cl_2 , benzene) but all our attempts to obtain gelification on cooling, at least for polymer concentrations ≤ 10 wt %, were unsuccessful.

However thermoreversible gels with PPPO can be also easily obtained for blends with syndiotactic polystyrene (s-PS), even for PPPO/s-PS ratios as high as 90/10 (Figure 3A). Moreover, as already observed for PPO/s-PS gels, ⁶ robust monolithic aerogels with good handling characteristics can be easily obtained from the mixed PPPO/s-PS gels by sudden solvent extraction by scCO_2 (Figure 3. 4B).

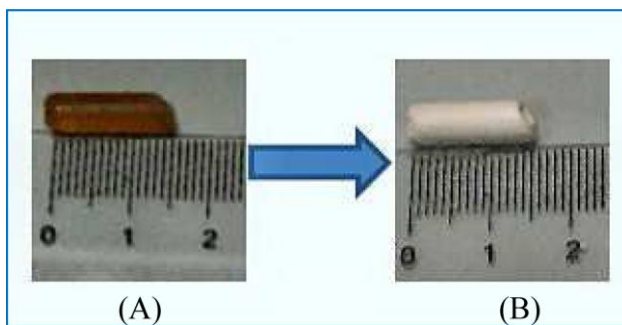


Figure 3.4 Photographs of (A) a cylindrical 90/10 PPPO/s-PS gel, with $C_{\text{pol}} = 10$ wt % and (B) the corresponding monolithic aerogel, with porosity $P = 90\%$ as obtained by scCO_2 drying.

Scanning electron microscopy (SEM) images of a 50/50 PPPO/s-PS aerogel are shown in Figure 3. 5.

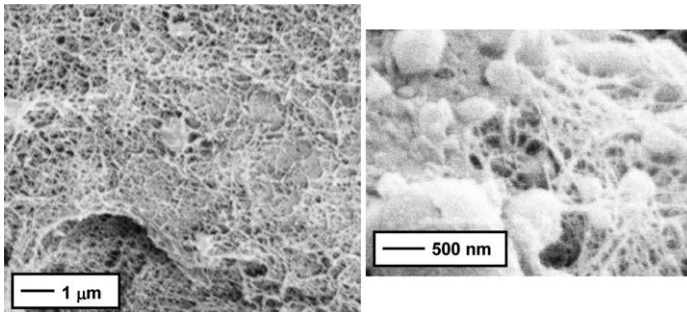


Figure 3.5. SEM images of a PPPO/s-PS aerogel with porosity $P = 90\%$ obtained from a 50/50 PPPO/s-PS gel prepared in chloroform with $C_{pol} = 10$ wt %, after complete solvent extraction by $scCO_2$.

The SEM images clearly show that as previously observed for PPO/s-PS aerogels, ⁶ the typical fibrillar morphology of s-PS aerogels ^{3b, 5, 19} is maintained in PPPO/s-PS aerogels while PPPO beads with diameter of 0.5–1 μm included in the fiber network can be also observed. Thus, we can assume that the maintenance of the s-PS fibrillar morphology allows the obtaining of robust monolithic PPPO/s-PS aerogels with good handling characteristics.

X-ray diffraction patterns of aerogels obtained from physical gels of s-PS and of 50/50 and 90/10 PPPO/s-PS blends, in

$CHCl_3$ and with polymer concentration $C_{pol} = 10$ wt %, are

reported in Figure 3. 6.

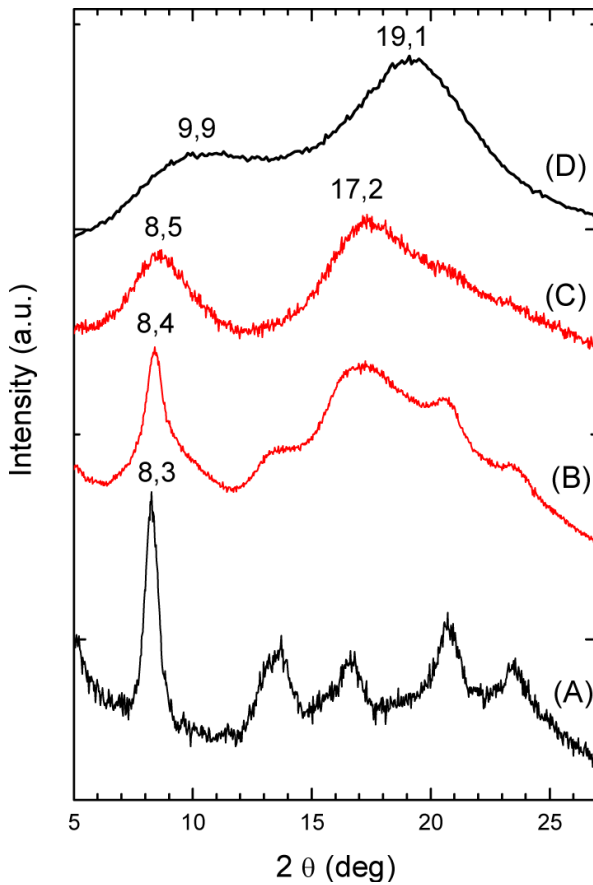


Figure 3.6. X-ray diffraction patterns (CuK α radiation) of aerogels as obtained by scCO₂ extraction of gels in chloroform, with C_{pol} = 10 wt %, of (A) s-PS (nanoporous-crystalline δ form) (B) s-PS/PPPO, 50/50 by wt; (C) s-PS/PPPO, 10/90 by wt. (D) For the sake of comparison, the diffraction of an amorphous sample of s-PS is also shown.

The 50/50 PPPO/s-PS aerogel (Figure 3. 6 B) presents, besides other broader peaks, a diffraction peak at $2\theta = 8.3^\circ$ corresponding to the 010 reflection of the nanoporous δ phase of s-PS.^{12a} The 90/10 PPPO/s-PS aerogel (Figure 3. 6 C) only shows two broad amorphous halos, whose maxima are slightly shifted to lower 2θ values (8.5 and 17.2°), also with respect to the high-free-volume PPPO amorphous powder of Figure 3. 6B. A comparison with the X-ray diffraction pattern of an amorphous s-PS film,^{25a, 38} presenting the typical halos roughly centered at $2\theta \approx 10^\circ$ and 20° (Figure 3. 6D), clearly indicates that this shift toward lower angles of the amorphous halos of PPPO is not due to the s-PS blend component.

3.4 Properties of aerogels based on PPPO

Adsorption–desorption N_2 isotherms (where the sorption is expressed as cm^3 of nitrogen in normal conditions per gram of polymer), for the aerogels of Figure 3.6 A–C are compared with those of the PPPO commercial semicrystalline powder, in Figure 3.7. The corresponding values for the total surface areas S_{BET} and total pore volume V_{tot} are compared in Table 3. 1.

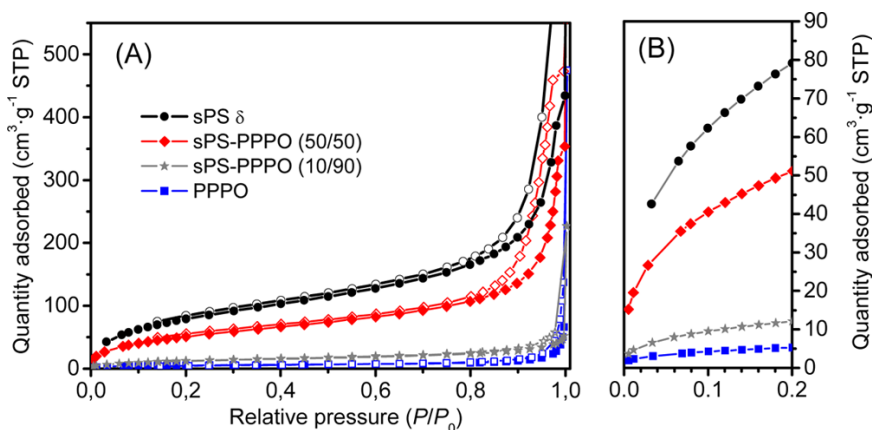


Figure 3.7. (A) Volumetric N_2 adsorption isotherms recorded at 77 K of the commercial Tenax powder (blue squares) and of aerogels of s-PS/PPPO 10/90 by wt (gray stars), s-PS/PPPO 50/50 by wt (reddiamonds), and s-PS (nanoporous δ crystalline form) (black circles). Filled and empty scatters refer to the adsorption and desorption branches, respectively. (B) Detail of the adsorption branch, for low pressures.

It is apparent from Table 3. 1 that both S_{BET} and V_{tot} largely increase moving from powders to aerogels. Relevant is the

increase of the surface area, by factors of roughly 2.3 and 10 moving from the PPPO powder to the 90/10 and 50/50 aerogels, respectively (3rd column of Table 3.1). This increase is due to the s-PS δ -form, which is characterized by nanopores having the same volume of ca. 115 \AA^3 .^{12c}

Samples	Polymer composition (wt/wt)	S_{BET}^a ($\text{m}^2 \text{ g}^{-1}$)	V_{tot}^b ($\text{cm}^3 \text{ g}^{-1}$)
Aerogels ^c	s-PS(δ -form)	290	0.31
	PPPO/s-PS, 50/50	197	0.20
	PPPO/s-PS, 90/10	47	0.04
Powders	s-PS(δ -form)	43	0.10
	PPPO	20	0.02

^aTotal area evaluated following the BET model in the standard $0.05 < p/p^0 < 0.25$ pressure range. ^bTotal pore volume calculated as volume of the liquid at $p/p^0 \approx 0.90$. ^cAs prepared from chloroform gels with a same polymer content ($C_{\text{pol}} = 10 \text{ wt } \%$). ^dIt is worth noting that as already reported in ref 33d, the measured specific surface area of PPPO is lower than the advertised value of $35 \text{ m}^2/\text{g}$.

Table 3.1. Total Surface Area (S_{BET}) and Total Pore Volume (V_{tot}) of Aerogels and Powders Based on s-PS and PPPO

As for aerogels based on PPO, also for aerogels based on PPPO sorption properties have been investigated.

CCl_4 sorption isotherms, at 35 °C and for p/p^0 up to 0.20, are reported in Figure 3.8, for the aerogels of Figure 3.6 and apparent that the PPPO/s-PS aerogels present CCl_4 uptake much higher than for the most efficient PPPO powders.

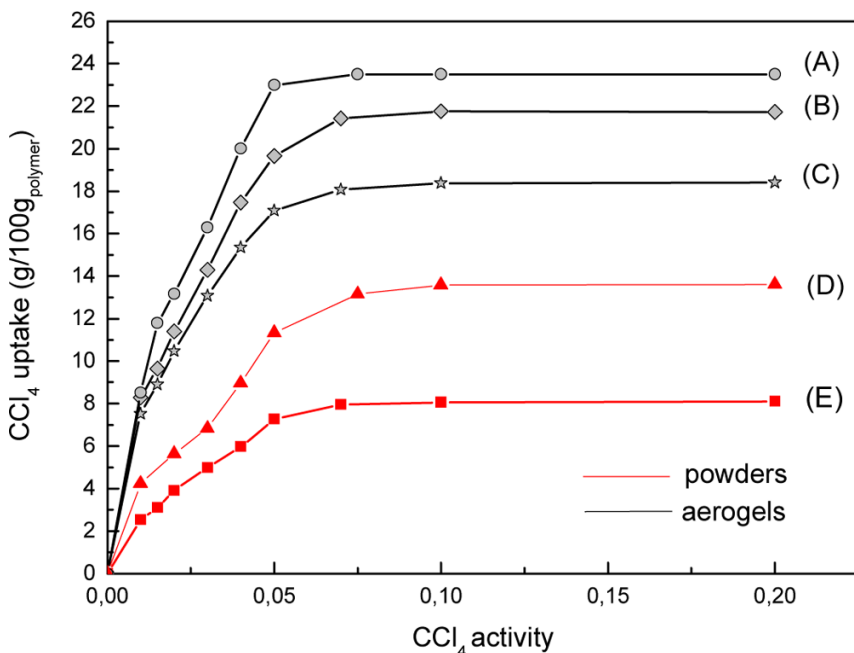


Figure 3. 8. CCl_4 sorption isotherms at 35 °C for the aerogels of Figure 3.6 A–C: (A) s-PS, δ form; (B) PPPO/s-PS 50/50 wt % (C) PPPO/s-PS 90/10 wt %. For the sake of comparison, the sorption isotherms of the (D) highly sorbent PPPO amorphous and (E) semicrystalline powders of Figure 3.2 are replotted.

This is only in part due to the higher sorption ability of the nanoporous δ form of s-PS (Figure 3.8 A). In fact, the aerogel containing only 10% of s-PS (Figure 3.8 C), which includes a negligible amount of nanoporous δ phase (as shown by the fully amorphous pattern of Figure 3.6 C), presents a guest uptake roughly 30% higher than the best PPPO powder (Figure 3. 8D). Although the evaluated surface areas (Table 3.1) and the CCl_4 equilibrium uptakes (Figures 3.8) are markedly larger for aerogels than for powders, the sorption kinetics are similar. This is shown, for instance in Figure 3.9, for the sorption kinetics relative to a sudden increase of CCl_4 activity from zero up to $p/p^\circ = 0.01$. It is apparent that the monolithic 90/10 PPPO/s-PS aerogel (circles) maintains the fast sorption kinetics of fine powders (triangles and stars) with a halftime for the equilibrium lower than 15 min.

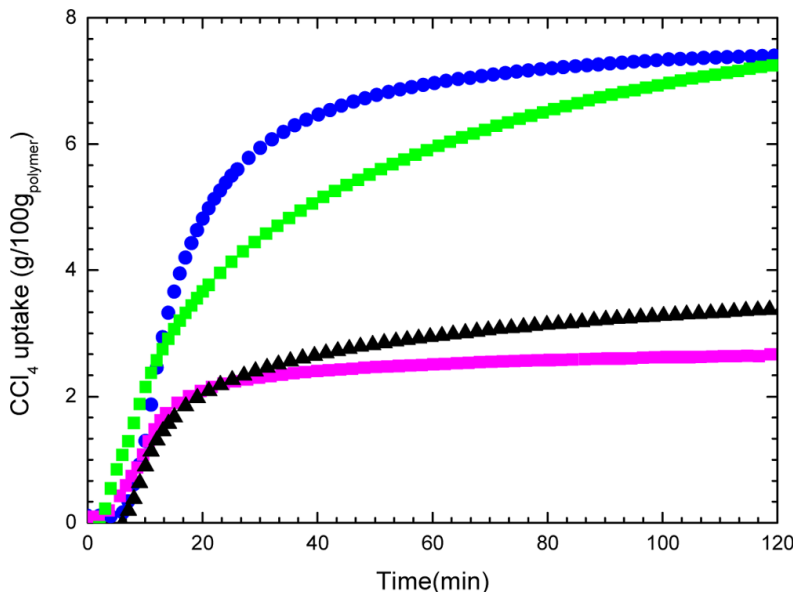


Figure 3.9. Sorption kinetics relative to a sudden increase of CCl_4 activity from zero up to $p/p^\circ = 0.01$, for the PPPO/s-PS 90/10 wt % aerogel (blue circles), for δ -s-PS aerogel (green squares), for PPPO amorphous powder (black triangles), and commercial PPPO semicrystalline powder (magenta squares).

In this respect, it is worth adding that the monolithic s-PS aerogel (squares in Figure 3.9), which exhibits the highest surface area (Table 3.1) and the highest CCl_4 uptake (Figure 7), presents a half time for the equilibrium higher than 20 min. This slower diffusivity of CCl_4 in s-PS samples can be easily rationalized on the basis of attractive interactions of CCl_4 molecules in the crystalline cavities of the δ form of s-PS, analogous to those studied in detail for other chlorinated organic guests.^{12b, 39, 40}

The same aerogels have been compared as for their ability to remove pollutants being present in traces in water. For instance

for PPPO/s-PS aerogels, the equilibrium uptake of CCl_4 and 1, 2-dichloroethane (DCE) from 10 ppm aqueous solutions are reported in Figure 3.10, versus the PPPO weight percent. It is worth noting that both the shape and the dimensions of the aerogels were not modified when immersed in aqueous solutions.

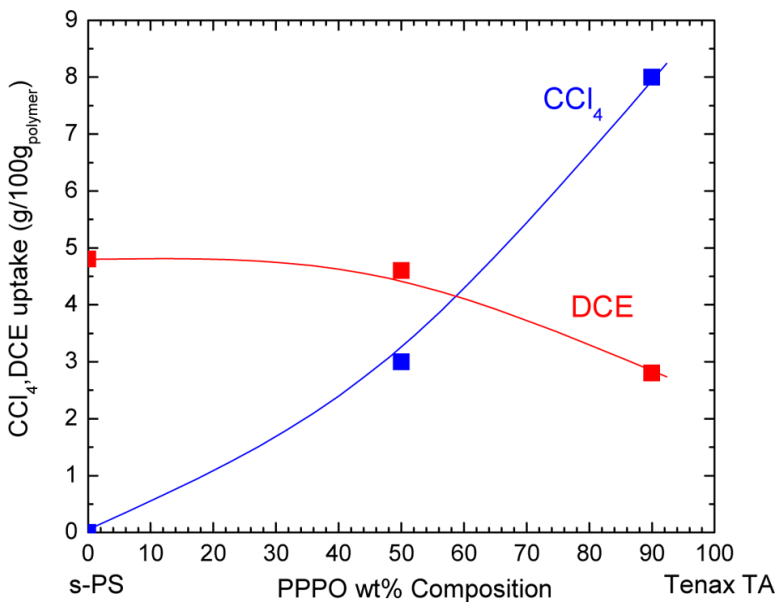


Figure 3. 10. Equilibrium uptake (wt %) of CCl_4 and DCE from dilute aqueous solutions (10 ppm) for PPPO/s-PS aerogels (as obtained from gels with $C_{\text{pol}} = 10$ wt %) vs the PPPO wt % composition. PPPO rich aerogels are particularly suitable for removal of CCl_4 traces from diluted aqueous solutions. Continuous lines are guide for eyes.

The uptake of CCl_4 by the PPPO/s-PS, 90/10 aerogel is large (nearly 8 wt %) also higher than for the commercial powder (7 wt %) and much higher than for the s-PS aerogel. In fact, s-PS aerogels, which are highly efficient in the removal of other similar organic guests, like DCE^{18f} (red curve in Figure 3. 10) and in the removal of the same CCl_4 guest from vapor phase (Figure 3. 8 and 3. 9), absorb a negligible amount of CCl_4 from diluted aqueous solutions.

3.5 Concluding remarks

Depending on the preparation procedure, fully amorphous PPPO samples with different amorphous halos indicating a different free volume can be obtained. The CCl_4 sorption measurements show that the guest uptake for fully amorphous powders, as obtained by scCO_2 extraction of concentrated solutions, can be much higher than for commercial sorbent materials based on semicrystalline PPPO (Tenax). Annealing procedures on both amorphous and semicrystalline samples can largely reduce the pollutant uptake, due to the densification of the amorphous phases. Hence, the sorption ability of PPPO samples is largely dependent on their preparation procedure as well as on their thermal history.

The comparison of molecular sorption behavior of the considered PPPO samples also allows to conclude that, differently from the case of PPO and as generally occurs for polymers, the guest uptake is essentially due to its amorphous phase while its crystalline phase is not nanoporous.

Although PPPO does not form physical gels from diluted solutions, gels can be easily obtained for blends with syndiotactic polystyrene (s-PS), also for PPPO/s-PS ratios as high as 90/10. These mixed gels lead to robust monolithic aerogels by sudden solvent extraction by scCO_2 . SEM experiments suggest that the obtaining of PPPO/s-PS aerogels

is due to the s-PS fibrillar morphology. The obtained aerogels exhibit fully amorphous PPPO with a high-free-volume amorphous phase. Moreover, s-PS rich (wt % > 50) aerogels exhibit, beside a high-free-volume PPPO amorphous phases, the highly sorbent nanoporous-crystalline δ phase of s-PS.

Monolithic PPPO/s-PS aerogels present many advantages as sorbent materials with respect to the commercially relevant PPPO powders. In fact, besides the obvious advantages in terms of easier and safer handling, the new monolithic aerogels generally present higher equilibrium guest uptake and maintain diffusivities similar to those of the powders. Volumetric N_2 adsorption isotherms show that the surface area (S_{BET}) increases in the aerogels with respect to the powders, by factors of roughly 2.3 and 10 for the monolithic 90/10 and 50/50 PPPO/s-PS aerogels. Particularly interesting is the CCl_4 uptake at low activities from the monolithic 90/10 PPPO/s-PS aerogel. In fact, the CCl_4 uptake from vapor phase at $p/p^\circ = 0.01$ (7.5 wt %) is nearly double than for the PPPO powders (in the range 2.5–4.5 wt %), whereas the uptake from diluted (10 ppm) aqueous solutions (8 wt %) is much higher than for the s-PS aerogel (<0.1%).

The observed increases of surface area and of guest uptakes in the aerogels, observed for the PPPO/s-PS aerogels with respect to the powders, are in part due the presence of the δ phase of s-PS and to its crystalline nanocavities and in part due to the less

dense packing of the amorphous phase in the aerogels. The whole set of results indicates that monolithic PPPO-based aerogels are particularly suitable for efficient, easy, and safe removal of pollutants from water and air.

Chapter 4

Monolithic Aerogels Based on Polyethylene

4. 1 Introduction

Polyethylene (PE) has become one of the most commonly used and widely investigated thermoplastic polymers with abundant applications that, depending on molecular architecture and molecular weight, range from common daily life objects (e. g. garbage bags and containers) to high-performance products such as ballistic protection items (e. g. bullet proof vests and shields) and medical implants.^{41a-d}

In literature the preparation of polyethylene gels with decaline are been already reported⁴² but aerogels of this polymer have never been achieved.

In this context, it must be stressed that high molecular masses promotes gel formation and thus, for this reason, among the various existing types of polyethylene, ultra high molecular weight polyethylene(UHMWPE) was chosen, also in accordance with the gelation procedure reported by Smith et al.⁴²

UHMWPE is a member of the polyethylene family with the repeat unit $[C_2H_4]_n$, with n denoting the degree of polymerization, is a linear (non-branching) semi-crystalline polymer. The crystalline phase contains chains folded into highly oriented lamellae, with the crystals being orthorhombic in

structure.⁴³ The lamellae are oriented randomly within the amorphous phase with tie molecules linking individual lamellae to one another.

This polymer combines many unique properties such as an abrasion resistance that is higher than of any known other thermoplastic; the highest impact toughness of all polymer materials, even at cryogenic temperatures; a good corrosion resistance; an excellent environmental stress-crack resistance and a low coefficient of surface friction.^{44a-b}

Furthermore, UHMWPE has been approved by the USDA, FDA, and National Bureau of Standards sanctions for pure water and food handling. For these reasons UHMWPE has found its way into many demanding applications, ranging from liners for hoppers and pipes in the food industry to medical and sport products.^{41b}

Because of the above, obtain a monolithic and highly porous morphology for this type of polyethylene is very interesting, since we have an innovative material with great capabilities.

4.2 Polyethylene gels

Physical crosslinked polyethylene gels were prepared from solutions of high molecular weight linear polyethylene ($M_w \sim 10^6$ g/mol). Smith et al.⁴² had previously investigated gelation / crystallization of polyethylene, however their goal was not the aerogel preparation, but to produce a solution spinning / drawing route.

In this study, the optimized procedure for the production of aerogels of polyethylene is described for the first time.

The gels were prepared from decaline solution at 160 °C, containing 10 % w/w of the polymer stabilized by 0.5 % w/w of the anti-oxidant di-t-butyl-p-cresol.

It is worth adding that the solution should be stirred, in order to favor fibrillar morphology, which, as mentioned above, is fundamental to obtaining a monolithic aerogel.

The SEM micrographs reported in the study by Smith et al. clearly show that the gel structure obtained from a solution that was kept at 160°C for 45 minutes after dissolution of the polymer included interconnected lamellar crystals, while the gel generated from a solution which was stirred at 160°C consist of fibrillar shish - kebab like crystal.

4.3 Preparation and structural characterization of polyethylene aerogels

By optimizing the gelation procedure reported by Smith et al., polyethylene gels were prepared from a decalin solution containing 10 wt% of polymer, and stabilized by 0.5 % w/w of the anti-oxidant di-t-butyl-p-cresol. The gel obtained was extracted with supercritical CO₂ and polyethylene aerogel was obtained (Figure 4.1).

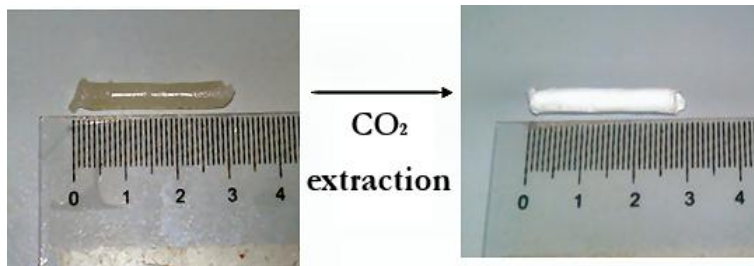


Figure 4. 1. Photographs of a piece of PE gel prepared in decaline at $C_{pol} = 0.10$ g/g, before and after complete solvent extraction via supercritical carbon dioxide (units of the ruler are cm).

In Figure 4.2 the X-ray diffraction patterns of the obtained PE aerogel and of commercial UHMWPE are reported.

The diffraction patterns of Figure 4.2 clearly show that the amorphous halo of polyethylene aerogel is significantly lower than the commercial polyethylene. This indicates that the polyethylene aerogel presents a higher degree of crystallinity

compared to the starting polyethylene. The degree of crystallinity of the samples was evaluated from X-ray diffraction data applying the standard procedure of resolving the diffraction pattern into two areas corresponding to the contributions of the crystalline and amorphous fractions for the 2Θ range 11–28°. For the PE aerogel, the observed degree of crystallinity is $X_c=80\%$, while for the commercial UHMWPE is $X_c=60\%$.

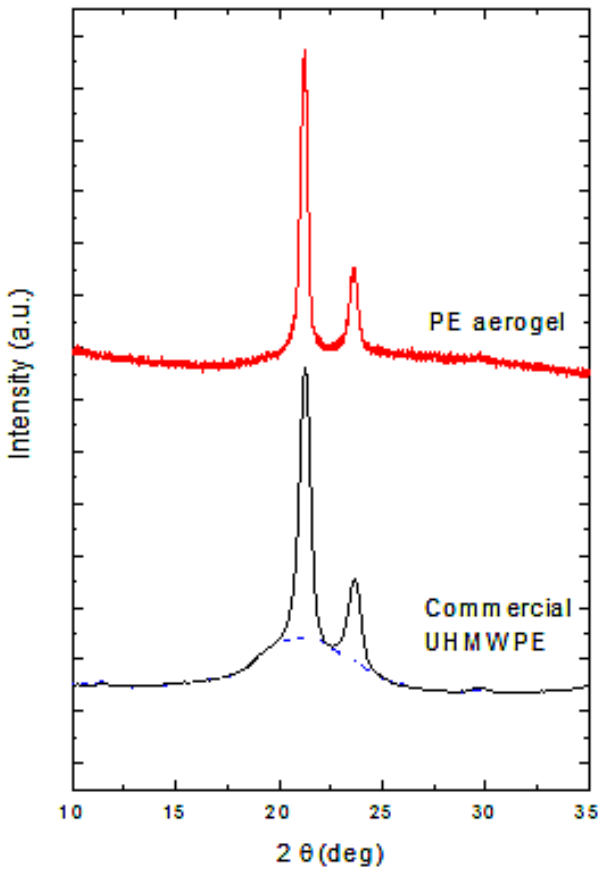


Figure 4. 2. X-ray diffraction patterns (CuK α radiation) of: polyethylene aerogel (red curve) and of the starting commercial UHMWPE (black curve).

Scanning Electron Microscopy (SEM) images of the aerogel are shown in Figure 4. 3.

As can clearly see, the typical morphology of lamellar polyethylene is maintained in the aerogel, but it is evident the presence of fibrils that maintain the monolithic structure.

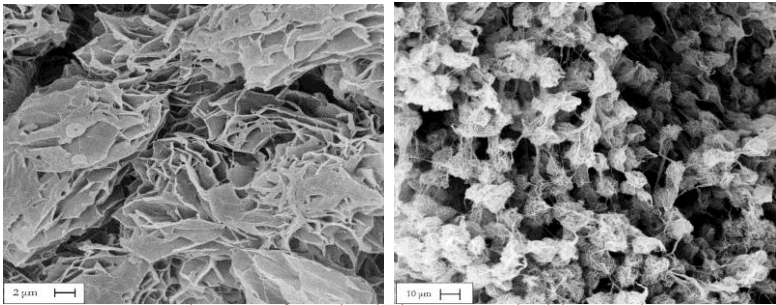


Figure 4. 3. SEM images of a polyethylene aerogel with porosity $P = 90\%$ obtained from a gel prepared in decaline with $C_{pol} = 10$ wt %, after complete solvent extraction by $scCO_2$.

Total surface areas, as obtained from N_2 isotherms (BET experiments) for UHMWPE aerogel and for the commercial polymer are compared in table 4. 1. As we can see, the surface area of the commercial UHMWPE is significantly lower compared to the aerogel surface area. This result is very interesting, because this data extends the range of application of the obtained aerogel.

Sample	$S_{\text{BET}}^{\text{a}}$ (m ² g ⁻¹)
Commercial UHMWPE	2,7
UHMWPE aerogel	66

^a Total area evaluated following the BET model in the standard 0. 05<P/P₀<0. 3 pressure range.

Table 4. 1. Total Surface Area (S_{BET}) of commercial HUMWPE and UHMWPE aerogel.

4.4 Concluding remarks

Procedures for obtaining polyethylene gels were studied, and literature suggests that aerogels based on this important polymer have never been prepared.

In this study aerogels preparation procedure has been optimized, starting from molecular ultra high molecular weight polyethylene, a polymer that has excellent properties, chosen to achieve the polyethylene gelation. X-ray diffraction patterns, shows that the aerogel preparation maximizes the degree of crystallinity compared to the commercial polyethylene. BET measurements also show that the aerogels surface area is significantly higher than the surface area of the commercial polyethylene powder. These polyethylene aerogels can be used for thermal insulation purposes, but also as a support for heterogeneous catalysis exploiting the preparation of its composite with metal catalysts.

References

- [1] a) R. W. Pekala, *J. Mater. Sci.* **1989**, *24*, 3221, b) R. W. Pekala, C. T. Alviso, X. Lu, J. Gross, J. Fricke, *J. Non-Cryst. Solids* **1995**, *188*, 34, c) W. C. Li, G. Reichenauer, J. Fricke, *Carbon* **2002**, *40*, 2955, d) Y. Tao, D. Noguchi, C. -M. Yang, H. Kanoh, H. Tanaka, M. Yudasaka, S. Iijima, K. Kaneko, *Langmuir* **2007**, *23*, 9155, e) P. Lorjai, T. Chaisuwan, S. Wongkasemjit, *J. Sol-Gel Sci. Technol.* **2009**, *52*, 56, f) W. F. Zhang, Z. H. Huang, C. Zhou, G. Cao, F. Kang, Y. Yang, *J. Mater. Chem.* **2012**, *22*, 7158, g) A. P. Katsoulidis, J. He, M. G. Kanatzidis, *Chem. Mater.* **2012**, *24*, 1937
- [2] a) J. M. Guenet, In *Thermoreversible Gelation of Polymers and Biopolymers*, Academic Press : London **1992**, b) C. Daniel, C. Dammer, J. M. Guenet, *Polymer* **1994**, *35*, 4243, c) A. Keller, *Faraday Discuss.* **1995**, *101*, 1, d) J. M. Guenet, In *Polymer- Solvent Molecular Compounds*, Elsevier Ltd. : Oxford **2008**, e) H. Itagaki, T. Tokami, J. Mochizuki, *Polymer* **2012**, *53*, 5304.
- [3] a) P. J. Bush, D. Pradhan, P. Ehrlich, *Macromolecules* **1991**, *24*, 1439, b) D. Pradhan, P. Ehrlich, *J. Polym. Sci. Polym. Phys.* **1995**, *33*, 1053, c) G. Beaucage, J. H. Aubert, R. R. Lagasse, D. W. Schaefer, T. P. Rieker, P. Erlich, R. S. Stein, S. Kulkarni, P. D. Whaley, *J. Polym. Sci. Part B Polym. Phys.* **1996**, *34*, 3063, d) D. Dasgupta, A. K. Nandi, *Macromolecules* **2007**, *40*, 2008, e) E. Reverchon, S. Cardea, C. Rapuano, *J. Supercrit. Fluids* **2008**, *45*, 365, f) E. Reverchon, P. Pisanti, S. Cardea, *Ind. Eng. Chem. Res.* **2009**, *48*, 5310, g) S. Cardea, A. Gugliuzza, M. Sessa, M. C. Aceto, E. Drioli, E. Reverchon, *ACS Appl. Mater. Interfaces* **2009**, *1*, 171, h) C. Daniel, J. G. Vitillo, G. Fasano, G. Guerra, *ACS Appl. Mater. Interfaces* **2011**, *3*, 969, i) J. M. Guenet, J. Parmentier, C. Daniel, *Soft Mater.* **2011**, *9*, 280, j) G. R. Peterson, K. A. Cychosz, M. Thommes, L. J. Hope-Weeks, *Chem. Commun.* **2012**, *48*, 11754.
- [4] a) H. Jin, Y. Nishiyama, M. Wada, S. Kuga, *Colloids Surf. A Physicochem. Eng. Aspects* **2004**, *240*, 63, b) R. Gavillon, T. Budtova, *Biomacromolecules* **2008**, *9*, 269, c) Z. J. Miao, K. L. Ding, T. B. Wu, Z. M. Liu, B. X. Han, G. M. An, S. D. Miao, G.

- Y. Yang, *Micropor. Mesopor. Mater.* **2008**, *111*, 104, d) M. Robitzler, L. David, C. Rochas, F. Di Renzo, F. Quignard, *Langmuir* **2008**, *24*, 12547, e) F. Quignard, R. Valentin, F. Di Renzo, *New J. Chem.* **2008**, *32*, 1300, f) S. Cardea, P. Pisanti, E. Reverchon, *J. Supercrit. Fluids* **2010**, *54*, 290, g) B. Ding, J. Cai, J. Huang, L. Zhang, Y. Chen, X. Shi, Y. Du, S. Kuga, *J. Mater. Chem.* **2012**, *22*, 5801, h) P. Del Gaudio, G. Auriemma, T. Mencherini, G. Della Porta, E. Reverchon, R. P. Aquino, *J. Pharm. Sci.* **2013**, *102*, 185.
- [5] S. S. Kistler, *J. Phys. Chem.* **1932**, *36*, 52.
- [6] C. Daniel, S. Longo, S. Cardea, J. G. Vitillo, G. Guerra, *RSC Adv.* **2012**, *2*, 12011
- [7] a) C. Daniel, C. Dammer, J. M. Guenet, *Polymer* **1994**, *35*, 4243, b) H. Itagaki, T. Tokami, J. Mochizuki, *Polymer* **2012**, *53*, 5304.
- [8] H. E. Bergna & W. O. Roberts, *Colloidal silica: Fundamentals and applications*, **2006**, 131, Boca Raton, Fla. : Taylor & Francis.
- [9] S. Sakka, *Handbook of sol-gel science and technology: processing, characterization and applications. Applications of sol-gel technology*. Kluwer academic, **2002**.
- [10] a) S. M. Kuznicki, V. A. Bell, S. Nair, H. W. Hillhouse, R. M. Jacobinas, C. M. Braunbarth, B. H. Toby, M. Tsapatsis, *Nature* **2001**, *412*, 720, b) W. J. Blau, A. J. Fleming, *Science* **2004**, *304*, 1457, c) A. Zecchina, S. Bordiga, J. G. Vitillo, G. Ricchiardi, C. Lamberti, G. Spoto, M. Bjorgen, K. P. Lillerud, *J. Am. Chem. Soc.* **2005**, *127*, 6361, d) A. R. Millward, O. M. Yaghi, *J. Am. Chem. Soc.* **2005**, *127*, 17998, e) P. K. Thallapally, B. P. McGrail, J. L. Atwood, C. Gaeta, C. Tedesco, P. Neri, *Chem. Mater.* **2007**, *19*, 3355.
- [11] a) M. Iuliano, G. Guerra, V. Petraccone, P. Corradini, C. Pellecchia, *New Polym. Mater.* **1992**, *3*, 133, b) N. Galdi, A. R. Alburnia, L. Oliva, G. Guerra, *Polymer* **2009**, *50*, 1901.
- [12] a) C. De Rosa, G. Guerra, V. Petraccone, B. Pirozzi, *Macromolecules* **1997**, *30*, 4147, b) G. Guerra, G. Milano, V. Venditto, P. Musto, C. De Rosa, L. Cavallo, *Chem. Mater.* **2000**, *12*, 363 c) G. Milano, V. Venditto, G. Guerra, L. Cavallo, P. Ciambelli, D. Sannino, *Chem. Mater.* **2001**, *13*, 1506, d) E. B.

- Gowd, N. Shibayama, K. Tashiro, *Macromolecules* **2006**, *39*, 8412, e) P. Rizzo, C. Daniel, A. De Girolamo Del Mauro, G. Guerra, *Chem. Mater.* **2007**, *19*, 3864, f) V. Petraccone, O. Ruiz de Ballesteros, O. Tarallo, P. Rizzo, G. Guerra, *Chem. Mater.* **2008**, *20*, 3663, g) A. R. Alburnia, P. Rizzo, G. Guerra, *Chem. Mater.* **2009**, *21*, 3370, h) G. Guerra, C. Daniel, P. Rizzo, O. Tarallo, *J. Polym. Sci. Polym. Phys. Ed.* **2012**, *50*, 305.
- [13] a) C. Daniel, Longo, S., J. G. Vitillo, G. Fasano, G. Guerra, *Chem. Mater.* **2011**, *23*, 3195, b) O. Tarallo, V. Petraccone, C. Daniel, G. Fasano, P. Rizzo, G. Guerra, *J. Mater. Chem.* **2012**, *22*, 11672, c) M. Galizia, C. Daniel, G. Fasano, G. Guerra, G. Mensitieri, *Macromolecules* **2012**, *45*, 3604, d) C. Daniel, D. Zhovner, G. Guerra, *Macromolecules* **2013**, *46*, 449, e) P. Rizzo, G. Ianniello, S. Longo, G. Guerra, *Macromolecules* **2013**, *46*, 399.
- [14] a) E. Reverchon, G. Guerra, V. Venditto, *J. Appl. Polym. Sci.* **1999**, *74*, 2077, b) W. Ma, J. Yu, J. He, *Macromolecules* **2005**, *38*, 4755, c) J. Fang, E. Kiran, *Macromolecules* **2008**, *41*, 7525.
- [15] a) Chatani Y., Shimane Y., Inagaki, T., Ijitsu T., Yukinari T., Shikuma H., *Polymer*, **1993**, *34*, 1620, b) De Rosa C., Rizzo P., Ruiz de Ballesteros O., Petraccone V., Guerra G., *Polymer*, **1999**, *40*, 2103 c) Tarallo O., Petraccone V., *Macromolecules*, **2004**, *205*, 1351.
- [16] a) V. Petraccone, O. Tarallo, V. Venditto, G. Guerra, *Macromolecules* **2005**, *38*, 6965, b) O. Tarallo, V. Petraccone, V. Venditto, G. Guerra, *Polymer* **2006**, *47*, 2402, c) C. D'Aniello, D. Dondi, A. Faucitano, G. Guerra, *Macromolecules* **2010**, *43*, 10560.
- [17] a) O. Tarallo, M. M. Schiavone, V. Petraccone, C. Daniel, P. Rizzo, G. Guerra, *Macromolecules* **2010**, *43*, 1455, b) A. R. Alburnia, C. D'Aniello, G. Guerra, *Cryst. Eng. Commun.* **2010**, *12*, 3942, c) A. R. Alburnia, P. Rizzo, M. Coppola, M. De Pascale, G. Guerra, *Polymer* **2012**, *53*, 2727.
- [18] a) C. Daniel, M. D. Deluca, J. M. Guenet, A. Brulet, A. Menelle, *Polymer* **1996**, *37*, 1273, b) S. Rastogi, J. G. P. Goossens, P. J. Lemstra, *Macromolecules* **1998**, *31*, 2983, c) C. S. J. van Hooy-Corstjens, P. C. M. M. Magusin, S. Rastogi, P. J. Lemstra, *Macromolecules* **2002**, *35*, 6630, d) C. Daniel, P. Musto, G. Guerra, *Macromolecules* **2002**, *35*, 2243, e) C. Daniel, D. Alfano, G.

- Guerra, P. Musto, *Macromolecules* **2003**, *36*, 1713, f) S. Malik, C. Rochas, J. M. Guenet, *Macromolecules* **2006**, *39*, 1000, g) C. Daniel, A. Avallone, P. Rizzo, G. Guerra, *Macromolecules* **2006**, *39*, 4820.
- [19] a) G. Guerra, G. Mensitieri, V. Venditto, E. Reverchon, C. Daniel, *PCT Int. Appl.* **2005**, WO 2005012402, b) C. Daniel, D. Alfano, V. Venditto, S. Cardea, E. Reverchon, D. Larobina, G. Mensitieri, G. Guerra, *Adv. Mater.* **2005**, *17*, 1515, c) S. Malik, C. Rochas, J. -M. Guenet, *Macromolecules* **2005**, *38*, 4888, d) S. Malik, D. Roizard, J. -M. Guenet, *Macromolecules* **2006**, *39*, 5957, e) C. Daniel, D. Sannino, G. Guerra, *Chem. Mater.* **2008**, *20*, 577, f) C. Daniel, S. Giudice, G. Guerra, *Chem. Mater.* **2009**, *21*, 1028, g) C. Daniel, F. Bernardo, *Macromol. Symp.* **2011**, *303*, 37.
- [20] a) A. Immirzi, F. de Candia, P. Iannelli, A. Zambelli, V. Vittoria, *Makromol. Chem., Rapid Commun.* **1988**, *9*, 761, b) P. Rizzo, M. Lamberti, A. R. Alburnia, O. Ruiz de Ballesteros, G. Guerra, *Macromolecules* **2002**, *35*, 5854, c) P. Rizzo, A. R. Alburnia, G. Guerra, *Polymer* **2005**, *46*, 9549.
- [21] a) C. De Rosa, M. Rapacciuolo, G. Guerra, V. Petraccone, P. Corradini, *Polymer* **1992**, *3*, 1423, b) Y. Chatani, Y. Shimane, T. Ijitsu, T. Yukinari, *Polymer* **1993**, *34*, 1625.
- [22] A. Buonerba, C. Cuomo, S. O. Sanchez, P. Canton and A. Grassi, *Chem. -Eur. J.*, **2012**, *18*, 709.
- [23] (a) M. Barrales-Rienda and J. M. G. Fatou, *Kolloid. Z. Z. Polym.*, **1971**, *244*, 317, (b) S. Horikiri, *J. Polym. Sci., Part A-2*, **1972**, *10*, 1167, (c) J. Hurek and E. Turska, *Acta Polym.*, **1984**, *35*, 201.
- [24] A. Factor, G. E. Heinsohn and L. H. Vogt Jr., *J. Polym. Sci., Part B: Polym. Lett.*, **1969**, *7*, 205, (b) O. M. Ilinitch, G. L. Semin, M. V. Chertova and K. I. Zamaraev, *J. Membr. Sci.*, **1992**, *66*, *1*, (c) M. Aguilar-Vega and D. R. Paul, *J. Polym. Sci., Part B: Polym. Phys.*, **1993**, *31*, 1577, (d) A. Alentiev, E. Drioli, M. Gokzhaev, G. Golemme, O. M. Ilinitch, A. A. Lapkin, V. Volkov and Yu Yampolskii, *J. Membr. Sci.*, **1998**, *138*, 99, (e) K. C. Khulbe, T. Matsuura, G. Lamarche and A. -M. Lamarche, *J. Membr. Sci.*, **2000**, *170*, 81, (f) D. M. Sterescu, D. F. Stamatialis,

- E. Mendes, J. Kruse, K. Ratzke, F. Faupel and M. Wessling, *Macromolecules*, **2007**, 40, 5400.
- [25] a) G. Guerra, C. De Rosa, V. M. Vitagliano, V. Petraccone, P. Corradini *J. Polym. Sci., Polym. Phys. Ed.* **1991**, 23, 265. b) G. Guerra, C. De Rosa, V. M. Vitagliano, V. Petraccone, P. Corradini, F. E. Karasz *Polym. Commun.* **1991**, 32, 30. c) Cimmino, S, Di Pace, E., Martuscelli, E., Silvestre, C. *Polymer* **1993**, 34, 2799. d) Woo E. M., Wu F. S. *Macromol. Chem. Phys.* **1998**, 199, 2041. e) Hong, B. K., Jo, W. H., Lee, S. C., Kim, J. *Polymer* **1998**, 39, 1793.
- [26] (a) C. De Rosa, M. Rapacciuolo, G. Guerra, V. Petraccone and P. Corradini, *Polymer*, **1992**, 33, 1423, (b) Y. Chatani, Y. Shimane, T. Ijitsu and T. Yukinari, *Polymer*, **1993**, 34, 1625.
- [27] (a) ATSDR. **2005**. *Toxicological Profile for Carbon Tetrachloride*. Agency for Toxic Substances and Disease Registry. <http://www.atsdr.cdc.gov/toxprofiles/tp30.pdf>. (b)W. F. Seifert, A. Bosma, A. Brouwer et al. *Hepatology*, 19 (1), 193-201. (c)K. X. Liu, Y. Kato, M. Yamazaki, O. Higuchi, T. Nakamura, Y. Sugiyama, *Hepatology*, **1993**, 17(4), 651-60. (d)R. O. Recknagel, E. A. Glende, J. A. Dolak, R. L. Waller. *Pharmacology Therapeutics*, **1989**, 43, 139-154. (e)R. O. Recknagel, *Pharmacol. Rev.*, **1967**, 19, 145-208. (f)A. S. Rood, P. D. McGavran, J. W. Aanenson, J. E. Till. *Risk Anal.*, **2001**, 21, 675-695. (g) P. Fraser, *Australian Meteorological Magazine*, **46**, 185-193. (h) W. F. J. Evans, E. Pukrin, *Geophysical Reserach Letters*, **1996**, 23(14), 1769-1772. (i) S. J. Walker, R. F. Weiss & P. K. Salameh, *Journal of Geophysical Research*, **2000**, 105, 14285-14296.
- [28] a) 1, 2-Dichoroethane MSDS. " Mallinckrodt Chemicals. 19 May 2008. Web. <http://hazard.com/msds/mf/baker/baker/files/d2440.htm>. b) ATSDR. 2005. *Toxicological Profile for 1, 2 Dichloroethane*. Agency for Toxic Substances and Disease Registry. <http://www.atsdr.cdc.gov/toxprofiles/tp38.pdf>. (accessed, november 2013)
- [29] (a) Sampson, James E., Blankenship, Forrest, *Proceedings of the Oklaboma Academy of Science* **1948**, 28, 112-13 (b) Kaloustian, J., Rosso, J. C., Caranoni, C., Carbonnel, L., *Revue de Chimie*

Minerale **1976**, 13, (4), 334-42.

[30] (a) CalEPA Air Resources Board Toxic Air Contaminant Summary (accessed, november 2013)(b) ChemFinder WebServer Project (1995) (accessed, november 2013)(c)Environmental Defense Fund - Summary, Uses, Consumer Products, Rank (industrial, by quantity)(accessed, november 2013)(d)IPCS International Chemical Safety Card (accessed, november 2013).

[31] Hay, A. S. U. S. Patent 3 432 466, March 11, 1969.

[32] Van Wijk, *Chromatogr. Sci.* **1970**, 8, 418–420.

[33] (a) I. Maier, M. Fieber, . *J. High Resolut. Chromatogr.* **1988**, 11, 566–576. (b) J. Jens Laaks, M. A. Jochmann, B. Schilling, T. C. Schmidt, *Anal. Chem.* **2010**, 82, 7641–7648. (c) Y. H. Kim, *Anal. Chem.* **2012**, 84, 8284–8293. (d) B. Alfeeli, L. T. Taylor, M. Agah, *Microchem. J.* **2010**, 95, 259–267. (e) B. Alfeeli, V. Jain, R. K. Johnson, F. L. Beyer, J. R. Heflin, M. Agah, *Microchem. J.* **2011**, 98, 240–245.

[34] K. Dettmer, W. Engewald, *Anal. Bioanal. Chem.* **2002**, 373, 49M0–500.

[35] (a) M. Harper, *J. Chromatogr.*, **2000**, 885, 129–151. (b) A. M. P Oen, G. D. Breedveld, S. Kalaitzidis, K. Christanis, G. Cornelissen, *Environ. Toxicol. Chem.* **2006**, 25, 1258–1267. (c) J. M. Barrero-Moreno, S. Tirendi, F. Reniero, G. Giordano, D. Kotzias, *Rapid Commun. Mass Spectrom.* **2008**, 22, 471–476. (d)P. Leva, A. Katsoyiannis, , J. Barrero-Morero, S. Kephelopoulos, D. J. Kotzias, *Environ. Sci. Health, Part B*, **2009**, 44, 51–57.

[36]W. Wrasidlo, *Macromolecules* **1971**, 5, 642–648.

[37] (a) A. H Chan, D. R. Paul, *J. Appl. Polym. Sci.* **1979**, 24, 1539–1550. (b) A. H. Chan, D. R. Paul, *Polym. Eng. Sci.* **1980**, 20, 87–94.

[38] T. Sago, H. Itagaki, *Soft Mater.* **2011**, 9, 199–223.

[39] Y. Tamai, Y. Tsujita, M. Fukuda, *J. Mol. Struct.* **2005**, 739, 33–40.

[40] G. Milano, G. Guerra, . *Progr. Mater. Sci.* **2009**, 54, 68–88.

[41] a)Polysciences, Inc., Polymer/Monomer Catalog **1998-**

2000. b) L. E. Smith, P. H. Verdier, in *Encyclopedia of Polymer Science and Engineering*, 2nd ed. H. F. Mark, N. M. Bikales, C. G. Overberger, G. Menges, Wiley:New York, **1988**, 12, 690. c) A. E. Zachariades, P. C. Watts, R. S. Porter, *Polym. Eng. Sci.*, **1980**, 20, 555 d) A. E. Zachariades, T. Kanamoto, *Polym. Eng. Sci.*, **1986**, 26, 658.
- [42] P. Smith, P. J. Lemstra, H. C. Booij, *J. Polym. Sci., Phys.*, **1981**, 19, 877.
- [43] L. Lin, A. S. Argon. *Journal of Materials Science*. **1994**, 29, 294–323.
- [44] a) J. Tong, M. Yunhai, R. D. Arnell, R. Ren, Luquan, *Composites Part A: Applied Science and Manufacturing* **2006**, 37, 1, 38-45 b) Budinski, G. Kenneth, *Wear*. **1997**, 203, 302-309.

Part II :

Nanocomposites

Physically Crosslinked

Polymeric Aerogels

Chapter 1

Nanocomposites Physically Crosslinked

Polymeric Aerogels

1.1 Introduction : the concept of Nanocomposites

Nanocomposites are composites in which at least one of the phases has dimensions in the nanometer range.¹ These are high performance materials that exhibit unusual property combinations and unique design possibilities and are thought of as the materials of the 21st century. With an estimated annual growth rate of about 25% and huge demand for engineering polymers, their potential is so promising that they are votes in several applications ranging from packaging to bio-medical. In the last two decades literature survey reveals that about 18, 000 publications, including papers and patents, have been published on nanocomposites. It is well known that at the nanoscale (below about 100 nm), a material's property can change dramatically. With only a reduction in size and no change in the substance itself, materials can exhibit new properties such as electrical conductivity, insulating behavior, elasticity, greater strength, different color, and greater reactivity-characteristics that the very same substances do not exhibit at the micro- or macroscale. Additionally, as dimensions reaches the nanometer

level, interactions at interfaces of phases become largely improved, and this is important to enhance materials properties. In this context, the surface area/volume ratio of reinforcement materials employed in the preparation of nanocomposites is crucial to the understanding of their structure–property relationships.

Among the various types of nanocomposites, polymer nanocomposites are the most promising. Polymer nanocomposites exhibit superior properties, such as mechanical, barrier, optical, etc. as compared to micro- or macrocomposites. Owing to this, polymer nanocomposites have shown ubiquitous presence in various fields of application. Polymer nanocomposites for various applications could be synthesized by proper selection of matrix, nanoreinforcement, synthesis method and surface modification of either the reinforcement or polymer (if required). Many products based on polymer nanocomposites have been commercialized.

With these premises, the importance of having highly porous materials, such as polymeric aerogels, with nanofillers can be easily understood.

In this section the achievement of monolithic nanocomposite aerogels with nanofillers such as organically modified montmorillonite (OMMT)² and reduced graphite oxide (r-GO) is described.

Monolithic nanocomposite aerogels, with large amounts of both intercalated and exfoliated OMMT and including the nanoporous-crystalline δ form of syndiotactic polystyrene (s-PS), have been prepared, by scCO_2 extractions of s-PS-based gels. Also for high OMMT content, the gel and aerogel preparation procedures occur without re-aggregation of the exfoliated clay, which is instead observed for other kinds of polymer processing. Analogous aerogels were prepared with GO. The most important result of the study is that the aerogel preparation allows the inclusion of also large amount of nanofillers, at least up to a content of 20 wt%.

Composite aerogels exhibiting large nanofiller content, can be used as catalyst support, in the case of r-GO, and generally, as masterbatches for polymer composites.

This is potentially very important because using masterbatches rather than dry powders means industrially a cleaner plant with minimal housekeeping effect.

Dust exposure is greatly reduced with masterbatches, as material handling is simplified with free-flowing, non bridging materials that can be transferred easily with pneumatic conveyors. It is worth adding that using masterbatches is especially important because eliminates employee exposure hazards associated with some powders and liquid.

1.2 The nanofillers

1.2.1 Organically modified montmorillonite

The clay known as montmorillonite consists of platelets with an inner octahedral layer sandwiched between two silicate tetrahedral layers ⁴ as illustrated in Figure 1.1. The octahedral layer may be thought of as an aluminum oxide sheet where some of the aluminum atoms have been replaced with magnesium; the difference in valences of Al and Mg creates negative charges distributed within the plane of the platelets that are balanced by positive counterions, typically sodium ions, located between the platelets or in the galleries as shown in Figure 1.1. In its natural state, this clay exists as stacks of many platelets. Hydration of the sodium ions causes the galleries to expand and the clay to swell; indeed, these platelets can be fully dispersed in water. The sodium ions can be exchanged with organic cations, such as those from an ammonium salt, to form an organoclay *OCs*.^{5a-h, 6}

The ammonium cation may have hydrocarbon tails and other groups attached and is referred to as a “surfactant” owing to its amphiphilic nature.

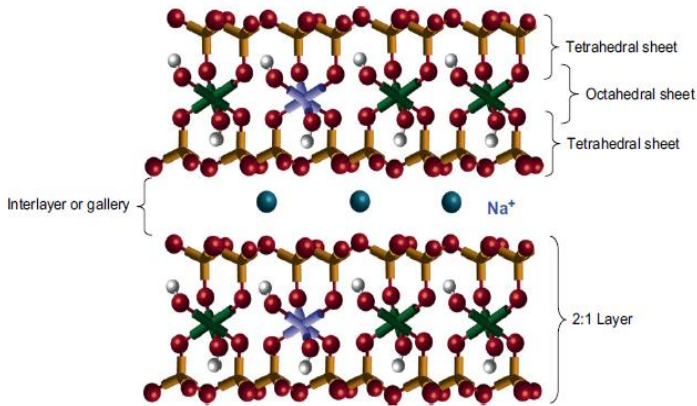


Figure 1.1. Structure of sodium montmorillonite.

The extent of the negative charge of the clay is characterized by the cation exchange capacity, i. e., CEC (here, we define the C. E.C. as the total amount of cations available for exchange at a given pH, which is commonly expressed as milliequivalent/100 g of calcined clay).

Alkylammonium salts act as compatibilizers with a hydrocarbon polymer matrix and the organization of the *OCs* in the polymeric matrix has a major influence on the properties of the composite material. As it is known, in the literature the following types of composites arising from the interaction of *OCs* and polymers are proposed (see figure 1.2), and they are called respectively microcomposite, exfoliated nanocomposite and intercalated nanocomposite.⁶⁻⁸

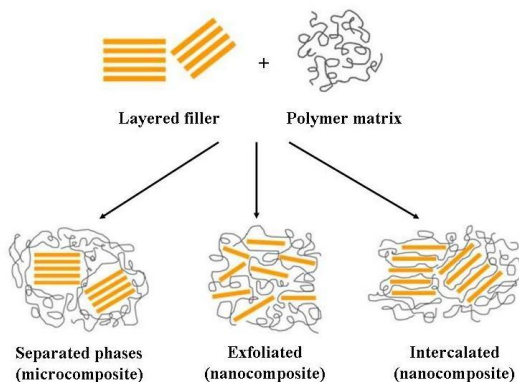
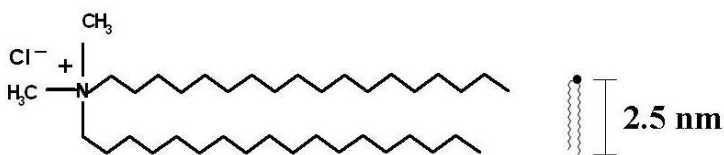


Figure 1.2 Schematic representation of the organizations proposed in the literature for polymeric composites containing *OCs*.

In our case the used organically modified clay, is a montmorillonite with 40 wt % of di(hydrogenated tallow)-dimethylammonium (2HT) commercially available as Dellite® 67G (Figure 1.3).



2HT: Di(hydrogenated tallow) dimethyl ammonium chloride

Figure 1.3. Chemical structure of *2HT* and its schematic representation.

1.2.2 Graphene Oxide

Graphene, a two dimensionally arranged and densely packed honeycomb lattice with sp^2 hybridized carbon atoms is the thinnest known material in the universe till date ⁹⁻¹¹. Graphene is one of the special allotrope of carbon, become 'rising star' among all other carbon nanomaterials in various fields of research owing to its unique physicochemical properties ^{12a-c}. Its unique properties include high surface area, tunable band gap, room temperature hall effect, excellent electrical, thermal and conducting properties. ^{12d, e}

It can be viewed as mother of other graphitic allotrope forms; it can wrap into fullerene (0D), rolled up into carbon nanotubes (1D) and stacked into multilayered graphite (3D) ^{13, 14} (Figure1.4).

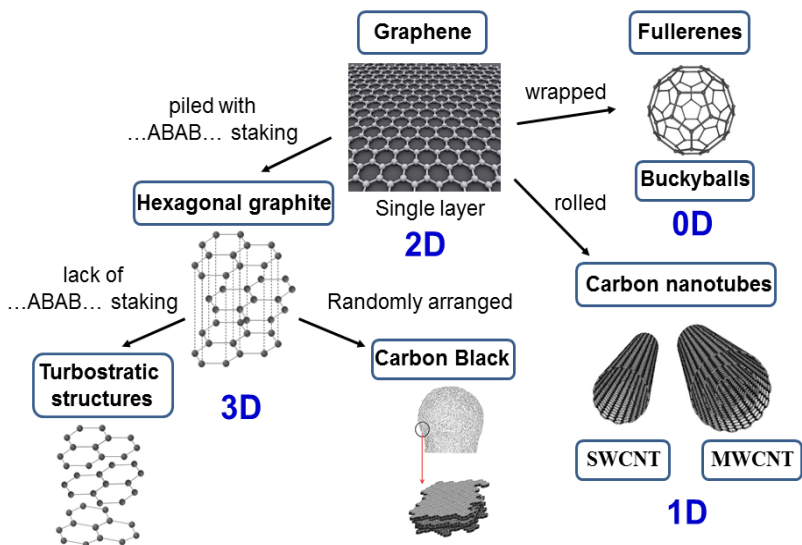


Figure 1.4 Mother of all graphitic forms. Graphene is a 2D building material for carbon materials of all other dimensionalities. It can be wrapped up into 0D buckyballs, rolled into 1D nanotubes, piled with a ...ABAB... stacking into 3D graphite or randomly stacked in primary particles of carbon black.

It shows great potential applications in various fields of research such as electronics ^{15a}, photocatalysis ^{15b}, solar cells ^{15c}, supercapacitors ^{15d}, medicine ^{15e} sensors ^{15f} and biosensors. ^{15g}

Graphene can be prepared by number of methods such as micromechanical exfoliation, epitaxial growth on silicon carbide, chemical vapor deposition (CVD), arc discharge method, small molecules intercalation within multilayered graphite, unzipping

of CNTs, electrochemical method and, as mentioned above, chemical reduction of exfoliated GO.^{14,16}

Each method holds its own advantages and disadvantages:

- Mechanical exfoliation of highly oriented pyrolytic graphite, also called as simple scotch tape method offer high quality graphene for the electronic applications with the associated disadvantages of low yield of graphene.⁹
- CVD growth of hydrocarbons on transition metal substrates (Cu, Ni, Co)^{17, 19, 20a-f} and epitaxial growth of graphene layers on silicon carbide can provide bulk quantity of graphene, but requires high temperature and high cost.^{17,18}
- Intercalation of small molecules and subsequent exfoliation (via thermal shock^{19c}, microwave exfoliation^{19d}, sonication approaches^{19e}) eventually break the multilayered graphite network into monolayered graphene sheets with high quality and defects free^{19f}.

Numbers of approaches were made to prepare high quality graphene sheets via unzipping of CNTs which has the disadvantage of time consuming process^{19g, 20a}. Chemical methods involve use of cheap and easily available graphite powder as the starting precursor with the simple set of process involving oxidation, exfoliation and reduction respectively.^{20b}

Chemical oxidation of graphite to graphite oxide, its exfoliation to monolayered graphene oxide (GO) and its subsequent reduction to graphene is one of the efficient approach to prepare scalable bulk quantity of graphene.^{20b}

Chemical oxidation of graphite can be achieved by Brodie method,^{20c} Staudenmaier method^{20d} and Hummer's method.^{20e,}^{20f} Exfoliation of graphite oxide can be achieved by microwave assistance,^{20g} ultrasonication^{20h} and thermally.²⁰ⁱ

Reduction of GO can be performed by using reducing agents (hydrazine,^{15f} sodium borohydride,^{21a} hydroquinone,^{21b} ascorbic acid,^{21c} alcohols,^{21d} alkali solutions,^{21e, f} and reducing sugars^{21g} such as glucose, fructose and sucrose) thermal methods,^{21h} and electrochemical reduction methods.^{21i,1}

Though the chemical oxidation-reduction approach give low quality graphene with residual oxygen functionalities and structural defects, until now this is the most versatile and desirable route for the production of bulk quantities of graphene for many applications.²² Specifically, chemical oxidation-reduction method has profound impact for the electrochemical applications where the defects and residual functional groups have specific advantageous. The ambitious vision to find a perfect method for the synthesis of defect free, bulk quantity of high quality graphene with 100% sp^2 carbon atoms of perfect

planar structure is a long time goal in the field of graphene based research.

Graphene oxide (GO), oxygenated derivative of graphene is an amphiphilic molecule having the structural network of interconnected random distribution of aliphatic and aromatic regions. ²³GO possess hydrophilicity owing to the presence of oxidized aliphatic regions containing tetrahedral sp^3 carbon atoms, whereas hydrophobicity is due to the presence of aromatic regions with unoxidised benzene rings containing planar sp^2 carbon atoms. ²⁴ It contains numerous functional groups mainly epoxy and hydroxyl groups on the plane, whereas carboxyl, carbonyl, ester, ether, diol, ketone, phenol, quinine and lactones groups present at the edge surfaces of the GO sheets. ^{25, 26}(Figure1.5)

The oxygen functionalities present on the basal and edge planes render it for the high dispersion in aqueous solutions and pave a way for the chemical functionalization, ²³such as amidation at the carboxylic groups ²⁷ and nucleophilic substitution via epoxy groups. ²⁸ On the other hand, the aromatic regions having sp^2 networks provide active sites to interact with other aromatic molecules through π - π supramolecular interactions. ²⁹

Thus GO is a very important precursor compound for the

preparation of graphene based composite materials with metals, metal oxides, polymers and CNTs for the diverse range of applications.

Chapter 2

Clay exfoliation and polymer/clay aerogels by supercritical carbon dioxide

2.1 Introduction

Over the last decades, clay polymer nanocomposites (CPN)^{5a, 6, 8, 30a-c} have been steadily increasing their importance in the field of material science, as they substantially improve polymer properties such as mechanical reinforcement, impermeability, thermal stability.^{31, 32} Superior properties are achieved when individual clay layers or stacks of few layers are evenly distributed in the polymer matrix and polymer-clay interfaces are maximized.^{33a-c} CPN exhibiting exfoliated clays are difficult to attain, particularly in the case of nonpolar polymers.^{34a-f}

Many reports show that different processing techniques based on supercritical carbon dioxide (scCO₂) constitute effective ways to increase dispersion and delamination in polymer/clay nanocomposites.^{35a-g} However, X-ray characterization of most samples show the presence of basal 00 ℓ reflections, clearly indicating that treatments with scCO₂ are generally unsuitable to induce complete organoclay exfoliation.^{35a-g}

Only some reports, from the Kannan's group, show that a

complete disappearance of the 00 l reflections (and hence a complete exfoliation) can be achieved by scCO₂ treatments on pure organoclays, where alkali counterions have been exchanged with long-chain alkylammoniums.^{36a, b} However, as a consequence of preparation of polymer nanocomposites, the 00 l reflections reappear with peak height and location essentially independent of the processing conditions.^{36b}

As mentioned above, scCO₂ treatments are also effective to prepare monolithic aerogels, by drying of wet gels.

In this chapter are described a deeper investigation of the scCO₂ induced organoclay exfoliation, by a more complete X-ray diffraction characterization of organoclays before and after scCO₂ treatments, and the preparation of composite aerogels containing large amounts of exfoliated organoclay as well as a nanoporous-crystalline polymer phase. The basic idea is that aerogel preparation processes, also based on scCO₂ extraction, could help to maintain the clay exfoliation, which is generally lost in the nanocomposite processing.^{36b} Advanced properties are pursued, through the synergy of aerogels and exfoliated clays. A montmorillonite (MMT) intercalated with dimethyl di(hydrogenated tallow) (2HT) ammonium cation was selected as the organoclay (OMMT in the following).

2.2 OMMT exfoliation by scCO_2

The X-ray diffraction pattern in the 2θ range $2-80^\circ$ of the OMMT, with 40 wt % of 2HT, is reported in Figure 2. 1A. Besides many $00l$ reflections (up to $l = 12$) that indicate a high degree of order perpendicular to the clay layers and an interlayer spacing of 3.5 nm, the pattern shows well defined weak peaks, corresponding to the typical 020, 210 and 060 in-plane MMT periodicities.^{34d, 37} It is worth adding that a well defined narrow peak is also present at $2\theta = 21.7^\circ$, corresponding to $d = 0.41$ nm, i. e. the distance between long hydrocarbon chains in their rotator order, analogous to those observed for long-chain alkylammoniums intercalated in anionic clays (layered double hydroxide, LDH)³⁸ as well as in graphite oxide.³⁹ The thickness of the clay layer (≈ 1 nm) and the length of the alkylammoniums (≈ 5 nm)⁴⁰ indicate that the tilting angle of the hydrocarbon chains is not far from $\alpha = 60^\circ$. Hence, the X-ray diffraction pattern of Figure 2. 5A indicates the presence of a MMT/2HT intercalate structure, whose schematic projections, parallel and perpendicular to the clay layers, are shown in Figures 2. 5A and 2. 5B, respectively.

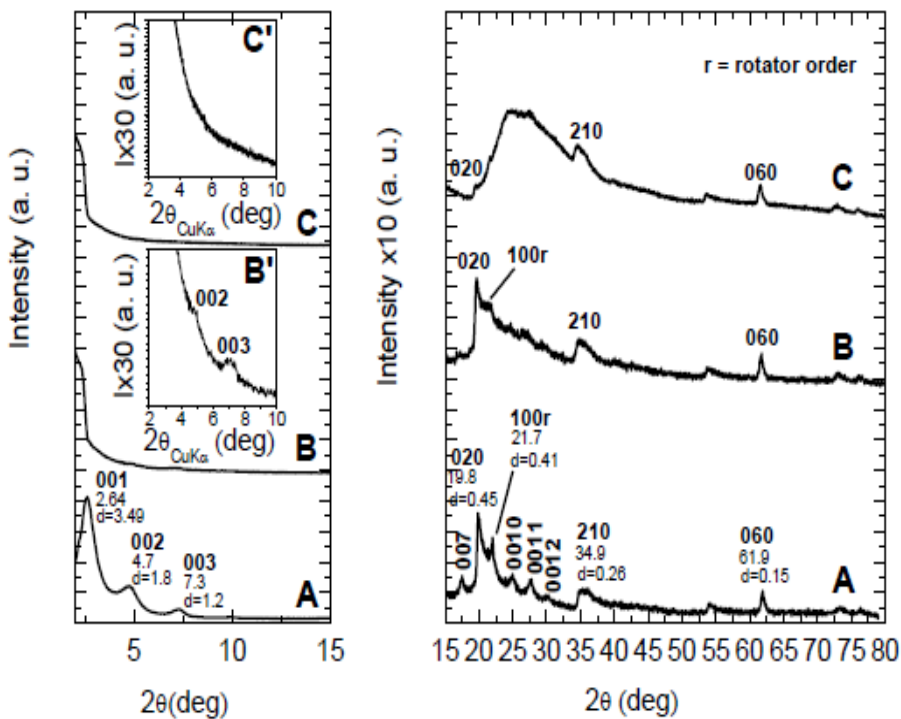


Figure 2.1 X-ray diffraction ($\text{CuK}\alpha$) patterns in the 2θ range $2\text{--}80^\circ$ of MMT, as intercalated with 40 wt % of 2HT ammonium before (A) and after 16h (B) and 32h (C) scCO_2 treatments. The inset in B and C enlarges the 2θ range $2\text{--}10^\circ$. The Miller index $110r$ indicate the reflection relative to the rotator order of the long hydrocarbon chains within the interlayer space.

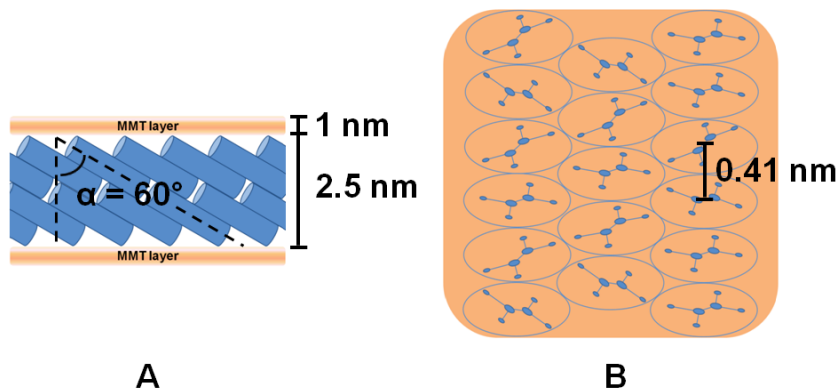


Figure 2. 2 Schematic projections parallel (A) and perpendicular (B) to the clay layers of the starting MMT/2HT (OMMT) intercalate structure. The hydrocarbon tails of the ammonium cations are represented as cylinders in the lateral view (A) and as ellipses in the top view (B). The distance between the axes of adjacent cylinders (0.41 nm) is shown in B while the definition of the alkyl chains tilt angle is shown in A.

The X-ray diffraction patterns of the OMMT of Figure 2.1 A, after short term and long term treatments by scCO_2 are shown in Figures 2.1B and 2.1C, respectively.

For the intermediate pattern of Figure 2.1B, the intensities of the $00l$ peaks as well as of the rotator order peak ($100r$) are strongly reduced (see also the inset of Figure 2. 1B). The in-plane 020 , 210 and 060 peaks maintain their intensity and narrowness. This indicates that short term scCO_2 treatments lead to a nearly complete clay exfoliation with maintenance of the in-plane order.

In agreement with previous results,^{36b} the X-ray diffraction

pattern of the OMMT, after long-term scCO_2 treatments, does not show anymore the $00l$ reflections (see also the inset of Figure 2. 1C): clay exfoliation is achieved.

It is worth adding that the in-plane 020 , 210 and 060 reflections are still present, although become less intense than a broad amorphous halo that appears in the 2θ range 20° - 30° . This amorphous halo can be attributed to a loss of order in the stacking of the clay layers, also associated with a complete loss of order in the packing of the hydrocarbon tails.

In summary, the described long-term scCO_2 treatments lead to exfoliation of the OMMT, and to a complete loss of long-range lateral order of the hydrocarbon tails of the cationic surfactant. The maintenance of $hk0$ reflections (mainly of the isolated 060 reflection), not yet reported in the literature, assures the maintenance of a long-range order in the clay layers. In this respect, it is worth adding that the half-height width of the 060 reflection, after exfoliation, remains equal to 0.45° indicating a correlation length $D_{060} = 28$ nm.

Relevant additional information, relative to the as received and scCO_2 -treated OMMT, can be obtained by DSC scans (Figure 2. 3). The scan of the as received OMMT (Figure 2. 3A) presents a reversible transition nearly located at 44°C ($\Delta H \approx 26$ J/g) that corresponds to the loss of rotator order of the hydrocarbon tails of the cations intercalated in the interlayer space. In this respect,

it is worth adding that endothermic peaks corresponding to the loss of order in the packing of the hydrocarbon tails have been observed, in the temperature range 25-80°C, not only for cationic organoclays,⁴¹ but also for other organically modified layered inorganic structures⁴² as well as for graphite oxide intercalation compounds.³⁹ The DSC scan of the scCO₂ treated OMMT does not present any thermal transition in the considered temperature range (Figure 2. 3B) and hence indicates the loss of 3D order in the packing of the hydrocarbon tails of the ammonium surfactant, which is compatible with clay exfoliation.

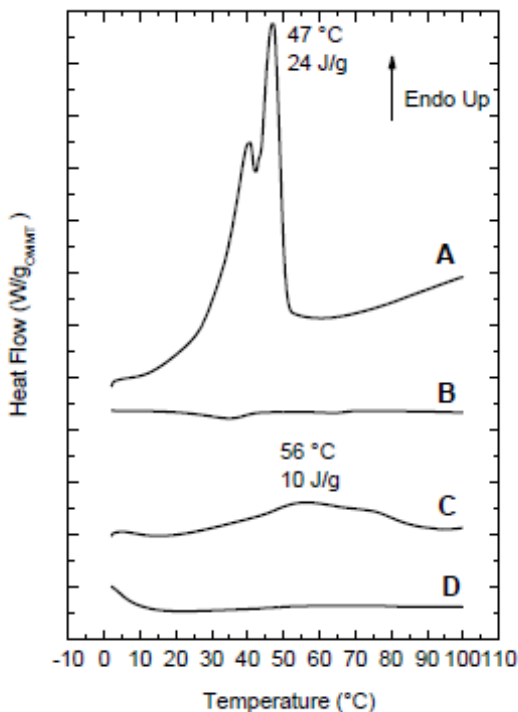


Figure 2. 3. DSC heating scans of: (A) as received MMT/2HT (intercalated); (B) MMT/2HT after treatment by scCO₂ (exfoliated); (C, D) aerogels with 90% of porosity, with 50/50 weight ratio of s-PS/as received OMMT (C) and of s-PS/exfoliated OMMT (D).

The overall information arising from X-ray diffraction and DSC characterization allows to conclude that the as received and scCO₂ treated OMMT can be described as intercalated and exfoliated OMMT, respectively.

2.3 Monolithic nanoporous-crystalline s-PS aerogels with large OMMT content

Monolithic composite aerogels, filled with large fractions of intercalated and exfoliated OMMT, have been prepared by using an s-PS matrix. This polymer choice is mainly due to the ability of s-PS to produce monolithic aerogels in a very broad range of porosity (from 50% up to 99%). An additional reason for this choice is the easy obtainment of aerogels exhibiting s-PS nanoporous-crystalline δ or ϵ phases.^{3a-c}

Aerogels with a porosity of nearly 90% were obtained by scCO₂ extraction of gels with a DCB content of 90 wt% and with different s-PS/OMMT weight ratios. For all aerogels with polymer/OMMT ratio equal or higher than 80/20, monolithic structures were obtained. Moreover, as usual for s-PS based aerogels,^{3a-f} the size and shape of s-PS/clay aerogels are essentially the same of the precursor gels. Aerogels with a 50/50 polymer/OMMT ratio are brittle and are generally obtained as powder X-ray diffraction patterns of s-PS based aerogels, containing intercalated and exfoliated OMMT, are shown in Figure 2. 4 and 2. 5, respectively.

All patterns of Figure 2. 4 show the typical reflections of the nanoporous-crystalline δ form. In particular, the isolated intense 010 reflection is always clearly apparent and located at $2\theta \approx 8$.

4°. The 00 l reflections of the OMMT are not detected for the aerogels with low clay content (4 and 8 wt%) while for higher clay contents (20 and 50 wt%) a narrow and intense 001 reflection is present, while the 002 and 003 reflections of the starting clay have disappeared. Moreover, the 001 reflection is markedly shifted with respect to its original position (from $2\theta = 2.6^\circ$ up to $2\theta = 3.8^\circ$), indicating a decrease of the interlayer spacing from $d = 3.5$ nm down to $d = 2.3$ nm.

The results of Figures 2. 4A-C suggest that the aerogel preparation procedure involving scCO₂ extraction, for low OMMT content, could lead to clay exfoliation, as already observed for scCO₂ treatment of the neat OMMT in Figure 2. 1. Figures 2. 4C-D show that, for high OMMT content in the aerogels, the used procedure is not suitable to generate OMMT exfoliation but, on the contrary, a reduction of the interlayer spacing is observed. An analogous phenomenon of reduction of interlayer spacing has been recently observed for organoclay extraction with different solvents, like e. g. ethyl acetate.⁴¹ As suggested in that paper, the observed reduction of basal spacing can be attributed to the extraction of excess cationic surfactant, not being ionically bonded to the negatively charged clay layers, but being simply included in the interlayer space by non-bonded interactions and contributing to the crystalline order of the hydrocarbon tails.

Additional information on the structural organization in the s-PS/OMMT aerogels comes from DSC analyses. In particular, DSC heating scan of a 50/50 by wt. s-PS/as-received-clay aerogel is shown in Figure 2. 3C. The endothermic peak, corresponding to loss of rotator order in the interlayer spacing (Figure 2. 1A) becomes broader and its maximum is shifted up to 50-60°C, with only a minor reduction of the related enthalpy ($\Delta H_r \approx 10 \text{ J/g} \approx 20 \text{ J/g}_{\text{OMMT}}$).

The combined information of the X-ray diffraction patterns of Figures 2. 4C-D and the DSC scans of Figures 2. 3C indicates that, for high clay content, the aerogel preparation procedure brings to a reduction of the OMMT basal spacing (d_{001}) from 3.5 nm down to 2.3 nm, with only partial loss of the hydrocarbon rotator order in the interlayer space.

The X-ray diffraction patterns of the s-PS aerogels prepared with the exfoliated OMMT (Figure 2. 5), independently of the aerogel composition, do not show 00 l clay reflections, while show the isolated weak 060 in-plane clay reflection (as shown by the inset of Figure 5C', D'). This clearly indicates that the gel and aerogel preparation procedures, also for high clay concentrations, allow to maintain clay exfoliation without re-aggregation, as instead observed for other common polymer processing.^{35c, 36b}

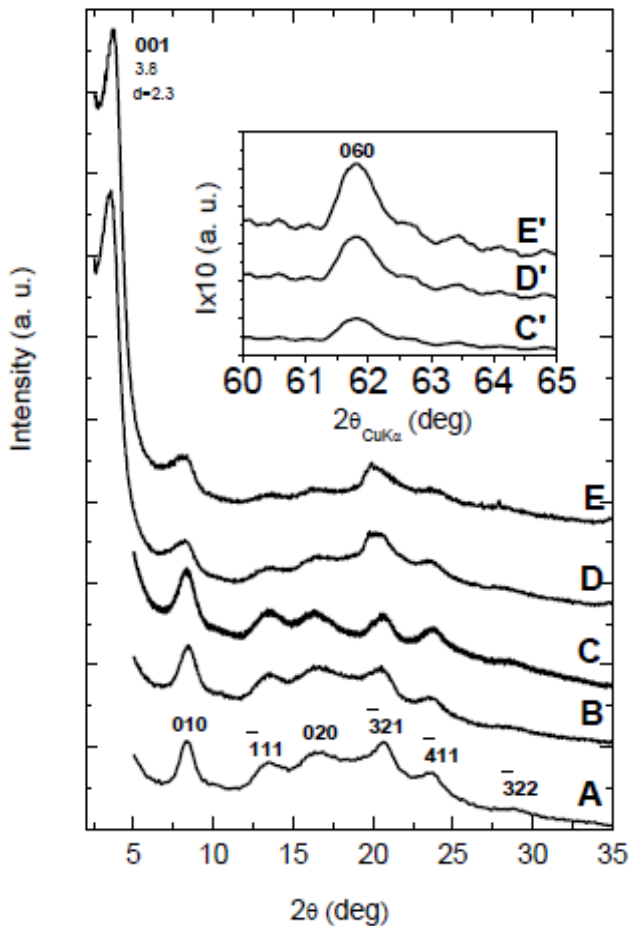


Figure 2. 4. X-ray diffraction ($CuK\alpha$) patterns in the 2θ range 2-35° of s-PS aerogels with as received OMMT, as obtained from gels with a solvent content of 90 wt% and presenting different polymer/OMMT weight ratios: (A) 100/0; (B) 96/4; (C) 92/8; (D) 80/20; (E) 50/50. The insets C', D' and E' enlarge the 060 in-plane reflection of the clay. The Miller indexes of the main reflections of the nanoporous-crystalline δ form of s-PS are indicated in A.

In this respect, it is worth citing that X-ray diffraction patterns of polymer-clay aerogels as obtained by freeze-drying of polymer solutions including clays^{43a-d} show the presence of 00/ clay reflections,^{43b, d} which exclude the occurrence of exfoliation. The patterns of Figure 2. 5 also show that s-PS is generally crystallized in the nanoporous δ form (Figure 2. 5A-C) while, for the 50/50 polymer/exfoliated-OMMT aerogel, the s-PS crystallization does not occur (broad amorphous halo of Figure 2. 5D). This is probably due to the good dispersion of a large amount of exfoliated OMMT, leading to a diluting effect on s-PS that reduces its crystallization kinetics. This loss of polymer crystallinity leads to a loss of the typical fibrillar structure, which in turn allows rationalizing the loss of monolithic structure. It is important to highlight some important differences between properties of s-PS monolithic aerogels exhibiting a porosity of 90% and a OMMT content of 20 wt%, as obtained by using intercalated or exfoliated OMMT, that present the X-ray diffraction patterns shown in Figure 2. 4 D and 2. 5 C. On the basis of quantitative evaluations on the X-ray diffraction patterns, the two aerogels present similar degree of polymer crystallinity ($\approx 40\%$). However, aerogels with the exfoliated clay (Figure 2. 6A) are much more homogeneous than aerogels obtained with the intercalated OMMT (Figure 2. 6B), which clearly present rough surfaces.

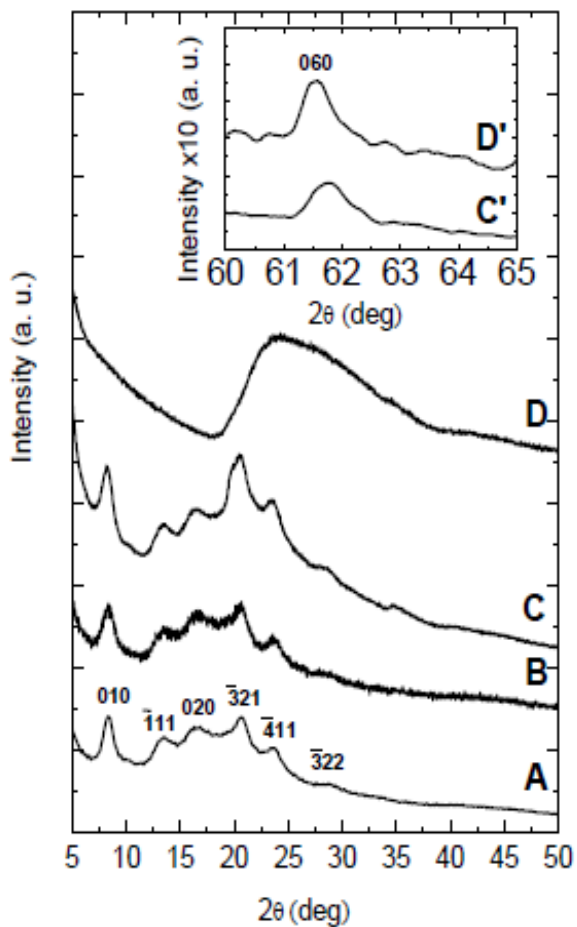


Figure 2. 5 X-ray diffraction ($\text{CuK}\alpha$) patterns in the 2θ range 5-50° of s-PS aerogels with exfoliated OMMT, as obtained from gels with a solvent content of 90 wt% and presenting different polymer/OMMT weight ratios: (A) 100/0; (B) 95/5; (C) 80/20; (D) 50/50. The inset C', D' enlarges the 060 in-plane reflection of the clay.

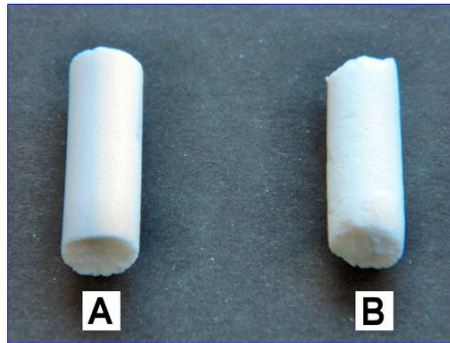


Figure 2.6. Photographs of cylindrical monolithic (diameter of 7 mm) s-PS/OMMT aerogels, with porosity $P=90\%$, as obtained by scCO_2 drying and exhibiting a 80/20 weight ratio: (A) with exfoliated clay; (B) with intercalated clay. The shown aerogels essentially present the same size and shape of the precursor gels.

Also the SEM images of the two aerogels are completely different. The SEM of the aerogel including the intercalated OMMT is dominated by the micrometric OMMT particles (Figure 2. 7B) while the SEM of the aerogel including the exfoliated OMMT (Figure 2. 7A) clearly show both nanometric clay platelets and nanometric s-PS fibrils (Figure 2. 7A'). The results of the SEM analyses suggest that also the large difference in the visual appearance between the two aerogels of Figure 2. 6 could be due to micrometric and nanometric size of intercalated and exfoliated clays, respectively.

DMA analyses indicate that aerogels based on the exfoliated clay

present an elastic modulus definitely higher than for those based on intercalated OMMT (36 MPa vs 15 MPa).

Surface areas S_{BET} , as obtained by N_2 adsorption data at 77 K, for the intercalated and exfoliated OMMT, as well as those of the corresponding aerogels, are compared in Table 1. For the sake of comparison, S_{BET} of the neat s-PS aerogel presenting the same porosity is shown in the last row of Table 1. As well known, s-PS aerogels exhibit high surface areas, mainly associated with the crystalline cavities of the δ crystalline phase, but also associated with the amorphous aerogel porosity.³ In agreement with literature data,⁴⁴ S_{BET} of the OMMT is rather low and is substantially increased for the exfoliated OMMT ($S_{\text{BET}} = 18 \text{ m}^2/\text{g}$). The s-PS/exfoliated-clay aerogels present values of S_{BET} ($281 \text{ m}^2\text{g}^{-1}$) much higher than those of the s-PS/intercalated-clay aerogels ($166 \text{ m}^2\text{g}^{-1}$) and not far from those observed for pure s-PS aerogels ($312 \text{ m}^2\text{g}^{-1}$). This indicates that, also for this high OMMT content (20 wt%), the exfoliated clay not only does not disturb the formation of the nanoporous crystalline phase but also does not alter the amorphous aerogel porosity.

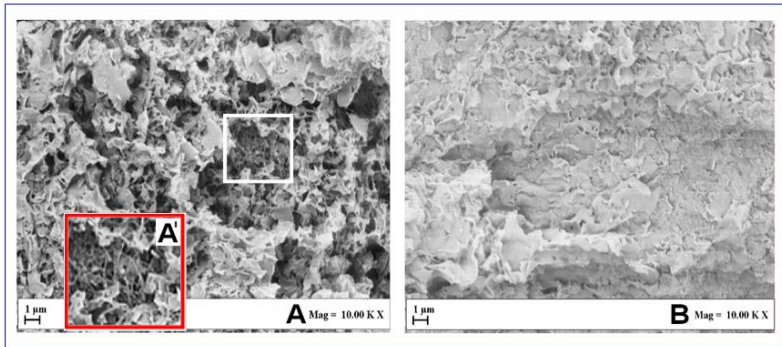


Figure 2. 7. SEM of aerogels with porosity $P= 90\%$, having 80/20 polymer/OMMT weight ratio: (A, A') with exfoliated OMMT; (B) with intercalated OMMT.

Sample	S_{BET}^a ($m^2 g^{-1}$)
Intercalated OMMT	10
Exfoliated OMMT (scCO ₂ treated)	18
s-PS/intercalated-OMMT, 80/20 aerogel	166
s-PS/exfoliated-OMMT, 80/20 aerogel	281
Aerogel δ s-PS	312

^a Total area evaluated following the BET model in the standard $0.05 < P/P_0 < 0.3$ pressure range.

Table 2.1 Total surface area (S_{BET}) of OMMT samples and of aerogels with porosity $P= 90\%$, having 80/20 polymer/OMMT weight ratio.

A schematic representation of the s-PS/exfoliated-OMMT aerogels is shown in Figure 2. 8

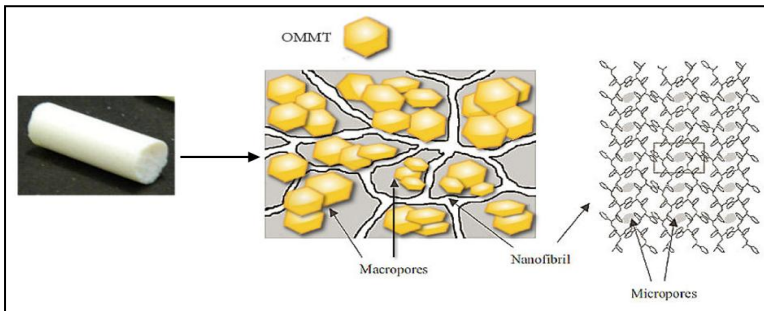


Figure 2. 8 Schematic representation of the s-PS/exfoliated-OMMT aerogels.

2. 5 Concluding remarks

A thorough investigation of scCO_2 -induced exfoliation of OMMT's has been conducted mainly by X-ray diffraction and DSC characterization techniques. The starting material is a MMT intercalated with ammonium cations bearing two long hydrocarbon tails. Suitable scCO_2 treatments led to exfoliation of the OMMT and also led to a complete loss of long-range order in the packing of the hydrocarbon tails of the cationic surfactant. The maintenance of $hk0$ reflections (mainly of the isolated 060 reflection), not yet reported in the literature, assures the maintenance of a long-range order in the clay layers. DSC scans of the intercalated OMMT present a reversible transition that corresponds to the loss of rotator order of the hydrocarbon chains in the interlayer spacing while those of the exfoliated OMMT do not present any thermal transition up to $100\text{ }^\circ\text{C}$. This confirms the absence of any 3-D order for the exfoliated clay.

Monolithic composite aerogels, filled with large amounts of both intercalated and exfoliated OMMT, have been prepared, starting from s-PS-based gels. In particular, for aerogels with high content of the intercalated OMMT, the preparation procedure brings to a reduction of the basal spacing (d_{001}) from 3.5 nm down to 2.3 nm , with only partial loss of the

hydrocarbon rotator order in the interlayer space. For aerogels with high content of the exfoliated OMMT, the gel and aerogel preparation procedures allow to maintain clay exfoliation without re-aggregation, as instead observed for other common polymer processing.

A strict comparison between s-PS monolithic aerogels with a porosity of 90% and a OMMT content of 20 wt %, as obtained by using intercalated or exfoliated OMMT, has been also reported. Although the two aerogels present similar degree of polymer crystallinity ($\approx 40\%$) as well as the same polymer crystalline form (the nanoporous-crystalline δ form), aerogels with the exfoliated OMMT are much more homogeneous than aerogels with the intercalated OMMT. This difference, clearly apparent both on visual inspection as well as on SEM analysis, is due to micrometric and nanometric size of intercalated and exfoliated clays, respectively. Aerogels based on the exfoliated clay also present elastic modulus definitely higher than those based on intercalated OMMT. Moreover, s-PS/exfoliated-clay aerogels present values of surface area ($281 \text{ m}^2\text{g}^{-1}$) much higher than those of the s-PS/intercalated-clay aerogels ($166 \text{ m}^2\text{g}^{-1}$) and not far from those observed for pure s-PS aerogels ($312 \text{ m}^2\text{g}^{-1}$). This indicates that, also for high content, the exfoliated clay does not alter the aerogel porosity.

The improvement of properties such as the modulus and the

surface area is definitely of interest in view of potential applications of aerogels with exfoliated OMMT, for example for achieving relevant transport properties with extremely light materials. Moreover, the clay rich aerogels (e. g. 50/50, w/w), could be helpful to an easier handling of exfoliated OMMT, removing the risks connected with inhalable nanoparticles.

Chapter 3

Graphene oxide / Syndiotactic Polystyrene

Aerogels

3.1 Introduction

As mentioned above, graphene is a two-dimensional structure of carbon atoms with unique electronic, chemical, and mechanical properties and with the potential to impact a wide range of technologies.^{9, 12e, f} The development of three-dimensional (3D) structures with graphene^{45, 46} is expected to further expand its relevance both in the number of applications and in manufacturability.

In many reports, 3D physically crosslinked graphene aerogels were obtained from graphene oxide (GO) suspensions, generally by drying followed by GO (thermal or chemical) reduction.⁴⁵

Monolithic graphene aerogels exhibiting covalent carbon bonding between the graphene sheets, rather than simple physical cross-links, have also been prepared by using organic sol-gel chemistry.⁴⁵ In particular, thermosetting (e. g., phenolic) resins are used to produce organogels, which are supercritically dried and then thermally reduced to yield graphene aerogels, with carbonization of the organic cross-links and thermal reduction of the GO to graphene occurring simultaneously

during pyrolysis.^{46a, b} These graphene aerogels can exhibit an improvement in bulk electrical conductivity of more than 2 orders of magnitude compared to graphene assemblies with physical cross-links alone as well as large surface areas, making these materials viable candidates for use in energy storage, catalysis, and sensing applications.^{46a, b}

In this chapter, the preparation process of GO aerogels by using suitable thermoplastic polymers rather than thermosetting resins is described. In particular, by using syndiotactic polystyrene (s-PS), robust aerogels are obtained for a very broad polymer/GO composition range. Our study also shows the relevance of polymer/graphene aerogels as obtained, exhibiting nanoporous-crystalline phases and relevant mechanical and molecular sorption properties that, due to their thermoplastic nature, can be used as graphene “masterbatches” for composite processing.

3.2 Monolithic nanoporous-crystalline s-PS aerogels with large GO content

The X-ray diffraction patterns of the starting high surface area graphite and of the derived GO, as obtained by the oxidation procedure described in the Experimental section, are shown in Figures 3.1 A and 3.1 B, respectively. The graphite oxidation leads to an increase of the distance between the layers from 0.399 nm up to 0.84 nm while the in-plane periodicities (d_{100} and d_{110}) remain unaltered.

Sonication at 100°C of the GO sample of Figure 3. 1B in an organic solvent (dichlorobenzene, DCB) leads to stable dispersions (Figure 3. 2). The X-ray diffraction of the powder as recovered by filtration after solvo-thermal reduction and, subsequently, extracted with scCO₂ is shown in Figure 3. 1C. The pattern shows the maintenance of the in-layer graphitic order (100 and 110 reflections) and the replacement of the peak at $d = 0.84$ nm with a peak at $d = 0.35$ nm clearly indicating the formation of reduced graphene oxide (rGO) by the used solvothermal procedure.¹⁵

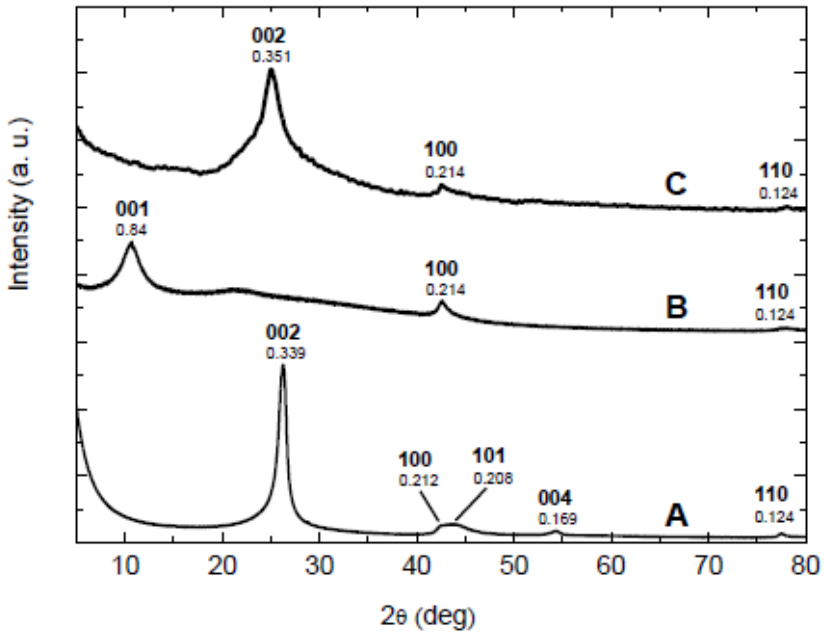


Figure 3. 1. X-ray diffraction patterns in the 2θ range $2\text{--}80^\circ$ of: the starting graphite (A), of the derived GO (B) and of the reduced GO, as coagulated from dispersions like those used for aerogel preparations (C). Miller indexes and d spacings are indicated close to the main diffraction peaks.

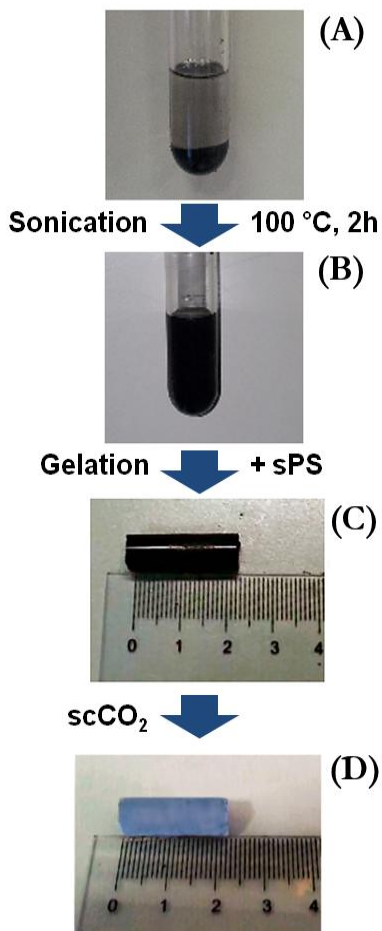


Figure 3 2. Preparation procedure for sPS/GO aerogels: (A, B) Dispersion of GO in the organic solvent, before (A) and after (B) sonication at 100°C for 2 hours; (C) Organogel as obtained after dissolution at 180°C of s-PS in the GO dispersion (sPS/GO, 80/20 by wt; overall solvent content in the gel: 90 wt%); (D) Aerogel with porosity of 90%, as obtained by solvent extraction by scCO₂.

sPS/rGO gels can be easily prepared by dissolution at 180 °C of

sPS in rGO dispersions, followed by cooling to room temperature of the hot solution. In particular, we have verified that stable gels can be obtained, at least for an overall amount of polymer and rGO in the gels being in the range 2 wt% – 20wt%. By extracting with supercritical carbon dioxide (scCO₂) these sPS/rGO organogels, monolithic aerogels, which essentially present the same size and shape of the precursor gels and hence roughly a porosity in the range 98% – 80% and a density in the range 0.02– 0.2 g/cm³, are obtained.

Visual inspection shows that light blue aerogels are obtained for rGO content lower than 30 wt%. For instance, a photograph of a monolithic sPS/rGO, 80/20 aerogel, with porosity $P= 90\%$, is shown in Figure 3. 3A. An optical micrograph of the same aerogel shows the presence of disordered GO aggregates, having average size of roughly 1-2 μm , dispersed in an uniform polymer-rich matrix. For the sake of comparison, monolithic sPS/graphite aerogels were also prepared from high surface area graphite (HSAG) dispersions in ortho-dichlorobenzene, by a preparation procedure strictly analogous to that one used for sPS/rGO aerogels. Aerogels with HSAG present much larger aggregates, even for low content of nanofiller (4 wt%), as shown by the photograph and the micrograph of Figures 3. 3B and 3. 3B', respectively. It is worth adding that s-PS/HSAG 80/20 aerogel appears to be black.

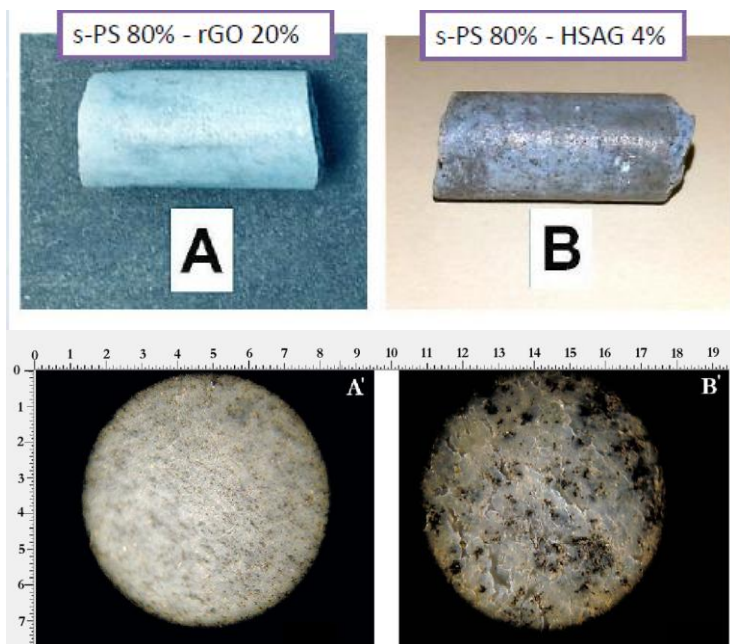


Figure 3.3. Photographs (A, B) and optical micrographs (A', B') of monolithic aerogels, with porosity $P=90\%$, as prepared with cylindrical molds (diameter of 7 mm): (A, A') sPS/rGO, 80/20 by wt. ; (B, B') sPS/HSAG 96/4 by wt. Both aerogels present the same size and shape of the precursor gel.

The occurrence of uniform light blue color for sPS/rGO aerogels, even for high rGO content (Figure 3. 3A) is rather unique, because known composites as well as foams containing carbonaceous fillers are generally black.

The large color difference between the obtained aerogels has been quantitatively compared by colorimetric measurements, as

shown in Figure 3. 4 for aerogels having a porosity of 90%. The white aerogels constituted only by sPS are highly reflective while the black aerogels with HSAG are of course highly absorbent. Aerogels with 20 wt% of GO present a higher reflectance with respect to the analogous aerogel with only 4 wt% of HSAG. Moreover, the reflectance markedly decreases going from blue to red, as expected on the basis of the aerogel color.

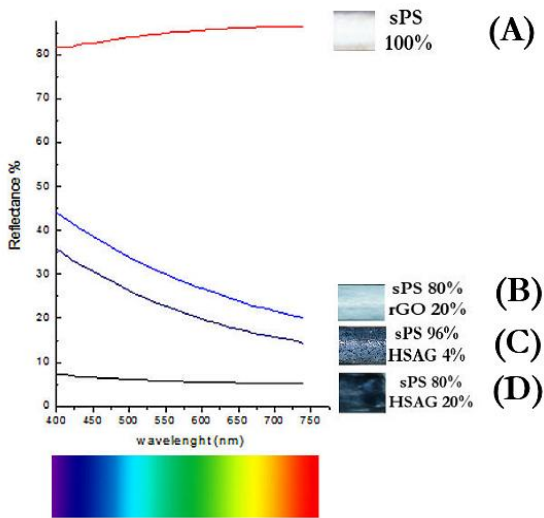


Figure 3. 4. Reflectance of sPS-based aerogels with porosity of 90%: (A) pure sPS; (B) sPS/rGO, 80/20 aerogel; (C) sPS/HSAG, 96/4 aerogel (D) sPS/HSAG, 80/20 aerogel.

The X-ray diffraction patterns of the sPS/rGO aerogels, with porosity of 90% and presenting different polymer/rGO weight ratios are shown in Figure 3. 5A-E. The patterns show the

presence of the diffraction peaks of the nanoporous-crystalline δ form of sPS (Miller indexes indicated close to the curve A of Figure 3. 5), for the entire composition range. In this respect, it is worth adding that the degree of crystallinity of the polymer increases, going from the pure sPS aerogel to the 95/5 aerogel (from nearly 45% up to 55%), suggesting a nucleating effect of graphitic layers on the crystalline δ form. The rGO diffraction peaks are clearly detected only for the sPS/rGO 50/50 aerogel, for which well defined in-plane 100 and 110 peaks and a broad 002 peak, whose broadness indicates a correlation length perpendicular to the graphitic planes $D_{\perp} = 3.5$ nm, are observed (Figure 3. 3E). For rGO content lower than or equal to 30 wt% (Figures 3. 3 B-D), the absence of the narrow 002 peak of the rGO (Figure 3. 1C) clearly indicates that most of rGO is constituted by structural layers exhibiting negligible order in the direction perpendicular to the graphitic plane.

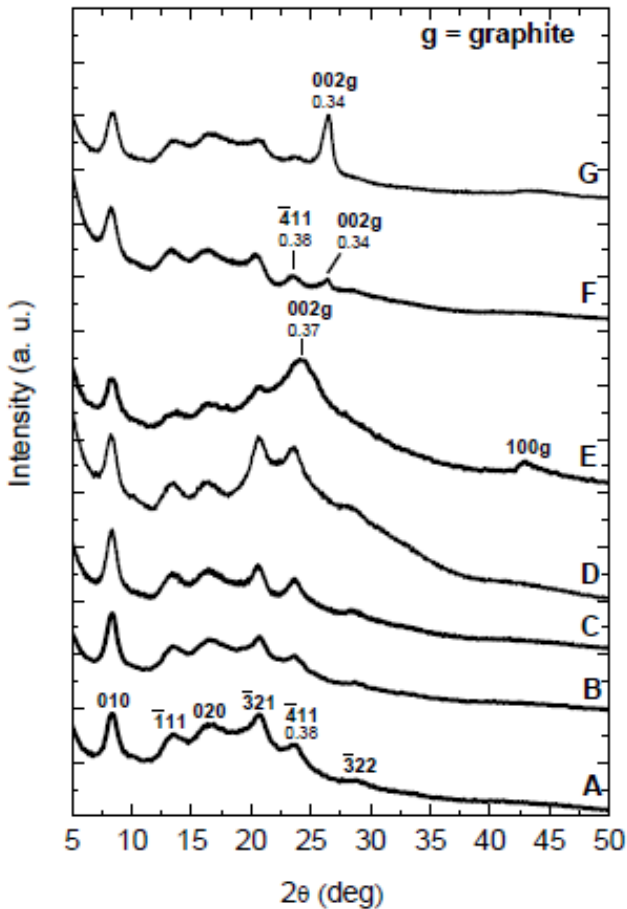


Figure 3. 5. X-ray diffraction patterns in the 2θ range $5\text{-}50^\circ$ of sPS-based aerogels with porosity of 90 wt% and presenting different polymer/filler weight ratios: (A) 100/0; (B) 95/5 with GO; (C) 80/20 with GO; (D) 70/30 with GO; (E) 50/50 with GO; (F) 96/4 with HSAG and (G) 80/20 with HSAG. The Miller indexes of the main reflections of the nanoporous-crystalline δ form of sPS are indicated in A. The symbol **g** indicates reflections relative to the graphitic component.

The X-ray diffraction patterns of the sPS/HSAG aerogels, with porosity of 90% and presenting different polymer/rGO weight ratios are shown in Figure 3.5 F-G. Differently from the case of sPS/rGO aerogels, sPS/HSAG aerogels exhibit an intense 002 diffraction peak, already clearly apparent for a HSAG content as low as 4 wt% (Figure 3. 5 F), indicating a correlation length perpendicular to the graphitic planes higher than 10 nm.

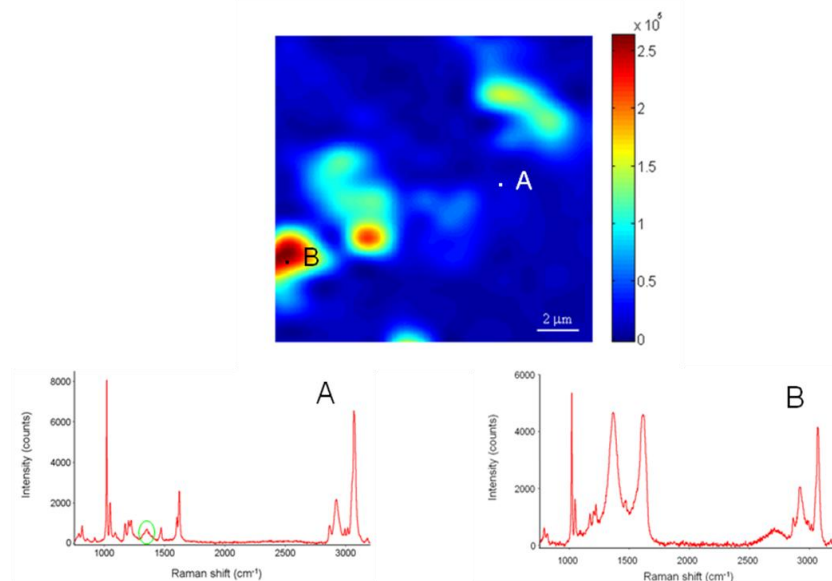


Figure 3. 6. RAMAN microscopy map ($16 \times 16 \mu\text{m}$) of a sPS/rGO aerogel with weight ratio 80/20 and $P = 90\%$, as based on the GO peak at 1345 cm^{-1} . RAMAN spectra correspond to points A and B in the map.

Additional information relative to the polymer and GO distribution in the aerogels has been achieved by the RAMAN

imaging technique.

Just as an example, a RAMAN microscopy map, for a size 16 x 16 μm and based on the GO peak at 1345 cm^{-1} , of a sPS/rGO aerogel with weight ratio 80/20 and $P = 90\%$ is shown in Figure 3.6. As observed for the entire aerogel, the polymer rich regions (blue in the map of Figure 3.6) also contain GO peaks (the main GO peak is encircled in spectrum A, in Figure 3.6) while the GO rich regions (red in the map of Figure 3.6) also contain the polymer (see, for instance, the intense sPS peak at 3060 cm^{-1} in spectrum B in Figure 3.6).

SEM images of polymer-rich regions of sPS-based aerogels are shown in Figure 3.7. In particular, SEM images of aerogels with porosity of 90%, for the pure polymer and for composite aerogels with GO and HSAG (polymer/filler ratio of 80/20 wt%) are shown in Figures 3.7 A, B and C, respectively. SEM images of s-PS/GO aerogels (Figure 3.7 B) are dominated by the typical fibrillar morphology (with diameters of roughly 50–100 nm) of δ form sPS aerogels (Figure 3.7 A). Moreover, the fibrillar polymer matrix presents uniformly distributed rGO platelets (white spots with diameters of roughly 80–200 nm in Figure 3.7 B). The SEM of the analogous sPS/HSAG aerogels, present completely different morphologies with a strongly reduced density of fibrils exhibiting increased diameters (300-500nm, Figures 3.7 C).

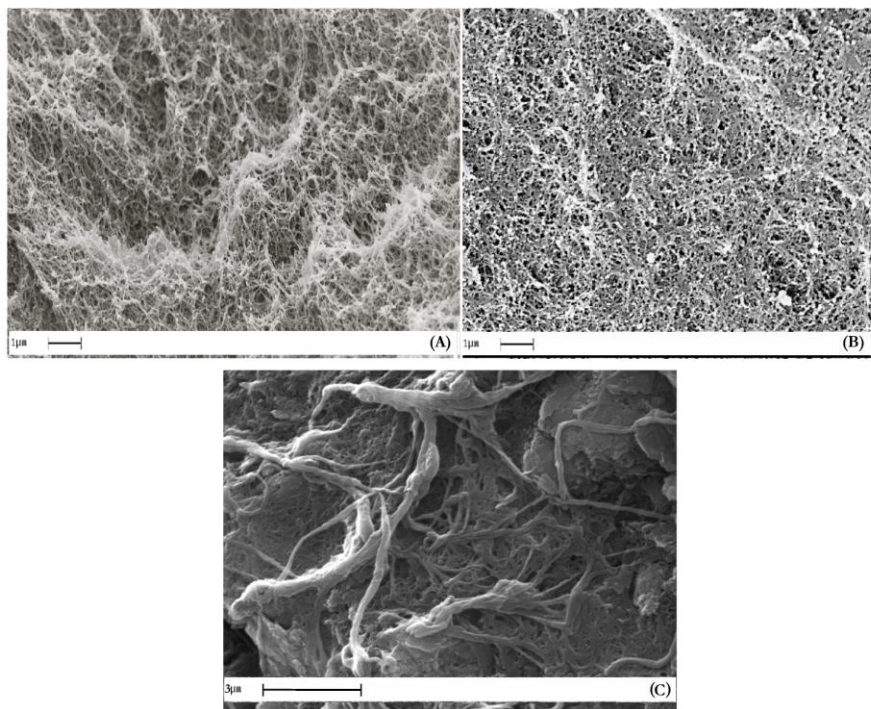


Figure 3. 7. SEM images of sPS-based aerogels with $P = 90\%$: pure s-PS (A); sPS/rGO, 80/20 by wt. (B); sPS/HSAG, 96/4 by wt. (C).

Relevant information relative to the sPS/rGO aerogels also comes from surface area evaluations, as conducted by the BET method. The data of Table 3. 1 show that, although the starting graphite exhibits a high surface area, the derived GO and rGO samples present low surface areas. The surface area of the composite sPS/rGO aerogels is, however, much closer to that one of the pure sPS aerogels ($312 \text{ m}^2/\text{g}$), i. e. much higher than

the weight-average calculated values.

It is worth noting that although the starting graphite as well as the graphite when subjected to the same procedures used for aerogel preparation exhibits high surface areas (308 and 233 m^2/g , respectively; Table 13.), the sPS/HSAG aerogels present surface areas much smaller than those observed for sPS/rGO aerogels (Table 3. 1). For instance, the sPS/HSAG, 80/20 aerogel presents S_{BET} (173 m^2/g) much smaller than for the sPS/rGO, 80/20 aerogel (289 m^2/g).

This much higher surface area values observed for sPS/rGO aerogels clearly supports the previous conclusion, mainly based on X-ray diffraction analyses, that rGO is mostly constituted by uncorrelated structural layers.

Sample	S_{BET}^a ($\text{m}^2 \text{g}^{-1}$)
HSAG	308
HSAG treated as in aerogel preparation	233
sPS/HSAG, 80/20	173
sPS/HSAG, 96/4	277
GO	0.8
rGO treated as in aerogel preparation	2.0
sPS/rGO, 50/50 aerogel	238
sPS/rGO, 70/30 aerogel	254
sPS/rGO 80/20 aerogel	289
sPS aerogel	312

^aTotal area evaluated following the BET model in the standard $0.05 < P/P_0 < 0.3$ pressure range.

Table 3. 1. Total surface area (S_{BET}) of the starting graphite, of the derived GO and rGO and of aerogels with $P = 90\%$ and exhibiting the nanoporous-crystalline δ form and different polymer/rGO weight ratios.

For the prepared aerogels, mechanical properties mainly in compression have been evaluated. In particular, compression stress-strain tests are compared for sPS and sPS/GO, 80/20 aerogels (both for porosity of 90%) in Figure 3. 8. The presence of GO slightly reduces the elastic modulus (from 1.9 to 1.6 MPa) while a good ductility is maintained, as also shown by the

photographs of the starting and compressed sPS/GO aerogels (insets in Figure 3.8).

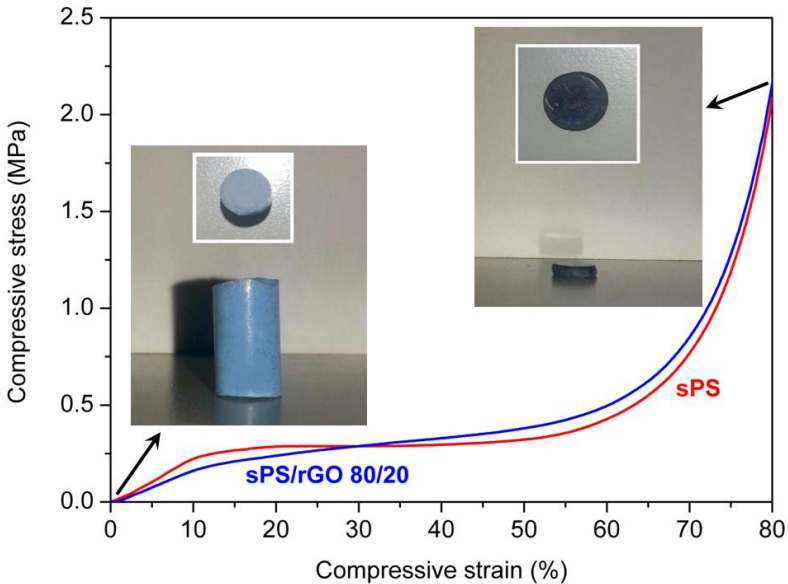


Figure 3. 8. Stress-strain curves in compression for aerogels, both with porosity of 90%.

sPS (red curve) and sPS/GO, 80/20 wt% (blue curve). The insets show photographs (parallel and perpendicular to the cylinder) of the sPS/GO aerogel before and after the compression test. Most monolithic solids with high porosity (e. g., activated carbons) are instead brittle and easily collapse under compression. Therefore, ultralight materials with good mechanical properties (mainly toughness) are in strong demand.

The present robust high-surface area sPS/rGO aerogels, exhibiting the nanoporous crystalline δ form and isolated rGO layers, are hence expected to find several applications. For instance, these composite aerogels can be used as monolithic supported catalysts, which can exploit the molecular sorption ability and diffusivity⁶ of the nanoporous-crystalline polymer phase and the catalytic activity³ of the GO nanoplatelets. Due to their thermoplastic nature, sPS/rGO aerogels can also facilitate the rGO dispersion in polymer melts, without rGO re-aggregation, i. e. could be possibly used as rGO “masterbatches” for melt polymer processing, which should allow to obtain GO-rich nanocomposites.¹⁴

3.3 Concluding remarks

Stable sPS/rGO organogels can be prepared by dissolution of sPS in GO dispersions in organic solvents, at least for an overall amount of polymer and GO in the gels being in the range 2 wt% – 20wt%.

By extracting these sPS/rGO organogels with supercritical carbon dioxide, monolithic aerogels, which essentially present the same size and shape of the precursor gels and hence roughly porosity in the range 98% – 80% and density in the range 0.02–0.2 g/cm³, are obtained.

These sPS/rGO aerogels show on visual inspection, for rGO content lower than 30 wt%, an homogeneous light blue color (rather than the black color of analogous sPS/graphite aerogels), which is due to much higher reflectance that significantly decreases going from blue to red light. This unusual light blue color suggests that, at least for rGO content lower or equal to 20 wt%, most of rGO is present as uncorrelated rather than as piled graphitic layers.

X-ray diffraction patterns show that the 002 graphitic reflection appears only as a broad peak and only for rGO content higher than 30 wt%, thus confirming that (at least for rGO content lower or equal to 20 wt%) most of rGO is constituted by structural layers that exhibit negligible order in the direction

perpendicular to the graphitic plane. The X-ray diffraction patterns also show that all the prepared aerogels exhibit the nanoporous-crystalline δ form of s-PS. The dispersion of the rGO platelets in the aerogels has been also studied by optical and electron microscopy (SEM) as well as by RAMAN imaging. Although rGO presents a low surface area (nearly 2 m²/g), the surface area of the composite sPS/rGO aerogels is high (240-290 m²/g) and close to those of pure sPS δ form aerogels. This again supports the conclusion that rGO is mostly present in the aerogels as uncorrelated graphitic layers. sPS/GO composite aerogels present mechanical properties, and in particular high ductility, close to those of analogous aerogels based on pure sPS. These robust high-surface area sPS/rGO aerogels, exhibiting the nanoporous crystalline δ form and uncorrelated rGO layers, are expected to have several possible applications, like e.g., as monolithic supported catalysts or as “masterbatches” for polymer composite processing.

References

- [1] R. Roy, R. A. Roy, D. M., *Materials Letters*, **1986**, 4(8-9), 323-328.
- [2] S. Longo, M. Mauro, C. Daniel, M. Galimberti, G. Guerra. *Frontiers in Polymer Chemistry*, **2013**, 1, 1-9.
- [3](a)C. Daniel, D. Alfano, V. Venditto, S. Cardea, E. Reverchon,, D. Larobina, G. Mensitieri, G. Guerra, G, *Adv. Mater.* **2005**, 17, 1515. (b) C. Daniel, S. Giudice, G. Guerra *Chem. Mater.*, **2009**, 21, 1028–1034 (c) C. Daniel, D. Sannino, G. Guerra, *Chem. Mater.*, **2008**, 20, 577–582d) C. Daniel, S. Longo, R. Ricciardi, E. Reverchon, G. Guerra, *Macromolecular Rapid Communications* **2013**, 34 (15), 1194-1207. (e) S. Longo, J. G. Vitillo, C. Daniel, G. Guerra, *ACS Applied Materials & Interfaces*, **2013**, 5(12), 5493-5499. (f)C. Daniel, S. Longo, S. Cardea, J. G. Vitillo., G. Guerra, *RSC Advances*, **2012**, 2(31), 12011-12018.
- [4] H. Van Olphen *New York, Interscience*, **1963**, 48-57.
- [5] a)P. C. Le Baron, Z. Wang, T. J Pinnavaia, *Appl Clay Sci*, **1999**, 15, 11–29 b) T. J. Pinnavaia, G. W. Beall editors, *Polymer-clay nanocomposites*. New York, John Wiley & Sons, **2000** c) S. Yariv, H. Cross, editors. *Organo-clay complexes and interactions*. New York, Marcel Dekker, **2002**. d) Y. Mai, Z. Yu editors. *Polymer nanocomposites*. Cambridge, Woodhead, **2006**. e) F. Hussain, M. Hojjati, *J. Compos. Mater.* **2006**, 40(17), 1511–65. f) D. L. Hunter, K. W. Kamena, D. R. Paul. *MRS Bull*, **2007**, 32, 2806 h)W. Xie, Z. Gao, K. Liu, W. P. Pan, R. Vaia, D. Hunter et al. *Thermochim Acta*, **2001**, 367–368, 339–50. g) W. Xie, Z. Gao, W. P. Pan, D. Hunter, A. Singh, R. Vaia, *Chem. Mater.* **2001**, 13, 2979–90. h) W. Xie, R. Xie, W. P. Pan, D. Hunter, B. Koene, L. S. Tan, et al. *Chem. Mater.* **2002**, 14, 4837–45.
- [6] S. S. Ray, M. Okamoto, *Progress in Polymer Science*, **2003**, 28, 1539-1641.
- [7] R. Sengupta, S. Chakraborty, S. Bandyopadhyay, S. Dasgupta, R. Mukhopadhyay, K. Auddy, A. S. Deuri, *Polymer*

Engineering and Science, **2007**, *47*, 1956-1974.

[8] B. Chen, J. R. G. Evans, H. C. Greenwell, P. Boulet, P. V. Coveney, A. A. Bowden, A. Whiting, *Chemical Society Reviews*, **2008**, *37*, 568-594.

[9] K. S. Novoselov, A. K. Geim, S. V. Morozov, D. Jiang, Y. Zhang, S. V. Dubonos, I. V. Grigorieva, A. A. Firsov, *Science*, **2004**, *306*, 666.

[10] S. W. Ting, A. P. Periasamy, S. -M. Chen, R. Saraswathi, *Int. J. Electrochem. Sci.*, **2011**, 4438-42

[11] K. S. Novoselov, V. I. Falko, L. Colombo, P. R. Gellert, M. G. Schwab, K. Kim, *Nature*, **2012**, *490*, 192.

[12] a) C. N. R. Rao, A. K. Sood, R. Voggu, K. S.

Subrahmanyam, **2010**, *J. Phys. Chem. Lett.*, *1*, 572. b) B. Devadas, M. Rajkumar, S. -M. Chen, R. Saraswathi, *Int. J. Electrochem. Sci.*,

2012, *7*, 3339. c) A. K. Geim, K. S. Novoselov, *Nat. Mater.* **2007**,

6, 183. d) A. K. Geim, *Science*, **2009**, *324*, 1530. e) L. Tang, Y. Wang, Y. Li, H. Feng, J. Lu, J. Li, *Adv. Funct. Mater.*, **2009**, *19*, 2782. f) C. Lee, X. Wei, J. W. Kysar, J. Hone, *Science* **2008**, *321*, 385

[13] J. W. Suk, R. D. Piner, J. An, R. S. Ruoff, *ACS Nano*, **2010**, *4*, 6567.

[14] X. M. Chen, G. H. Wu, Y. Q. Jiang, Y. Wang, X. Chen, *Analyst*, **2011**, *136*, 4631.

[15] a) P. Avouris, F. Xia, *MRS Bull.*, **2012**, *37*, 1225. b) N.

Zhang, Y. Zhang, Y. J. Xu, *Nanoscale*, **2012**, *4*, 5792. c) T. H.

Tsai, S. C. Chiou, S. M. Chen, *Int. J. Electrochem. Sci.*, **2011**, *6*,

3333. d) K. Zhang, L. L. Zhang, X. S. Zhao, J. Wu, *Chem. Mater.*

2010, *22*, 1392. e) K. Yang, L. Feng, X. Shi, Z. Liu, *Chem. Soc.*

Rev., **2013**, *42*, 530. f) V. Mani, A. P. Periasamy, S. M. Chen,

Electrochem. Commun., **2012**, 1775 g) S. W. Ting, A. P. Periasamy,

S. M. Chen, R. Saraswathi, *Int. J. Electrochem. Sci.*, **2011**, *6*, 4438.

[16] D. Chen, L. Tang, J. Li, *Chem. Soc. Rev.*, **2010**, *39*, 3157.

[17] C. Mattevi, H. Kim, M. Chhowall, *J. Mater. Chem.*, **2011**, *21*, 3324

- [18] D. Wei, B. Wu, Y. Guo, G. Yu, Y. Liu, *Acc. Chem. Res.*, **2013**, 46, 106.
- [19] (a) T. Peng, H. Lv, D. He, M. Pan, S. Mu, *Sci Rep.*, **2013**, 3, 1148. b) S. W. Poon, W. Chen, E. S. Tok, A. T. Wee, *Appl. Phys. Lett.*, **2008**, 92, 104102. c) A. D. Lueking, L. Pan, D. L. Narayanan, C. E. B. Clifford, *J. Phys. Chem. B*, **2005**, 109, 12710. d) E. H. L. Falcao, R. G. Blair, J. J. Mack, L. M. Viculis, C. W. Kwon, M. Bendikov, R. B. Kaner, B. S. Dunn, F. Wudl, *Carbon*, **2007**, 45, 1364. e) R. Hao, W. Qian, L. Zhang, Y. Hou, *Chem. Commun.*, **2008**, 0, 6576. f) H. Huang, Y. Xia, X. Tao, J. Du, J. Fang, Y. Gan, W. Zhang, *J. Mater. Chem.*, **2012**, 22, 10452. g) R. P. B. D. Santos, E. Perim, P. A. S. Autreto, G. Brunetto, D. S. Galvao, *Nanotechnology*, **2012**, 23, 465702.
- [20] a) N. L. Rangel, J. C. Sotelo, J. M. Seminario, *J. Chem. Phys.* **2009**, 131, 031105. b) S. Park, J. An, J. R. Potts, A. Velamakanni, S. Murali, R. S. Ruoff, *carbon*, **2011**, 49, 3019. c) B. C. Brodie, *Philos. Trans. R. Soc. London*, **1859**, 149, 249. d) L. Staudenmaier, *Ber. Dtsch. Chem. Ges.*, **1898**, 31, 1481. e) W. S. Hummers, R. E. Offeman, *J. Am. Chem. Soc.*, **1958**, 80, 1339. f) S. Park, R. S. Ruoff, *Nat. Nanotechnol.*, **2009**, 4, 217. g) Y. Zhu, S. Murali, M. D. Stoller, A. Velamakanni, R. D. Piner, R. S. Ruoff, *Carbon*, **2010**, 48, 2106. h) H. A. Becerril, J. Mao, Z. Liu, R. M. Stoltenberg, Z. Bao, Y. Chen, *ACS Nano*, **2008**, 2, 463. i) T. -Y. Zhang, D. Zhang, *Bull. Mater. Sci.*, **2011**, 34, 25.
- [21] a) H. J. Shin, K. K. Kim, A. Benayad, S. M. Yoon, H. K. Park, I. S. Jung, M. H. Jin, H. -K. Jeong, J. M. Kim, J. Y. Choi, Y. H. Lee, *Adv. Funct. Mater.*, **2009**, 19, 1987. b) G. Wang, J. Yang, J. Park, X. Gou, B. Wang, H. Liu, J. Yao, *J. Phys. Chem., C*, **2008**, 112, 8192. c) J. Zhang, H. Yang, G. Shen, P. Cheng, J. Zhang, S. Guo, *Chem. Commun.*, **2010**, 46, 1112. d) D. R. Dreyer, S. Murali, Y. Zhu, R. S. Ruoff, C. W. Bielawski, *J. Mater. Chem.*, **2011**, 21, 3443. e) X. Fan, W. Peng, Y. Li, X. Li, S. Wang, G. Zhang and F. Zhang, *Adv. Mater.*, **2008**, 20, 4490. f) T. Zhou, F. Chen, K. Liu, H. Deng, Q. Zhang, J. Feng, Q. Fu, *Nanotechnology*, **2011**, 22, 045704. g) C. Zhu, S. Guo, Y. Fang, S. Dong, *ACS Nano*, **2010**, 4, 2429. h) H. C. Schniepp, J. -L. Li, M.

- J. McAllister, H. Sai, M. H. -Alonso, D. H. Adamson, R. K. Prudhomme, R. Car, D. A. Saville, I. A. Aksay, *J. Phys. Chem. B*, **2006**, 110, 8535.
- i) M. Zhou, Y. Wang, Y. Zhai, J. Zhai, W. Ren, F. Wang, S. Dong, *Chem. Eur. J.*, **2009**, 15, 6116.
- l) H. L. Guo, X. F. Wang, Q. Y. Qian, F. B. Wang, X. H. Xia, *ACS nano*, **2009**, 3, 2653.
- [22] W. Choi, I. Lahiri, R. Seelaboyina, Y. S. Kang, *Crit. Rev. Solid State Mater. Sci.*, **2010**, 35, 52.
- [23] D. R. Dreyer, S. Park, C. W. Bielawski, R. S. Ruoff, *Chem. Soc. Rev.*, **2010**, 39, 228.
- [24] L. Qiu, X. Yang, X. Gou, W. Yang, Z. F. Ma, G. G. Wallace, D. Li, *Chem. Eur. J.*, **2010**, 16, 10653
- [25] F. Kim, L. J. Cote, J. Huang, *Adv. Mater.*, **2010**, 22, 1954.
- [26] T. Szabo, O. Berkesi, P. Forgo, K. Josepovits, Y. Sanakis, D. Petridis, I. Dekany, *Chem. Mater.*, **2006**, 18, 2740.
- [27] Z. Liu, J. T. Robinson, X. Sun, H. Dai, *J. Am. Chem. Soc.*, **2008**, 130, 10876
- [28] H. Yang, F. Li, C. Shan, D. Han, Q. Zhang, L. Niu, A. Ivaska, *J. Mater. Chem.*, **2009**, 19, 4632
- [29] Y. X. Xu, H. Bai, G. W. Lu, C. Li, G. Q. Shi, *J. Am. Chem. Soc.*, **2008**, 130, 585
- [30] a) M. Alexandre, and P. Dubois, *Mater. Sci. Eng. R. Rep.* **2000**, 28, 1–63. b) F. A. Bergaya, *Microp. Mesop. Mater.* **2001**, 107, 141–148. c) Galimberti, M. (ed.). *Rubber Clay Nanocomposites-Science, Technology and Applications*. New York, NY, WileyandSons, **2011**.
- [31] Paul, D. R., and Robeson, L. M. **2008**. *Polymer* 49, 3187–3204.
- [32] F. Bergaya, and G. Lagaly, G. *Handbook of Clay Science*. 2nd Edn. Elsevier, Amsterdam, **2013**.
- [33] a) Y. Kojima, A. Usuki, M. Kawasumi, A. Okada, Y. Fukushima, Y. Kurauchi, et al. *J. Mater. Res.*, **1993**, 8, 1179–1185. b) R. A. Vaia, H. Ishii, E. P. Giannelis, *Chem. Mater.*, **1993**, 5, 1694–1696.

- c) E. Manias, A. Touny, L. Wu, K. Strawhecker, B. Lu, and T. C. Chung, *Chem. Mater.*, **2001**, 13, 3516–3523.
- [34] a) Y. S. Choi, H. T. Ham, and I. Chung, *J. Chem. Mater.*, **2004**, 16, 2522–2529.
- b) C. C. Chou, and J. Lin, *Macromolecules*, **2005**, 38, 230–233.
- c) M. Galimberti, S. Giudice, V. Cipolletti, and G. Guerra, *Polym. Adv. Tech*, **2010**, 21, 1–6.
- d) M. Galimberti, A. Lostritto, A. Spatola, and G. Guerra, *Chem. Mater.*, **2007**, 19, 2495–2499.
- e) M. Galimberti, S. Senatore, L. Conzatti, G. Costa, G. Giuliano, and G. Guerra, *Polym. Adv. Technol.*, **2009**, 20, 135–142.
- f) D. R. Robello, N. Yamaguchi, T. Blanton, and C. Barnes, *J. Am. Chem. Soc.*, **2004**, 126, 8118–8119.
- [35] a) K. C. Baker, M. Manitiu, R. Bellair, C. A. Gratopp, H. N. Herkowitz and R. M. Kannan, *Acta Biomater.* **2011**, 7, 3382–3389.
- b) C. Chen, J. Samaniuk, D. G. Baird, G. Devoux, M. Zhang, R. B. Moore et al. *Polymer*, **2012**, 53, 1373–1382.
- c) S. Feng-hua, H. Han-Xiong, and Z. Yang, *Compos. Part B*, **2011**, 42, 421–428.
- d) J. Ma, E. Bilotti, T. Peijs, J. A. Darr, *Eur. Polym. J.*, **2007**, 43, 4931–4939
- e) Q. T. Nguyen, D. G. Baird, *Polymer*, **2007**, 48, 6923–6933.
- f) J. Samaniuk, D. Litchfield, Baird D. *Polym. Eng. & Sci.*, **2009**, 49, 2329–2341.
- e) M. A. Treece, J. P. Oberhauser, *J. Appl. Polym. Sci.*, **2007**, 103, 884–892.
- [36] a) S. Horsch, G. Serhatkulu, E. Gulari, R. M. Kannan. *Polymer*, **2006**, 47, 7485–7496. b) M. Manitiu, R. J. Bellair, S. Horsch, E. Gulari, and R. M. Kannan, *Macromolecules*, **2009**, 41, 8038–8046.
- [37] Powder diffraction data base 70-2151 International Centre for Diffraction Data. (1999). *PCPDF win. Version 2.02*.
- [38] T. Itoh, N. Ohta, T. Shichi, T. Yui, K. Takagi, *Langmuir*, **2003**, 19, 9120–9126.
- [39] M. Mauro, M. Maggio, V. Cipolletti, M. Galimberti, P. Longo, G. Guerra, *Carbon*, **2013**, 61, 395–403.

- [40] M. A. Osman, M. Ernst, B. H. Meier, U. W. Suter, *J. Phys. Chem. B*, **2002**, 106, 653–662.
- [41] V. Cipolletti, M. Galimberti, G. Guerra, and M. Mauro *Appl. Clay Sci.*, **2013**, doi, 10.1016/j. clay. 2013. 11.001.
- [42] Y. Ide, M. Ogawa, *J. Colloid. Interface Sci.*, **2005**, 296, 141–149.
- [43](a) S. Bandi, M. Bell, D. A. Schiraldi, *Macromolecules*, **2005**, 38, 9216–9220
(b) T. Pojanavaraphan, D. A. Schiraldi, R. Magaraphan, *Appl. Clay Sci.*, **2010**, 50, 271–279
(c) T. Pojanavaraphan, L. Liu, D. Ceylan, O. Okay, R. Magaraphan, D. A. Schiraldi, *Macromolecules*, **2011**, 44, 923–931.
(d) Y. Wang, S. M Alhassan, V. H. Yang, D. A. Schiraldi, *Composites, Part B*, **2013**, 45, 625–630
- [44] Y. Park, G. A. Ayoko, R. L. Frost, *J. Colloid Interface Sci.*, **2011**, 360, 440–456.
- [45] (a) X. Zhang, Z. Sui, B. Xu, S. Yue, Y. Luo, W. Zhan, B. Liu, *J. Mater. Chem.*, **2011**, 21, 6494-6497. (b) F. Liu, S. Song, D. Xue, H. Zhang, *Adv. Mater.*, **2012**, 24, 1089-1094. (c) S. Nardecchia, D. Carriazo, M. L. Ferrer, M. C. Gutiérrez and F. del Monte *Chem. Soc. Rev.*, **2013**, 42, 794-830. (d) H. Hu, Z. Zhao, W. Wan, Y. Gogotsi, J. Qiu *Adv. Mater.* **2013**, 24, 2219-2223. (e) T. Wu, M. Chen, L. Zhang, X. Xu, Y. Liu, J. Yan, W. Wang, J. J Gao, *Mater. Chem. A: Mater. Energy and Sustainability*, **2013**, 1, 7612-7621. (f) S. Ye, J. Feng, P. Wu *ACS Appl. Mater. Interfaces*, Article ASAPDOI: 10.1021/am401458x.
- [46] (a) M. A. Worsley, P. J. Pauzauskie, T. Y. Olson, J. Biener, J. H. Satcher, Jr., T. F. Baumann *J. Am. Chem. Soc.* **2010**, 132, 14067–14069. (b) M. A. Worsley, T. Y. Olson, J. R. I. Lee, T. M. Willey, M. H. Nielsen, S. K. Roberts, P. J. Pauzauskie, J. Biener, J. H. Satcher, Jr., and T. F. Baumann *J. Phys. Chem. Lett.*, **2011**, 2, pp 921–925. (c) J. Li, F. Wang, C. Liu *Journal of Colloid and Interface Science*, Volume 382, 2012, Pages 13–16 (d) S. Ye, J. Feng and P. Wu *J. Mater. Chem. A*, 2013, 1, 3495-3502.

[47] a) R. W. Pekala, . *J. Mater. Sci.*, **1989**, 24, 3221. b) R. W. Pekala, C. T. Alviso, ; X. Lu, J. Gross, J. Fricke, *J. Non-Cryst. Solids*, **1995**, 188, 34. c) W. C. Li, G. Reichenauer, J. Fricke, *Carbon*, **2002**, 40, 2955. d) Y. Tao, D. Noguchi, C-M. Yang, H. Kanoh, H. Tanaka, M. Yudasaka, S. Iijima, K. Kaneko, *Langmuir*, **2007**, 23, 9155. e)P. Lorjai, T. Chaisuwan, S. Wongkasemjit, . *J. Sol-Gel Sci. Techn.* **2009**, 52, 56. f) W. F. Zhang Z. H. Huang, C. Zhou, G. Cao, F. Kang, Y. Yang, *J. Mater. Chem.* **2012**, 22, 7158. g) A. P. Katsoulidis, J. He, M. G. Kanatzidis, *Chem. Mater.*, **2012**, 24, 1937.

Part III : Experimental Section

Chapter 1

Experimental section

Materials and Samples preparation

1.1. Syndiotactic Polystyrene (s-PS)

The syndiotactic polystyrene used in this study was manufactured by Dow Chemicals under the trademark Questra 101. ^{13}C nuclear magnetic resonance characterization showed that the content of syndiotactic triads was over 98%. 1 Weight-averaged and number-averaged molecular masses were found to be $M_w = 320000 \text{ g mol}^{-1}$ and $M_n = 82000 \text{ g mol}^{-1}$.

1.2 Poly(2, 6-dimethyl-1, 4-phenylene)oxide (PPO)

The PPO used in this study was purchased by Sigma Aldrich and presents weight-averaged and number-averaged molecular masses $M_w = 58500 \text{ g mol}^{-1}$ and $M_n = 17000 \text{ g mol}^{-1}$, respectively.

1.3 Poly(2,6-diphenyl-1,4-phenylene oxide) (PPPO)

Poly(2, 6-diphenyl-1, 4-phenylene oxide) used in this work was purchased from Sigma Aldrich (Tenax TA 60–80 mesh).

1.4 Ultra High Molecular weight polyethylene (UHMWPE)

The ultra high molecular weight polyethylene used in this study was purchased by Sigma Aldrich and presents weight-averaged and molecular mass $M_w = 3,000,000-6,000,000$.

1.5 High surface area graphite and GO preparation

High surface area graphite, with Synthetic Graphite 8427[®] as trademark, was purchased from Asbury Graphite Mills Inc., with a minimum carbon wt% of 99.8.

Graphite oxide (GO) samples were prepared by Dr. Marco Mauro using Hummers' method,² from graphite samples. 120 mL of sulfuric acid and 2.5 g of sodium nitrate were introduced into a 2000 mL three-neck round bottomed flask immersed into an ice bath and 5 g of graphite were added, under nitrogen, with a magnetic stirring. After obtaining an uniform dispersion of graphite powders, 15 g of potassium permanganate were added very slowly to minimize the risk of explosion. The reaction mixture was thus heated to 35 °C and stirred for 24 h. The resulting dark green slurry was firstly poured into a copious amount of deionized water, and then centrifuged at 10000 rpm for 15 min with a Hermle Z 323 K centrifuge. The isolated GO powder was washed twice with 100 mL of a 5 wt% HCl aqueous solution and subsequently with deionized water. Finally, it was

dried at 60 °C for 12 h.

Reduced graphite oxide (rGO) dispersions were obtained by adding the appropriate GO amount in 5 mL of DCB, following by solvothermal reduction of GO in a 5000 mL batch bath ultrasound (Badelin Sonorex RK 1028 H) at 100 °C for 2h. ³

1.6 Preparation of Physically Crosslinked Polymeric Aerogels

All gel samples were prepared in hermetically sealed test tubes by heating the mixtures until complete dissolution of the polymer and the appearance of a transparent and homogeneous solution had occurred. Only for UHMWPE solutions, a constant agitation was necessary to facilitate the rearrangement of the chains in a fibrillar morphology. Moreover the polyethylene was stabilized by 0.5 % w/w of the anti-oxidant di-*t*-butyl-*p*-cresol. ⁴ Then the hot solution was cooled down to room temperature where gelation occurred.

Gels were extracted with a SFX 200 supercritical carbon dioxide extractor (ISCO Inc.), generally using the following conditions: T= 40°C, P = 250 bar, extraction time t = 300 min.

For monolithic aerogels with a regular cylindrical shape, the total porosity, including macroporosity, mesoporosity and microporosity, can be estimated from the volume/mass ratio of the aerogel.

Then, the percentage of porosity P of the aerogel samples can be expressed as:

$$P = 100 \left(1 - \frac{\rho_{app}}{\rho_{pol}} \right)$$

where ρ_{pol} is the density of the polymer matrix and ρ_{app} is the aerogel apparent density calculated from the mass/volume ratio of the monolithic aerogels.

1.7 Preparation of s-PS/Clay Gels and Aerogels

Dispersions of the clays in DCB were obtained with both as received and exfoliated samples. A clay dispersion was initially prepared by adding the appropriate clay amount in 5ml of DCB. The mixtures were homogenized for 1 h under magnetic stirring and sonicated in a 5000mL batch bath ultrasound (Badelin Sonorex RK 1028 H) for 1 h.

s-PS/clay gels were prepared, in hermetically sealed test tubes, by heating the clay dispersions above the boiling point of the solvent until complete dissolution of the polymer and the appearance of a transparent and homogeneous solution had occurred. The hot solution was then cooled to room temperature, where gelation occurred. For instance, 655 mg of s-PS and 5mL of 2 wt % clay dispersion were mixed to obtain clay/polymer gels. The overall amount of polymer and clay in the gels was generally fixed to 10 wt %.

Also in this case Aerogels were obtained by treating s-PS/claygels with a SFX200 supercritical carbon dioxide extractor (ISCO Inc.) using the following conditions: $T = 40^{\circ}\text{C}$, $P = 200$ bar, extraction time $t = 300$ min. The prepared s-PS/clay aerogels present a weight composition ranging between 96/4 and 50/50. The aerogels, as prepared from gels with an overall polymer-clay content of 10wt%, present a porosity close to 90%.

1.8 Preparation of s-PS/rGO Gels and Aerogels

The preparation procedure is quite similar to the procedure described above for s-PS-Clay gels and aerogels. The prepared s-PS/rGO aerogels present a weight composition ranging between 95/5 and 50/50. The aerogels, as prepared from gels with an overall polymer-rGO content of 10 wt%, present a porosity close to 90%.

Chapter 2

Experimental section

Techniques

2. 1 Wide angle X-ray diffraction (WAXD)

Wide-angle X-ray diffraction (WAXD) patterns with nickel filtered Cu-K α radiation were obtained, with an automatic Bruker D8 Advance diffractometer, in reflection. The intensities of the WAXD patterns were not corrected for polarization and Lorentz factors, to allow an easier comparison with most literature data. The D_{hkl} correlation length of crystals was determined applying the Scherrer equation:

$$D_{hkl} = K \lambda / (\beta_{hkl} \cos\Theta_{hkl})$$

where: K is the Scherrer constant, λ is the wavelength of the irradiating beam (1.5419 Å, CuK α), β_{hkl} is the width at half height, and Θ_{hkl} is the diffraction angle. The instrumental broadening, b, was determined by obtaining a WAXD pattern of a standard silicon powder 325 mesh (purity > 99%), under the same experimental conditions. For each observed reflection with $\beta_{hkl} < 1^\circ$, the width at half height was evaluated by subtracting the unavoidable instrumental broadening of the closest silicon reflection from the experimental width at half height, B_{hkl} , using the following relationship:

$$\beta_{hkl}^2 = (B_{hkl}^2 - b^2)$$

The degree of crystallinity of the samples was evaluated from x-ray diffraction data applying the standard procedure of resolving the diffraction pattern into two areas corresponding to the contributions of the crystalline and amorphous fractions .

2.2 Fourier Transform Infrared (FTIR)

Fourier Transform Infrared (FTIR) spectra were obtained at a resolution of 2.0 cm^{-1} with a Vertex 70 Bruker spectrometer equipped with deuterated triglycine sulfate (DTGS) detector and a Ge/KBr beam splitter. The frequency scale was internally calibrated to 0.01 cm^{-1} using a He-Ne laser. A total of 32 scans were signal averaged to reduce the noise. The content of the guest molecules was determined by the intensity of FTIR guest peaks, as calibrated by thermogravimetric measurements.

2.3 Raman spectroscopy

The Raman spectra were collected by a confocal Raman spectrometer (Horiba-Jobin Yvon Mod. Aramis) operating with a diode laser excitation source emitting at 532 nm. The 180° back-scattered radiation was collected by an Olympus metallurgical objective (MPlan 50x, NA = 0.75) with confocal and slit apertures both set to 200 μm. A grating with 600 grooves/mm was used throughout. The radiation was focused onto a Peltier-cooled CCD detector (Synapse Mod. 354308) operating in the Raman-shift range 3200 – 800 cm⁻¹.

2.4 Scanning electron microscopy (SEM)

The internal morphology of the aerogelic monoliths was characterized by means of a scanning electron microscope (SEM, Zeiss Evo50 equipped with an Oxford energy dispersive X-ray detector). Samples were prepared by fracturing small pieces of the monoliths in order to make accessible the internal part of the specimen. In fact, the external lateral surface of all samples resulted to be flat and free of porosity. Low energy was used (5 keV) in order to obtain the highest possible surface resolution. Before imaging, all the specimens were coated with gold using a VCR high resolution indirect ion-beam sputtering system. The samples were coated depositing approximately 20 nm of gold. The coating procedure was necessary in order to

prevent the surface charging during the measurement and to increase the images resolution.

2.5 Porosimetry

For all physically crosslinked polymeric aerogels, surface area, pore volume and pore size distribution were obtained by N₂ adsorption measurements carried out at 77 K on a Micromeritics ASAP 2020 sorption analyzer.

Instead for all nanocomposites physically crosslinked polymeric aerogels surface area, pore volume and pore size distribution were obtained by N₂ adsorption measurements carried out at 77 K on Nova Quantachrome 4200e instrument.

All the samples were outgassed for 24 h at 30°C before the analysis. The specific surfaces areas were calculated using the Brunauer–Emmet–Teller method.⁵ The micropore volume has been determinate with the t-plot method.

2.6 Thermogravimetric measurements (TGA)

The content of the guest molecules in the samples was determined by thermogravimetric measurements (TGA) performed with a TG 209 F1 equipment from Netzsch under nitrogen atmosphere at a heating rate of 10 °C min⁻¹.

2.7 Colorimetric measurements

Colorimetric measurement have been carried out using a KONICA MINOLTA Spectrophotometer (CM-2500d).

2.8 Dynamic-mechanical analysis

Foe the s-PS-Clay aerogels dynamic-mechanical properties were studied using a Triton dynamic-mechanical thermal analyzer. The spectra were recorded in the three-point bending mode, on samples with the following dimensions: length 15 mm, width 10 mm, and thickness 2mm. The modulus E' was obtained, as a function of temperature, at a frequency of 1Hz and an amplitude of 0. 03mm. The heating rate was 2°C/min in the range of 0, +100°C.

References

- [1] A. Grassi, C. Pellicchia, P. Longo, A. Zambelli. *Gazzetta Chimica Italiana*, **1987**, 117, (4), 249-50.
- [2] W. S. Hummers, R. E. Offeman, *J. Am. Chem. Soc.*, **1958**, 80, 1339.
- [3] C. Nethravathi, M. Rajamathi. *Carbon* **2008**, 46, 1994-1998.
- [4] P. Smith, P. J. Lemstra, H. C. Booiij, *J. Polym. Sci., Phys.*, **1981**, 19, 877.
- [5] S. Brunauer, P. H. Emmett, E. Teller, *Adsorption of Gases in Multimolecular Layers*, **1938**, (60), 309.

Ringraziamenti

Desidero innanzitutto ringraziare il Prof. Gaetano Guerra e il Dr. Christophe Daniel, per tutto ciò che ho imparato durante questo corso di Dottorato. Ogni volta che ho avuto dubbi o perplessità mi hanno aiutato con incommensurabile pazienza, ho potuto maturare competenze e fare esperienze che senza loro non sarebbero state possibili; ma soprattutto, non mi sono mai sentita sola, per questa assidua presenza, grazie di cuore.

Ringrazio inoltre il Prof. Antonio Proto, il Prof. Vincenzo Venditto e la Dr.ssa Paola Rizzo per i preziosi consigli e per il loro aiuto .

Voglio ringraziare tutti i ragazzi del laboratorio 9, per il fantastico clima di divertimento e di collaborazione che sul posto di lavoro è fondamentale.

In particolare voglio ringraziare la Dr.ssa Maria Rosaria Acocella, mia cara amica che ha saputo rendersi indispensabile in ogni senso, ed è diventata importantissima per me.

Ancora vorrei ringraziare la Dr.ssa Graziella Ianniello, che per me c'è da sempre e spero per sempre. Un ringraziamento sincero al Dr. Marco Mauro, per la collaborazione scientifica, e non solo, per tutto l'aiuto che ci siamo dati avendo iniziato insieme questo percorso.

Il ringraziamento più grande, quello che esplode dal cuore, va al mio Papà e alla mia Mamma che mi hanno permesso di perseguire ogni mio obiettivo spalleggiandomi sempre, non lasciandomi mai sola; voi siete la mia vera forza, vi devo ogni cosa. Grazie.

Grazie a mia sorella Ilaria, amica e complice, perchè è sempre riuscita a farmi stare bene e a farmi ridere. Mi è stata vicino in un modo speciale come solo una sorella può fare.

Grazie al mio Diego, per tutto l'amore e la pazienza che mi ha dimostrato ogni giorno e continua a dimostrarmi, il punto cardine delle mie giornate e della mia vita.

Grazie alle mie Nonne, che mi hanno sempre incoraggiata e amata, fin da bambina, mostrandosi sempre orgogliose per ogni mio piccolo passo.

Grazie alla Signora Maddalena e al Signor Gianfranco, per il sostegno, l'entusiasmo e la fiducia dimostratami in ogni occasione.

Grazie a Lia e Nunzia, perchè ci comprendiamo al volo e siamo l'una per l'altra, per tutte le risate fino alle lacrime e per la forza che viene da ogni nostro abbraccio.

Grazie alla mia amica Matilde lontana solo sulla cartina, ma per me sempre vicina.

Grazie di cuore alla mia amica Rosaria, per aver camminato accanto a me, per avermi consigliata, e per non avermi mai fatto mancare il suo affetto e la sua presenza.

Un ringraziamento speciale va alla mia amica Lucia che con il suo sorriso ha portato allegria nelle mie giornate, facendo svanire ogni preoccupazione.

Voglio ringraziare inoltre, chi mi ha guardato, guidato e protetto da lassù. Vi ho sentito sempre.

Per ultimo, ma non meno importante, voglio ringraziare il Sorriso del mio cuore, Rocky.